2 copy

MASTER

STS INCORPORATED
SCIENTIFIC TRANSLATION SERVICE
formerly Technical Library Research Service
Ann Arbor, Michigan

ORNL-tr-2415

SPECTRUM MEASUREMENTS OF RADIOACTIVE NEUTRON SOURCES IN THE 10 keV-10 MeV ENERGY REGION WITH PROTON-RECOIL PROPORTIONAL COUNTERS

By H. Werle

Karlsruhe Nuclear Research Center
External Report, INR-4170-25, February 1970
(NP-18359)

LEGAL NOTICE
This report was prepared as an account of work sponsored by the United States Government. Neither the United States nor the United States Atomic Energy Commission, nor any of their employees, nor any of their contractors, subcontractors, or their employees, makes any warranty, express or implied, or assumes any legal liability or responsibility for the accuracy, completeness or usefulness of any information, apparatus, product or process disclosed, or represents that its use would not infringe privately owned rights.

Translated from the German
For Oak Ridge National Laboratory
Purchase Order No. 34B-83481-V
Letter Release T-67

STS Order No. 9935

DISTRIBUTION OF THIS DOCUMENT IS UNLIMITED

sTs®
Ann Arbor, Michigan

STS INCORPORATED
SCIENTIFIC TRANSLATION SERVICE
formerly Technical Library Research Service

SPECTRUM MEASUREMENTS OF RADIOACTIVE NEUTRON SOURCES IN THE 10 keV-10 MeV ENERGY REGION WITH PROTON-RECOIL PROPORTIONAL COUNTERS

By H. Werle

Karlsruhe Nuclear Research Center
External Report, February 1970, INR-4170-25

Institute of Neutron Physics and Reactor Engineering

Gesellschaft für Kernforschung mbH, Karlsruhe

Contents

		Page
1.	Introduction	1
2.	Choice of the Neutron Spectrometer	3
3.	Measuring Method	10
3.1	Proton-Recoil Proportional Counters	10
3.2	Measurement of Proton Spectra	15
3.2.1	Construction, filling and energy resolution of the counters	15
3.2.2	Gas amplification and rise times	21
3.2.3	Energy calibration and relation between proton energy and ionization	26
3.2.4	Electronics with and without γ,n-discrimination	38
3.2.5	Source-detector geometry and counters utilized	45
3.3	Analysis of the Proton Spectra	48
3.3.1	Monoenergetic neutrons	48
3.3.2	Analysis program	51
3.3.3	Estimate of systematic errors	61
4.	Spectrum Measurements	66
4.1	Comparison Measurements with Other Methods in SUAK	66
4.2	Sb-Be(γ,n)-source	69
4.3	Cf^{252}-source	78
4.4	α,n-sources	80
4.4.1	Theoretical background	80
4.4.2	Am-Li-source	83
4.4.3	Am-F source	85
4.4.4	Am-B^{10}-source	87
4.4.5	Am-B-source	89
4.4.6	Am-Be sources	91
4.4.7	Ra-Be source	98

4.5 Source strengths 100

5. Summary 101

6. Literature 102

Abstract:

Proton recoil proportional counters are used since some years with success for neutron spectrum measurements in the energy range between about 20 keV and 1.5 MeV. In this work it is shown by measurements with monoenergetic neutrons and by comparison measurements with other methods, that with proton recoil counters reliable measurements are also possible below 20 keV and in the energy range between 1.5 and 10 MeV.

The spectra of most of the normally used, radioactive neutron sources (α,n-sources: Ra-Be, Am-Be, Am-B, Am-B^{10}, Am-F, Am-Li; Cf^{252} spontaneous-fission source) were measured in the whole interesting energy range, especially also in the range below 1 - 2 MeV and the influence of the size of the radioactive particles on the neutron spectrum was proved experimentally. The differential neutron spectrum of a Sb-Be (γ,n)-source could be determined for the first time with good accuracy, in spite of the very high γ-background, by using the γ-n-discrimination technique.

1. Introduction

For differential investigations of fast neutron reactions, radioactive neutron sources have been extensively replaced by accelerators which furnish higher neutron fluxes and permit a continuous variation of neutron energy, while reactors are used practically exclusively for the generation of induced radioactivities. In spite of this development, radioactive neutron sources are still highly useful for some applications. They are extremely compact, have a constant or only slowly changing source strength and are practically maintenance-free. Consequently, radioactive neutron sources continue to be employed as standards for the determination of absolute neutron source strengths, calibration of neutron detectors, investigation of slowing-down and diffusion properties in different materials, measurement of scattering and absorption cross-sections, and for importance measurements in fast reactors.

In order to attain the limit of error of 1% for importance measurements, a precise knowledge of the source spectra is necessary. For most radioactive neutron sources, the spectrum in the lower energy region has not been known thus far because the measuring methods utilized cannot be employed below about 1 MeV, especially with a strong γ-background. In the upper energy region, the spectra measured by different authors frequently diverge highly from each other and since usually no information is given on systematic errors, the reliability and accuracy can hardly be evaluated. Consequently, differences of up to 5% result in the importance measurements, depending on which of the published spectra is used and what assumptions were made for the trend in the low-energy region. General information concerning the necessary accuracy with which source spectra must be known to attain a 1% limit of error for importance measurements cannot be given because the spectra are very different. However, it is sufficient if the relative trend of the spectrum is known within 10% in the entire energy region from 10 keV to 10 MeV which is of interest for radioactive neutron sources.

The objective of the present study therefore was (1) to develop a sufficiently sensitive method for radioactive neutron sources with which neutron spectra can be measured with an accuracy of 10% in the range of 10 keV-10 MeV with an energy resolution of 10%, and (2) to

determine the spectra of the neutron sources listed in Table 1 which are used for importance measurements in particular.

Table 1.--Investigated sources.

Source	Type	Radioactive isotope	Target material	Source strength (n/sec)
Sb-Be	γ,n	Sb^{124}	Be	$5 \cdot 10^4$
Cf^{252}	spontan. fission	Cf^{252}	-	$1,7 \cdot 10^6$
Am-Li	α,n	Am^{241}	Li	$1,1 \cdot 10^6$
Am-F	α,n	Am^{241}	F	$4,6 \cdot 10^5$
Am-B^{10}	α,n	Am^{241}	B^{10}	$4,3 \cdot 10^5$
Am-B	α,n	Am^{241}	B	$1,2 \cdot 10^6$
Am-Be(5C)	α,n	Am^{241}	Be	10^7
Am-Be(0,4C)	α,n	Am^{241}	Be	$1,1 \cdot 10^6$
Am-Be(1,5C)	α,n	Am^{241}	Be	$1,3 \cdot 10^6$
Ra-Be	α,n	Ra^{226}	Be	$1,2 \cdot 10^6$

In Section 2, the various methods to be considered are compared on the basis of the requirements made of the spectrometer and the choice of recoil-proton proportional counters is explained; these have been used successfully for several years to measure fast reactor neutron spectra in the energy region from about 20 keV to 1.5 MeV.

In Section 3, the problems which occur below 20 keV and above 1.5 MeV with the use of this technique are discussed. By an accurate determination of the relationship between proton energy and ionization for hydrogen produced in the counter with the use of a so-called slowing-down time spectrometer, it was possible to increase the reliability and accuracy in the lower energy region. For the energy region above 1.5 MeV, the applicability of this method with the use of suitable counters is demonstrated by measurements with monoenergetic neutrons.

In Section 4, the neutron spectrum measurements of the sources listed in Table 1 are discussed. First, however, the spectra measured for two SUAK systems with the use of proton recoil counters in the range of 20 keV to 5 MeV are compared with the results of other methods, showing that proton recoil counters can also be employed above 1.5 MeV to measure the neutron spectra of fast reactors. In connection with the neutron spectra of radioactive sources, the following needs to be pointed out: (1) For most α,n-sources, the trend of the neutron spectrum

below 1-2 MeV is not well known and measurements below 500 keV do not exist for any of these sources. However, it can be anticipated [1] that a considerable number of neutrons with energies below 1 MeV are emitted at least from some α,n-sources. The spectra in the low-energy region are of great significance for importance measurements and of some physical interest, and their determination is an important part of this study. (2) For the Sb-Be(γ-n)-source, which is still used today for standard measurements of absorption cross-sections, the differential neutron spectrum was determined for the first time. (3) In the studies published thus far on radioactive source spectra, only one or two sources were investigated and since data on possible systematic errors are usually not furnished, it is difficult to evaluate the accuracy and reliability of results. In this connection, we should notethe estimate of systematic errors, the comparison measurements with other methods in SUAK and the fact that the spectra of all sources used typically were determined by the same method in the present study.

2. Choice of the Neutron Spectrometer

The spectra of a number of different neutron sources, some of which have very small source strengths (≈ 10^5 n/sec) are to be determined with the neutron spectrometer. The spectrometer must therefore be usable in the energy region from about 10 keV to 10 MeV and must have a high response probability. The energy resolution should be not less than 10% over the entire energy region, so that the structures present in different source spectra are well resolved and the mean total error in the measured energy distribution should not be greater than about 10%. In the following, the choice of the spectrometer utilized will be explained by a critical comparison of the different methods to be considered. Three points are of particular interest here: (1) Measurable energy region, (2) Sensitivity, and (3) Accuracy.

The methods for the determination of differential neutron spectra can be divided into three groups:

1. Time-of-flight methods,
2. Neutron-induced nuclear reaction,
3. Recoil processes.

Generally, the time-of-flight method cannot be used for the measurement of neutron spectra of stationary sources, since another radiation coincident with the neutrons, which is suitable to establish the start of the flight time, is emitted only in exceptional cases. The exceptions include nuclei undergoing spontaneous fission, such as Cf^{252}.

The methods of group two make use of reactions of the following type:

$$n + A \rightarrow B + C + Q$$

The capture of a neutron in nucleus A leads to the product nuclei B and C, with the release of energy Q. The sum of Q and of the kinetic energy of the neutron appears as kinetic energy of the product nuclei if no product nucleus excitation occurs. Consequently, the neutron energy can be clearly determined by measuring the total released energy. However, for a reaction to be useful for neutron spectrometry, the following conditions must be at least partially satisfied:

The cross section may not be too small and should be a continuous function of energy (no sharp resonances).

In the energy region of interest ($\leq$ 10 MeV), no interefering competing reactions should occur.

The Q-value should be positive, so that measurements can also be made in the region of low neutron energies. However, Q should also not be too large, since the energy resolution becomes poorer with increasing Q-values, particularly at low neutron energies.

The reacting isotope A must be present in a form which permits the construction of a spectrometer.

There is no reaction which satisfies all conditions. Because of the first two conditions, our choice is limited to light nuclei, and of these, He^3, Li^6, B^{10} and N^{14} should be given closer attention. The reactions $N^{14}(n,p)C^{14}$ and $B^{10}(n,\alpha)Li^7$, however, both have very small cross-sections. The $B^{10}(n,\alpha)Li^7$-reaction furthermore leads to an excited level in Li^7 with a 6% probability and contains resonances in the cross-section. Consequently, only the reactions:

$$Li^6 + n \longrightarrow H^3 + \alpha + 4{,}786 \text{ MeV},$$

$$He^3 + n \longrightarrow H^3 + p + 0{,}764 \text{ MeV}.$$

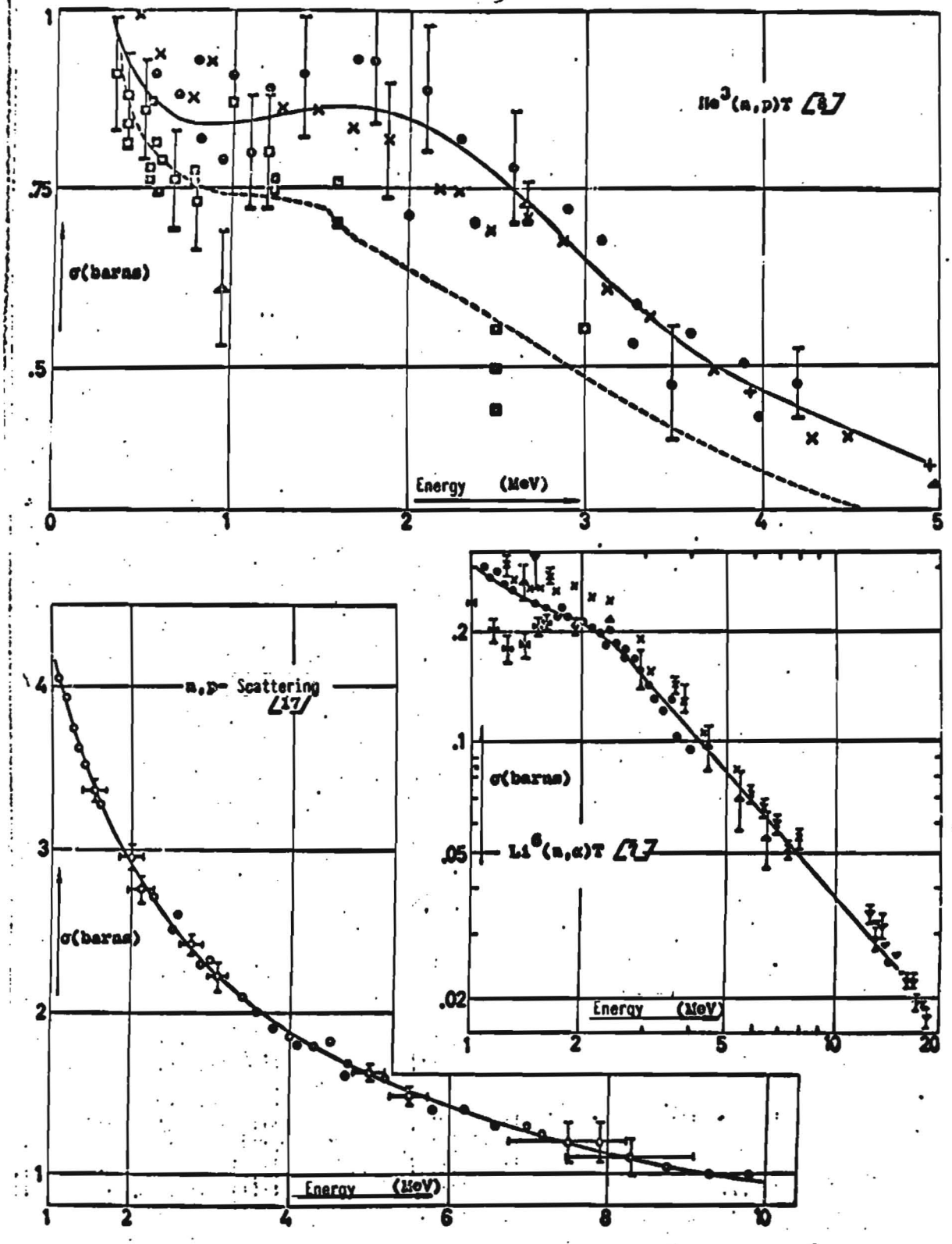

Fig. 1.--Cross-sections for the reactions $He^3(n,p)T$ $Li^6(n,\alpha)T$, and n,p-scattering.

are useable for neutron spectroscopy. The $Li^6(n,\alpha)H^3$-reaction was used for the first time for neutron spectroscopy by Love and Murray [2] in the form of the Li^6-sandwich-semiconductor spectrometer. This spectrometer is already being used frequently to measure fast reactor neutron spectra, but it is not suited to measure source spectra for the following reasons:

1. The sensitivity is very low because the cross-section is very small and because the Li^6F-layer must be very thin so that the energy loss of product nuclei occurring in it will remain small.

2. Because of the large Q-value and the finite energy resolution of semiconductor detectors, measurements are possible only above about 500 keV.

3. Above 5 MeV, the n,α-cross section decreases extensively, so that the ratio of measuring reactions to secondary reactions in the semiconductor-detector silicon becomes very unfavorable.

4. The relative curve of the n,α-cross section at the present time does not seem to be known within better than ±10% as indicated by Fig. 1. In principle, all spectrum measurements contain the same error.

Two types of spectrometers are known which are based on the $He^3(n,p)H^3$-reaction. He^3-filled proportional counters were used for the first time as spectrometers by Batchelor, Aves and Skyrme [3]. A summary of these studies up to and including 1957 has been published by Batchelor and Morrison [4]. Essentially, two problems remain which have not yet been solved to satisfaction:

1. Calculation of wall effects,

2. Elimination of competing reactions: He^3-recoils, $He^3(n,D)D$ above 4.36 MeV and $He^3(n,pn)D$ above 7.32 MeV.

A calculation of wall effects is particularly difficult here because a three-particle reaction is involved. Moreover, the nuclear data required for the calculation are not completely known. A mathematical correction of the spectrum which is considerably deformed by competing reactions also fails because accurate nuclear data are lacking. The method of Sayres and Coppola [5], who separate the various processes by means of the pulse shape is more promising. A complete separation is not possible, however, and in particular, $He^3(n,p)T$-processes, in which the product nuclei release their energy only

partially in the counter, cannot be differentiated from other reactions. Consequently, an effective cross section must be introduced and the determination of the latter becomes extremely complicated due to coupling of wall effects and competing reactions, as was demonstrated by Bair [6]. With regard to the accuracy of the relative variation of the cross section, an error of ±10% must be expected again as shown by Fig. 1. Furthermore, it must be kept in mind that measurements below about 200 keV are impossible with an energy resolution of about 10% because of the Q-value of 764 keV.

The other spectrometer type in which the $He^3(n,p)T$-reaction is used is a He^3-sandwich-semiconductor spectrometer. Its sensitivity is about 10 times higher than that of the Li^6 spectrometer. The reason for this is that the cross section is about 3 times greater than that of Li^6 and that the number of He^3-atoms may be about 4 times greater than that of Li^6-atoms because of the lower specific ionization of product nuclei. Because of the higher sensitivity, the ratio of primary-to-secondary reactions is considerably more favorable than in the Li^6-spectrometer, and therefore, spectra can be measured up to 10 MeV. If a considerable γ-background is present, which is always true for radioactive sources, the lower thresholds of the coincidence circuits must be raised; as a result, (1) the measurable energy region has a lower limit of about 2 MeV and (2) an effective cross section which is modified over the entire energy region is obtained, whose precise calculation again fails because of the lack of nuclear data [9].

Recoil processes have been used for the detection and energy determination of neutrons since the beginnings of neutron physics and accordingly, a large number of different methods exists by now [4]. Most of them use proton recoil processes. This has three reasons:

1. The entire neutron energy can be transferred to the proton.

2. n,p-scattering in the CM system is isotropic below 10 MeV, leading to the well-known box-shaped distribution of recoil protons produced by monoenergetic neutrons.

3. The n,p-scattering process is the cross-section which is best known in general.

In the following, only those methods will be briefly discussed which can be basically used for the measurement of source spectra.

Scintillators: Protons produced by fast neutrons excite scintillators (anthracene, stilben, liquid scintillators) to light emission, the intensity of which depends on the released proton energy and is measured with a photomultiplier. The detection probability of scintillators is very high. It is a disadvantage that the relation between proton energy and light yield is not linear and that double-scattering also occurs as a result of the very high response probability, leading to very complicated proton distributions, especially at higher neutron energies [10]. The γ-radiation produces fast electrons in the scintillators and these have a considerably higher light yield than protons. Consequently, discrimination over the pulse shape is necessary over the entire energy region to eliminate fast electrons. The resolution between protons and electrons becomes more difficult with decreasing energy, so that measurements below about 1 MeV are impossible.

Nuclear emulsions: This method permits a very good energy resolution (≈ 3%) and good discrimination with respect to background radiation. Disadvantages are the low sensitivity and extremely complicated analyses of tracks. The lower limit of the measuring range falls at about 500 keV.

Telescope systems: These systems consist of a hydrogen-containing radiator and one or several detectors connected in coincidence which detect the protons emitted in a very small angular interval and measure their energy. Good discrimination with respect to the background is possible as a result of the coincidence circuit. The detection probability of such systems is very small, however, because (1) the neutron beam must be collimated, (2) the radiator must be thin to avoid energy losses, and (3) the detectors may detect only protons from a small angular interval.

Proportional counters: In addition to the simple recoil-proton proportional counter which is used in the present study, a number of other techniques exists. The difficulties due to wall effects can be reduced considerably if heavier gases are used as the filling, for example, deuterium or helium. However, in these nuclei, scattering is anisotropic and therefore, the differential, angle-dependent scattering cross sections are contained in the neutron spectrum obtained. However, at the present time, these scattering cross sections are not yet known well enough that the desired accuracy of 10% can be attained in the spectral measurements.

Monoenergetic neutrons result in a broad recoil-nucleus distribution which extends from zero energy up to a maximum energy. Several possibilities exist to obtain a clearer relationship between neutron and proton energy for neutrons incident parallel to the counting wire and thus to simplify the evaluation of recoil spectra. Giles [11] used a counter with a small diameter compared to the length and proton range. In this manner, it is possible to detect only the tracks parallel to the axis which originate from recoil nuclei to which the maximum possible energy was transmitted. Perlow [12] uses the same principle in a somewhat modified form. All versions of this type result in a small detection probability because of the telescope-like geometry. Another possibility for making this selection without necessarily reducing the detection probability is that of pulse shape discrimination, since the rise of the voltage pulse in the counter depends highly on the radial extent of the track. Whether a clean separation of the tracks running parallel to the counting wire is possible in this manner is very doubtful, however, for the following reasons: (1) The rise time of the counter pulses also depends highly on the radial distance of the track from the counting wire. This dependence can be reduced only by decreasing the counter diameter and therefore, at the expense of the detection probability. (2) If scattering takes place preferentially in the forward direction, as is the case with helium and deuterium, the radial extent of all tracks is small.

Table 2 summarizes the most important results of this study. The energy resolution of all methods listed there is smaller than or equal to 10%. A quantitative comparison of the detection probabilities is very difficult because these depend on many factors. The data listed in column 5 of Table 2 represent measuring times for an Am-B(α,n)-source with a source strength of 10^6 n/sec. The data were obtained from published studies [13-16] by converting the listed measuring periods to the same subdivision of the energy region (10% group width)and to the same mean statistical error per group (10%).

The decisive reasons for the choice of the simple proton-recoil proportional counter can be briefly summarized once more as follows:

1. Below 10 MeV, n,p-scattering is isotropic and does not produce competing reactions. The cross section is the best one known of all (Fig. 1) and the mean error of the measured values is less than 2%. In this connection, it is worthy of note that only a small number of the source-spectrum measurements published to date makes use of different reactions.

2. The simple proportional counter was selected because (a) it can be used in the entire energy region between 10 keV and 10 MeV, (b) its sensitivity is sufficient even for weak sources (10^5 n/sec), (c) all data are known for an exact analysis of the relatively simple proton spectra--in contrast to scintillators--and (d) it has proved to be highly useful in the measurement of fast reactor neutron spectra in the energy region below 1.5 MeV as a result of advances made in recent years in counter development [19,20].

3. Measuring Method

3.1 Proton-Recoil Proportional Counters

Proportional counters filled with hydrogen-containing gases have played an important role as neutron detectors since the beginnings of experimental neutron physics. Up to about ten years ago, however, it was generally believed that they were unsuitable for the measurement of continuous neutron spectra [4,18]. This opinion was refuted by Benjamin et al. [19] who determined differential neutron spectra of fast reactors in the energy region between about 30 keV and 1 MeV with small spherical proton-recoil counters. In 1964, Bennett [20] was able to expand the measurable energy range down to about 1 keV by pulse-shape discrimination. Since then, the 4π-proton-recoil method has become one of the most common techniques for the determination of differential neutron spectra in fast reactors.

If E_n is the neutron energy before collision and θ is the angle between the path of the incident neutron and the recoil nucleus (atomic weight A) in the laboratory system, then, the energy of the recoil nucleus according to the law of conservation of energy and momentum is given by:

$$E = \frac{4A}{(1+A)^2} E_n \cdot \cos^2 \theta \quad (1)$$

Table 2.--Comparison of different methods for the measurement of radioactive neutron source spectra.

Reaction		Spectrometer type	Measuring range (MeV)	Precision of relative cross-section trend	Measuring time (hours)	Remarks
$Li^6(n,\alpha)H^3$		Semiconductor sandwich	0,5 - 5	± 10%	500	
$He^3(n,p)H^3$		Proportional counter	> 0,2	± 10%	5	Pulse shape discrimination needed; sensitivity can not be precisely calculated.
		Semiconductor sandwich	> 2	± 10%	50	Sensitivity cannot be precisely calculated
Recoil	D, He	Proportional counter	> 0	± 5%	5	Anisotropic scattering σ_{diff} not precisely known
	P	Scintillator	> 1	± 2%	2	Pulse shape discrimination needed; complicated response functions
		Emulsion	> 1	± 2%	500	Very complicated analysis
		Proportional counter	> 0	± 2%	5	Complicated analysis

The recoil energy is highest for a central collision ($\theta = o$). Then we have:

$$E_{max} = \frac{4A}{(1+A)^2} E_n \, . \tag{2}$$

The following relation is valid between the recoil energy in the laboratory system and the scattering angle of the neutron in the center-of-mass system ω:

$$E = \frac{2A}{(1+A)^2} E_n (1 - \cos\omega) \, . \tag{3}$$

If σ_i is the integral scattering cross section and $\sigma(\omega)$ is the differential scattering cross section in the CM system, then $\sigma(\omega)d\Omega/\sigma_i$ is the probability that the neutron will be scattered in a collision by the angle ω into the solid angle element $d\Omega$. Because $d\Omega = 2\pi \sin\omega \, d\omega$, the probability that the recoil nucleus will absorb an energy of between E and E + dE then is:

$$p(E)\, dE = \frac{\sigma(\omega)}{\sigma_i} 2\pi \sin\omega \, d\omega \, . \tag{4}$$

With (3), it then follows that:

$$p(E) = \frac{\sigma(\omega)}{\sigma_i} \frac{\pi}{E_n} \cdot \frac{(A+1)^2}{A} \, . \tag{5}$$

For hydrogen, scattering below 10 MeV is isotropic in the CM system, i.e. $\sigma(\omega) = \sigma_i/4\pi$, and therefore, we have:

$$\begin{aligned} p(E) &= \frac{1}{E_n} = \text{const.} && \text{for } E < E_n \\ p(E) &= 0 && \text{for } E > E_n \, . \end{aligned} \tag{6}$$

The proton spectrum (per MeV) produced by a continuous neutron distribution $\varphi(E_n)$ (neutrons per $cm^2 \cdot sec.MeV$) therefore is:

$$P(E) = N \cdot T \int_E^{\infty} \frac{\sigma_1(E_n)}{E_n} \varphi(E_n)\, dE_n \,. \tag{7}$$

Inversely, by differentiating (7) for E, we obtain the well-known relation:

$$\varphi(E) = -\frac{1}{N \cdot T} \frac{E}{\sigma(E)} \frac{dP(E)}{dE} \,. \tag{8}$$

which is the basis for the determination of neutron spectra from the recoil-proton distribution. In the above, N is the number of protons in the sensitive volume of the counter and T is the measuring time.

The proton spectrum measured in a counter is significantly modified by two unavoidable effects: Some recoil protons are incident on the counter wall before they have released their total energies to the counter gas. In addition to neutrons, the counters also detect the fast electrons which are produced mainly in the counter wall by γ-quanta.

The square proton distribution described by (6) consequently is deformed as shown schematically in Fig. 2. (The sharp drop at the maximum proton energy is rounded as a result of the finite counter resolution.)

As long as the wall effects are sufficiently small, they can be corrected. There are two possibilities to measure spectra over a wide energy region in spite of the γ-background: One of these is to eliminate the γ-induced pulses by the pulse shape. The other is based on the fact that the maximum energy released by the electrons is considerably smaller than that of protons because of the considerably lower specific ionization. If E_{max} is the proton energy up to which the proton spectrum can be analyzed, the γ-induced pulses are all below about $E_{max}/10$. With a suitable set of approximately four different counters, the entire energy region from 10 keV to MeV can therefore be determined.

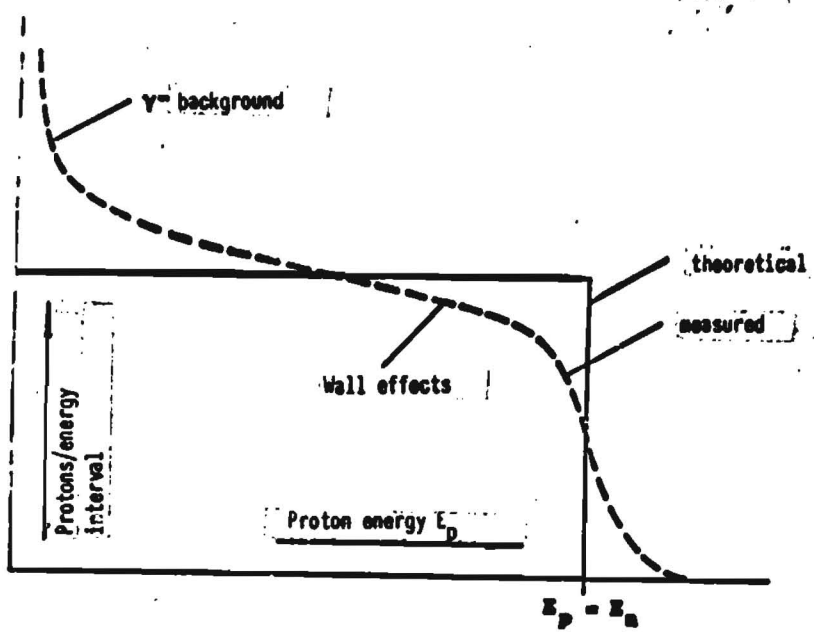

Fig. 2.--Recoil-proton spectra for monoenergetic neutrons.

Up until now, simple recoil-proton proportional counters have not been used for spectral measurements above about 1.5 MeV. The reason for this is that high pressures and large counter dimensions are necessary to maintain sufficiently small wall effects of the high-energy protons. The filling gases therefore should have a high slowing-down power and, to attain a high detection probability, should also have a large number of hydrogen atoms per molecule. Consequently, practically only hydrocarbons or mixtures of hydrocarbons and heavy rare gases can be considered. Of the rare gases Xe and Kr to be considered, Kr was used in spite of its smaller slowing-down power because its total reaction cross section is so small (a few mb) that no interferences with the recoil proton spectrum by Kr reaction products are to be expected with the mixture utilized here (2 atm Kr + 2 atm CH_4); this has been fully explained by Bair [6]. Table 3 lists the ranges (R) in hydrogen, methane and krypton for different proton energies for comparison purposes.

We assume that the neutrons are incident parallel to the counting wire of a cylindrical counter having a large length compared to the diameter D. As will be demonstrated fully in Section 3.1, the proton spectrum can then be analyzed up to a proton energy E_{max} which

Table 3.--Range (cm) of protons (760 mm Hg, 15°C)

Proton energy (MeV)	Hydrogen	Methane	Krypton
1 2	9,91 33,8	2,51 8,24	1,91 5,27
3 4	70,3 118,0	16,7 27,9	9,79 15,3
5 6	177,0 246,0	41,6 57,8	21,9 29,3
7 8	326,0 417,0	76,3 97,2	37,8 47,1
9 10	518,0 628,0	120,0 146,0	57,4 68,7

is given by $R(E_{max}) \approx 2D$. The largest counter used here has a diameter of 9 cm. The range of 10 MeV protons therefore may not be greater than about 20 cm. The counter therefore must be filled with at least 7 atm methane, 4 atm propane or 4 atm of a krypton-methane mixture.

The determination of neutron spectra can be divided into two parts: (1) Determination of the proton energy distribution. This is accomplished by measuring and storing the amplified counter pulse amplitudes. The relation between released proton energy and recorded voltage amplitude therefore must be accurately known and will be investigated more fully in point 3.2.3. (2) Determination of the neutron spectrum from the measured proton energy distribution. This point is explained in 3.3 The main problem here is the calculation of wall effects.

3.2 Measurement of Proton Spectra

3.2.1. Construction, filling and energy resolution of the counters: We used two types of counters. For in-core measurements in fast reactor systems (such as SUAK) in the energy region below 1 MeV, we used primarily so-called spherical counters (20th Century Electronics Ltd., New Addington, Nr. Croydon, Surrey, England.) [19] in which the cathode has the shape of a sphere, with the result that the measured proton spectra are extensively independent of the direction of neutron incidence on the counter. By careful design of the

insulators it is furthermore possible to obtain a highly constant field of cylindrical symmetry along the entire wire, so that the dead spaces at the wire ends become very small and end effects become negligible. For the measurement of radioactive neutron source spectra, cylindrical counters (Laboratory of Prof. Dr. Berthold, Wildbad, Black Forest) were used primarily in the energy region above 150 keV; their diameter (9 cm maximum) is small compared to their length (100 cm maximum). Consequently, end effects do not play a great role compared to wall effects and no special efforts were made to eliminate end effects, such as by the so-called "field tubes." It is true, that the counter tubes are equipped with so-called "safety rings" so that they can be operated at high voltages of up to 6 kV.

In some counter types, the ends have a region in which no gas amplification occurs any longer, but the primary charge is collected nevertheless. This is the case particularly in counter tubes with "hypodermic needles" [20] in which the counter wire diameter is enlarged at the ends so that a well-defined active volume is obtained. However, as shown by Fig. 3, two peaks are generally obtained for monoenergetic protons (764 keV from the $He^3(n,p)T$-reaction with the use of such counters. The peak with a small pulse height originates from protons produced in the dead space, i.e. their primary charge is only collected. As long as no gas amplification occurs on the counting wire proper, the two peaks coincide. With increasing gas amplification, the position of one of the peaks shifts. This effect which permits the determination of the absolute gas amplification and of the ratio of dead to active space may completely falsify the low-energy proton spectrum, on the other hand, because the "collection" spectrum is superimposed on the "gas-amplified" spectrum. In measurements of the low-energy regions of a neutron spectrum extending up to high energies, it is therefore necessary to use counters with very small dead volumes or high gas amplification.

The counters were filled with commercial high-purity gases (Edelgas GmbH., Düsseldorf). The maximum impurities are listed in Table 4. Filling was performed in such a way that repeated flushing with the filling gas was followed by heating the filling system for several hours at about 100°C while evacuating to less than 10^{-4} torr. After filling, the filling nipple consisting of soft-annealed copper was pinched closed.

Table 4.--Purity of filling gas.

Filling gas	Purity	Impurities, max. (vpm)		
		H_2O	N_2	O_2
Hydrogen H_2	≥ 99,9997	≤ 2	≤ 0,5	≤ 0,5
Methane CH_4	≥ 99,99	≤ 5	≤ 30	≤ 5
Propane C_3H_8	≥ 99,95	≤ 5	≤ 40	≤ 10
Krypton Kr	≥99,998	Total < 5		

In addition to propane, which produced a poor energy resolution even at pressures below 2 atm, all other gases used here were well suited as filling gases up to pressures of about 4 atm. Methane was best; it furnished energy resolutions of about 5% up to pressures of 3 atm even with the largest counters (9 cm diameter). The energy resolution became rapidly poorer with increasing pressure above 3 atm with all gases, particularly in the large counters, and at 4 atm, it already amounted to about 20%.

The cylindrical counters contained a trace of He^3(≈1 ‰). During irradiation with thermal neutrons, monoenergetic protons with 764 keV are obtained from the $He^3(n,p)T$-reaction. This He^3-peak (shown in Fig. 4 for some of the counters utilized) serves to verify the counters and particularly, to determine the gas amplification and constancy of the energy calibration made with monoenergetic neutrons. In the spherical counters, use is made of a weak Pu-α-specimen (a few disintegrations per sec) instead of He^3; it is mounted in the center of the anode wire. The energy resolution of the counters utilized here was better than 10% except for the large cylindrical counter (9 cm diameter) which was filled with 2 atm Kr and 2 atm CH_4 and which was used in the energy region above 3 MeV and had an energy resolution of about 20%.

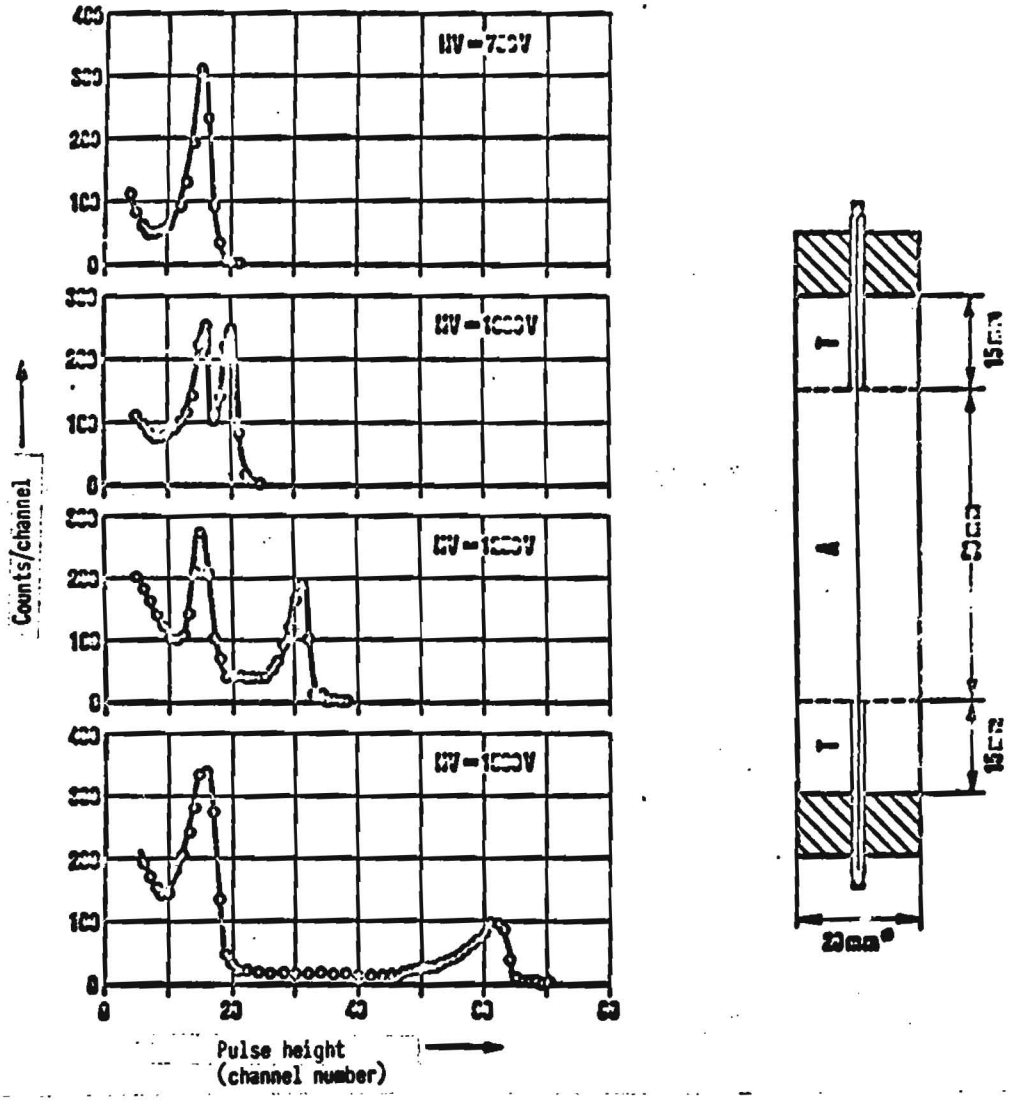

Fig. 3.--Dead volume effect in a cylindrical counter with "hypodermic needles" (2 atm CH_4 + 1%, ^3He filling).

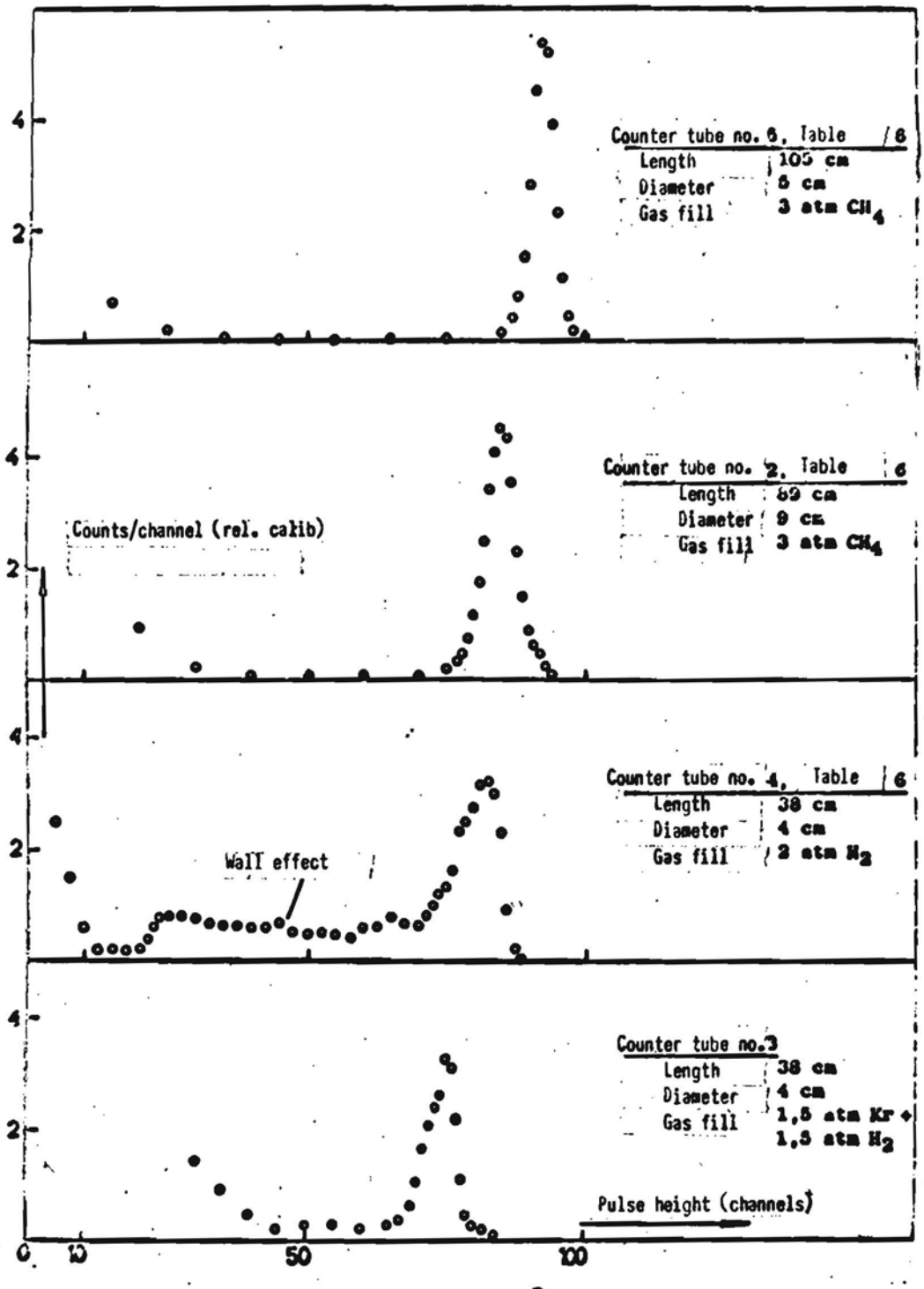

Fig. 4.--Spectra of the 764 keV ^{3}He line in different counters.

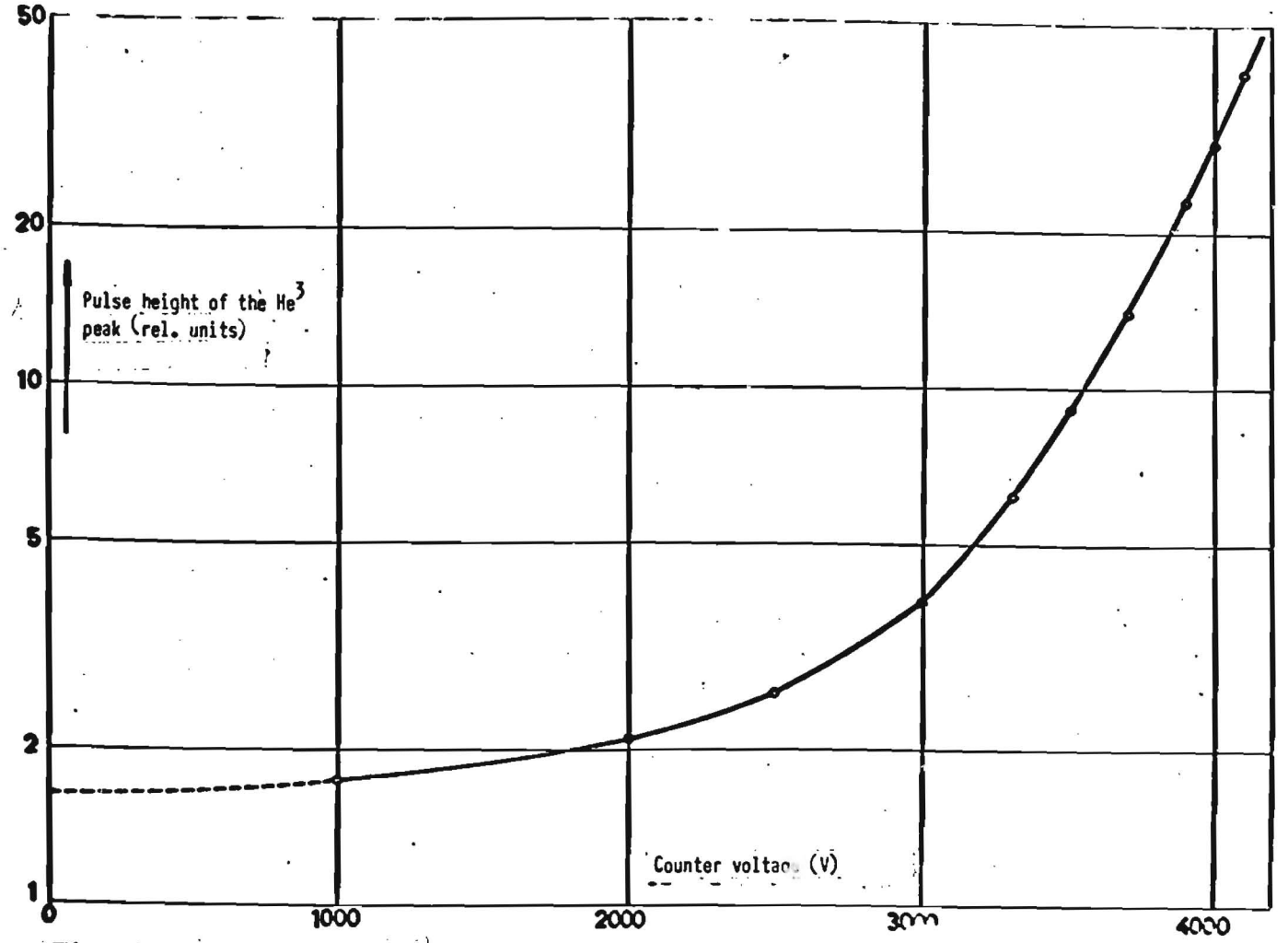

Fig. 5.--Gas amplifiecation as a function of the counter voltage. Counter No. 5 (Table 6); Height 100 cm, diam. 5 cm, gas fill 3 atm CH_4.

3.2.2 Gas amplification and rise times: No exact theory exists for the gas amplification process. For not too large values of the gas amplification factor A, the following is valid [21]:

$$A = A\left(\frac{V}{\ln(b/a)} \cdot pa\right) . \qquad (9)$$

A increases approximately exponentially with the counter voltage V over a broad range and decreases when the gas pressure p or radius A of the wire is increased (b = cathode radius). For reasons of stability of the gas amplification process, A should be as small as possible but not much smaller than 10 so that the energy resolution is not impaired. In the large cylindrical counters, which measure the region above 1 MeV, a gas amplification of 10 is sufficient. To measure the region around 10 keV, gas amplifications of up to about 100 must be used so that the energy resolution will not be impaired by amplifier noise. Fig. 5 shows an example. The pulse height of the He^3 peak was measured as a function of counter voltage. The gas amplification factor is obtained by dividing the ordinate by the pulse heights corresponding to zero voltage which is obtained by extrapolation.

The formation of a voltage pulse on the counter wire can be described as follows: The electrons originating from the primary ionization migrate to the wire under the influence of the electrical field. In the immediate vicinity of the wire (a few wire diameters), the electrons absorb sufficient energy between successive collisions to be able to ionize. As a result of this so-called gas amplification, a secondary ionization proportional to the primary ionization is produced. The electrons from this avalanche migrate very rapidly to the wire, but because of the approximately equal and opposite charge induced by the positive ions, a pulse is produced only when the ions move away from the wire. The pulse first rises very rapidly as long as the ions move in the strong field near the wire, then rises much more slowly and reaches its maximum after the so-called collecting time when the ions are incident on the counter wall. According to Wilkinson [22], the voltage rise with time in a cylindrical counter tube can be described as follows for a point-shaped primary ionization:

$$P(\tau) = \frac{\ln\left(\frac{b^2}{a^2}\tau + 1\right)}{2 \ln \frac{b}{a}} . \tag{10}$$

$P(\tau)$ is the pulse height referred to the asymptotic value, τ is the time measured in units of collecting time, and a and b are the wire and counter radius, respectively.

The collecting time amounts to 1-10 msec and is given by:

$$t_c = \frac{(b^2-a^2) \ln \frac{b}{a}}{2 V K} . \tag{11}$$

V is the anode voltage and $K = K_o \frac{P_0}{p}$ is the positive ion mobility at pressure p (K_o = mobility at 1 atm).

However, the ionization tracks produced by the fast protons are by no means point-shaped; rather, their length is comparable to the counter dimensions. In this case, the voltage pulse generated is described by a superposition of expressions (10) and can be given numerically with some insignificant simplifications [23]. If r_i and r_a are the shortest and longest distance of the track from the wire, the time difference between arrival of the first and last electrons at the wire is given by:

$$\Delta T = \int_{r_i}^{r_a} \frac{dr}{v\left(\frac{E}{p}\right)} ; \qquad \Delta T_{max} = \int_{a}^{b} \frac{dr}{v\left(\frac{E}{p}\right)} , \tag{12}$$

where $v(E/p)$ is the electron drift velocity which depends on the ratio of field strengths and pressure. The finite electron drift velocity results in a dependence of the pulse rise time on the position and radial extension of the primary ionization. In order to permit an analysis of the pulses falling into the range of mV and having a duration of up to 10 msec, they must be amplified to a few Volts and shortened to a few µsec, so that overlapping effects are prevented and storage in customary pulse height analyzers becomes possible.

The voltage rise described by (10) is very rapid at first and accordingly, the times T(25%) until 25% of the asymptotic amplitude are attained are short compared to ΔT_{max} (12), as can be seen from the values compiled in Table 5 for the counters utilized here.

From (10) and (11), it follows that:

$$T(25\%) = \left(\frac{b}{a}\right)^{\frac{1}{2}} a^2 \frac{\ln \frac{b}{a}}{2VK} . \tag{13}$$

For ΔT_{max}, (12) results in:

$$\Delta T_{max} \approx \frac{1}{2} \frac{p \ln \frac{b}{a}}{mV} b^2 , \tag{14}$$

if $v(E/p) = m.E/p$ is introduced with a constant mobility m, which can be assumed to be correct for small values of E/p (and these small values essentially determine ΔT_{max}). For the calculation of the values in Table 5, the following data were used [22, 24, 25]: K_o(cm/sec/V/cm) = 10(H_2), 1.7(Kr), 10(CH_4) and m(cm/μsec/V/cm.cm.Hg) = 0.18(H_2), 1.0(Kr), 1.65(CH_4). The relation [25]

$$\frac{1}{m} = \frac{p_1}{p} \frac{1}{m_1} + \frac{p_2}{p} \frac{1}{m_2} \tag{15}$$

was used to calculate the ion and electron mobility in mixtures (p = total pressure, p_1, p_2 = partial pressures, m_1, m_2 = mobilities of the components of the mixture), even though the values thus obtained for the electron mobility can be considered only a rough approximation.

In the following, it is therefore assumed that the counter pulses have rise times of between 0 and ΔT_{max}. For times longer than ΔT_{max}, the pulses rise only slowly and in addition, this rise is the same for all pulses and can therefore be neglected in the following.

Table 5.--Rise times of the counter pulses.

Counter	Form	Radius (cm)		Fill (atm)	V (Volt)	T(25%) (μsec)	ΔT_{max} (μsec)	τ (μsec)
		Housing b	Wire a					
1	Cyl.	5	$2,5 \cdot 10^{-3}$	$2Xr+2CH_4$	3600	0,4	6	8
2	Cyl.	5	$2,5 \cdot 10^{-3}$	$3CH_4$	3800	0,1	3,5	4
3	Cyl.	2,1	$2,5 \cdot 10^{-3}$	1,5 Kr + 1,5 H_2	2000	0,3	5	8
4	Cyl.	2,1	$2,5 \cdot 10^{-3}$	2 H_2	2500	0,05	4,5	4

If pulses of identical amplitude but different rise times ($0-\Delta T_{max}$) are amplified in a system whose differentiation time constant is equal to ΔT_{max} and whose upper frequency limit is infinite, the initial amplitudes [22] vary between 1 and e^{-1}, i.e. by about 60%.

This is shown schematically in Fig. 6. This amplitude dispersion can be improved by reducing the upper limit frequency. With a view toward minimum amplitude dispersion as well as toward an optimum signal-noise ratio [26], it is most favorable to select the integration time constant τ_I to be equal to the differentiation time constant τ_D. For $\tau_I = \tau_D = \Delta T_{max}$, the relative amplitude dispersion [22] amounts only to 4% and for $\tau_I = \tau_D = 2\Delta T_{max}$, only to 1%. These theoretical values were verified with the amplifier-analyzer system utilized here. The rise time ΔT of pulse generator signals was varied and the amplitude was amplified in the amplifier system ($\tau = \tau_I = \tau_D = 4$ usec) and recorded in the analyzer. The results in Fig. 7 show that the amplitude has dropped to 88% already for $\Delta T/\tau = 0.5$. However, these results are not representative for those obtained with counters, because the rapid decay of the generator signal (50 usec) already causes the generator output amplitude to be reduced with an increase of the rise time. In counters this effect plays no role because of the much greater RC-time constant of at least 10 msec (working resistance R of a few MΩ, counter capacity >10 pF). If this generator effect is compensated, a reduction of about 6% is obtained for $\Delta T/\tau = 1$ as shown in Fig. 7, which is in agreement with the theoretical values in order of magnitude [22].

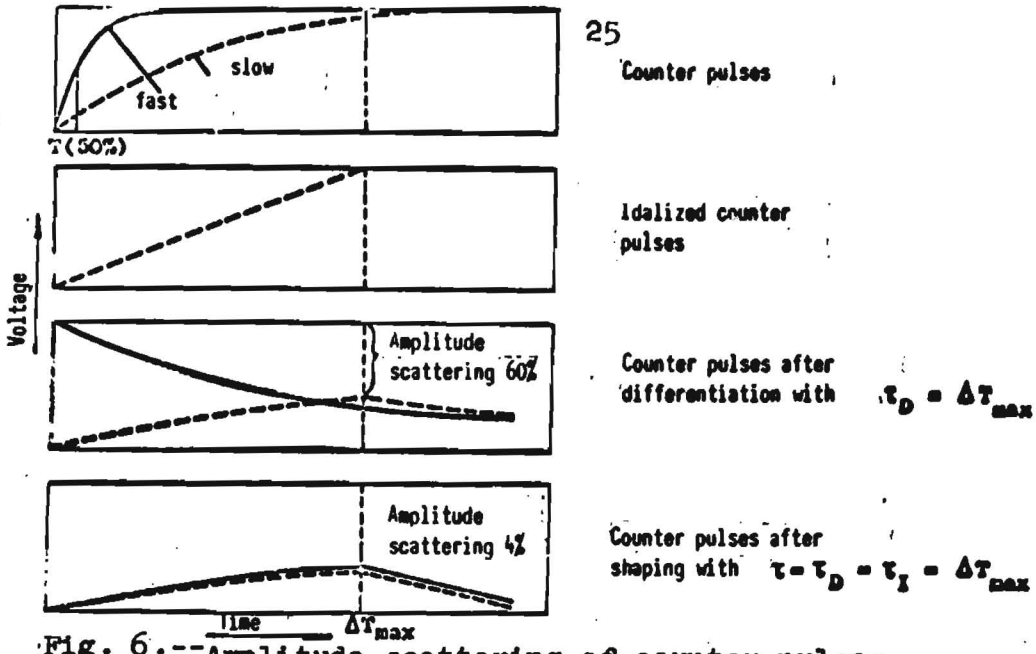

Fig. 6.--Amplitude scattering of counter pulses.

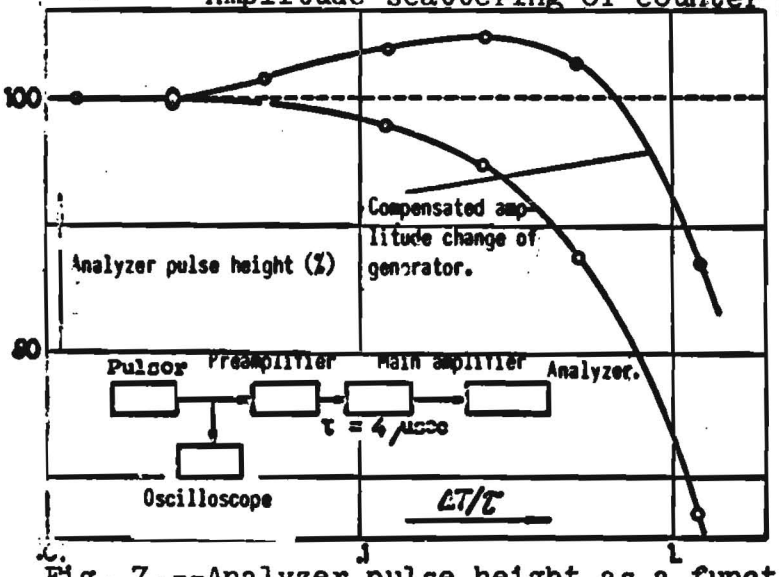

Fig. 7.--Analyzer pulse height as a function of the rise time ΔT generator signals (preamplifier time constant $\tau = 4\mu sec$.)

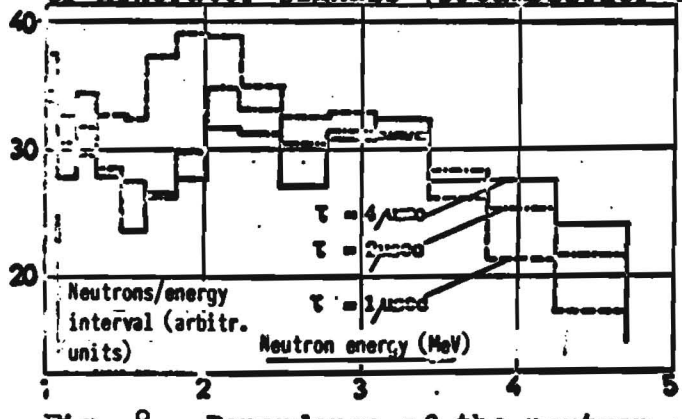

Fig. 8.--Dependence of the neutron spectra on the preamplifier time constant τ (Am-Be (TC) source, counter No. 2, Table 6).

The results obtained here were verified by measurements with counters. Fig. 8 shows the spectra of an Am-Be-source in the energy region below 5 MeV measured with counter No. 2 (Table 5, ΔT_{max} = 3.5 usec) with amplifier time constants τ = 1, 2 and 4 usec. It can be seen that the spectra measured with τ = 2 and 4 usec already agree practically within the statistical errors of about 5%. The amplifier time constants were therefore selected with $\tau > \Delta T_{max}$ (Table 5) in such a way that significant deformations of the measured proton spectrum due to rise time effects can be ruled out.

3.2.3 Energy calibration and relation between proton energy and ionization: The dependence of the ionization produced in the counter on the proton energy must be exactly known since calculation of the neutron spectrum requires a conversion of the measured ionization spectrum N(I) to the proton recoil spectrum P(E):

$$P(E) = \frac{N(I)}{W(I)}, \tag{16}$$

where

$$W(I) = \frac{dE(I)}{dI} \tag{17}$$

is the proton energy necessary for production of an ion pair. For higher energies, W is very constant and ionization then depends linearly on the proton energy, and in many cases, direct proportionality can be assumed.

Hydrogen: Precise measurements of the relation between ionization and proton energy are available only above 10 keV [27], while very little is known below 10 keV. Accordingly, the relation is linear above 10 keV, but extrapolation leads to an intersection with the energy axis at an energy E_o between zero and 2 keV. According to Bennett [20], E_o amounts to about 0.4 keV. Since the value of E_o undoubtedly depends on impurities and additions of quenching agent, and since measurements to below 10 keV are necessary for the Sb-Be(γ,n)-source and for fast reactors, the energy region below 10 keV was investigated more fully with the counters utilized here. The details of these measurements have been described fully in [28], and only the principle and results will be briefly described here. We measured the maximum ionization produced by monoenergetic neutrons of known energy in the counters. The slowing-down-time spectrometer

[29] shown in Fig. 9 was used to produce monoenergetic neutrons. Brief 14 MeV neutron pulses were moderated in lead. After a very short time, the neutrons have lost so much energy that only elastic collisions can take place. In this range, the following applies [29]:

$$\bar{E}_n = \frac{c}{(T+t_0)^2} , \qquad (18)$$

i.e. the mean neutron energy $\bar{E}_n$ can be calculated from the measured slowing-down time T. Below 30 keV, the neutron energy distribution with a fixed T has nearly a Gaussian shape. The energy resolution depends highly on the time resolution of the counters and is shown in Fig. 10.

Since lead has a very small neutron capture cross section and excellent shielding properties for γ-radiations, the γ-background in the counter is so small that it does not significantly falsify the measured proton spectra. The electronic instrumentation is shown in Fig. 11. The counter signals are transmitted through the preamplifier and two main amplifiers. The output amplitudes of the Hamner N 302-amplifier are proportional to the ionization and are recorded in 128 channels of the 128 x 16 storage. The fast output signal of the HVL-L 120 amplifier supplies the time mark for the determination of the slowing-down time T. In this manner, the ionization spectrum produced by scattering processes between T and T + ΔT is stored in each of the 16 time groups. Fig. 12 shows one of the measured two-dimensional spectra. Short slowing-down times correspond to high neutron energies and the spectra accordingly extend to high ionization values. With increasing slowing-down time, the drop of the spectra shifts to smaller ionization values. Because of the mediocre energy resolution of the slowing-down time spectrometer, the drop in the spectra is not sharp, but in some of them, it can be recognized that a region in which the distribution decreases relatively little is followed by one with a steeper drop. In the "contour display" the maximum ionization decrease with increasing slowing-down time can be easily recognized.

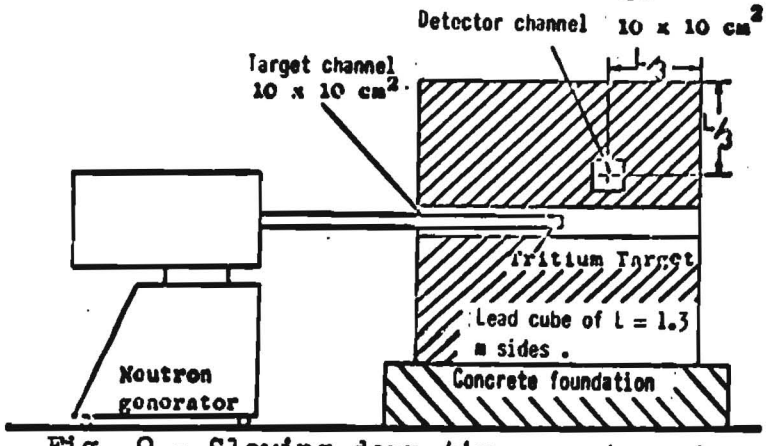

Fig. 9.--Slowing-down time spectrometer with detector system.

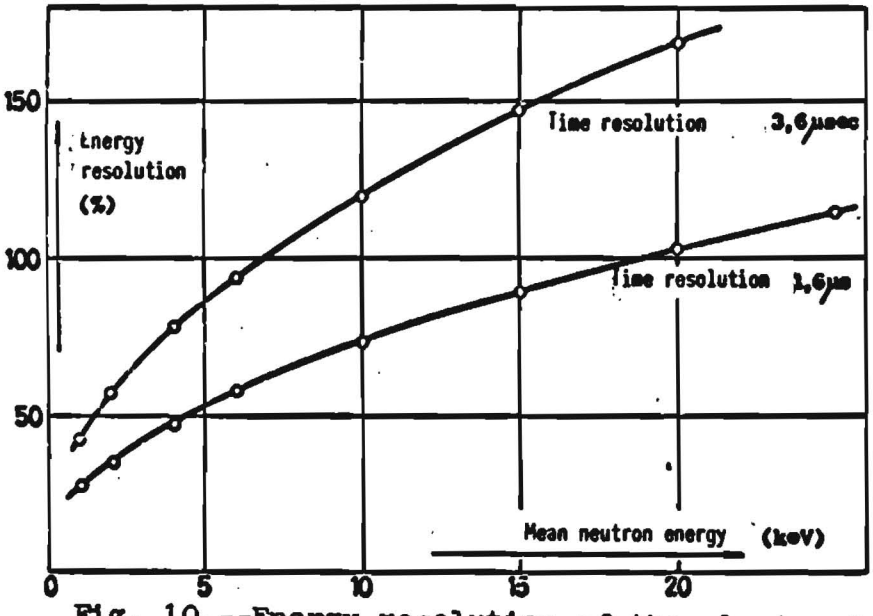

Fig. 10.--Energy resolution of the slowing-down time spectrometer.

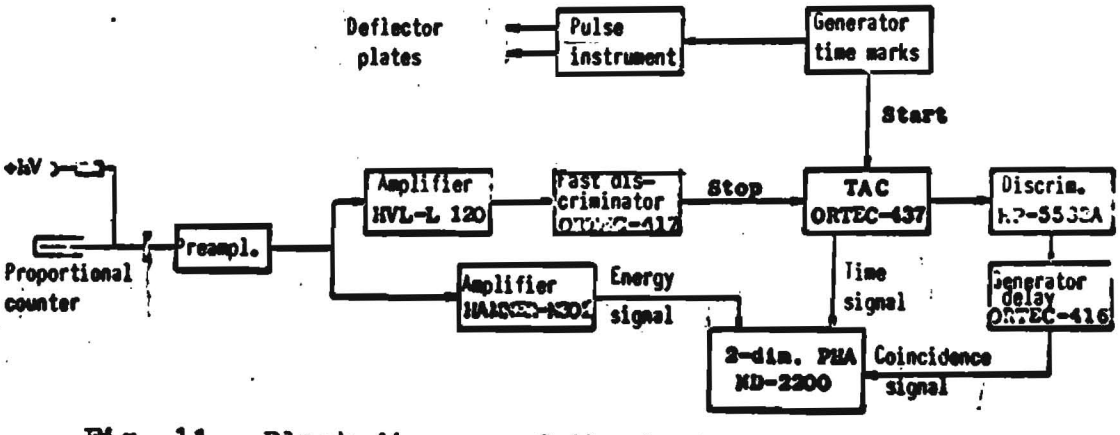

Fig. 11.--Block diagram of the instrumentation.

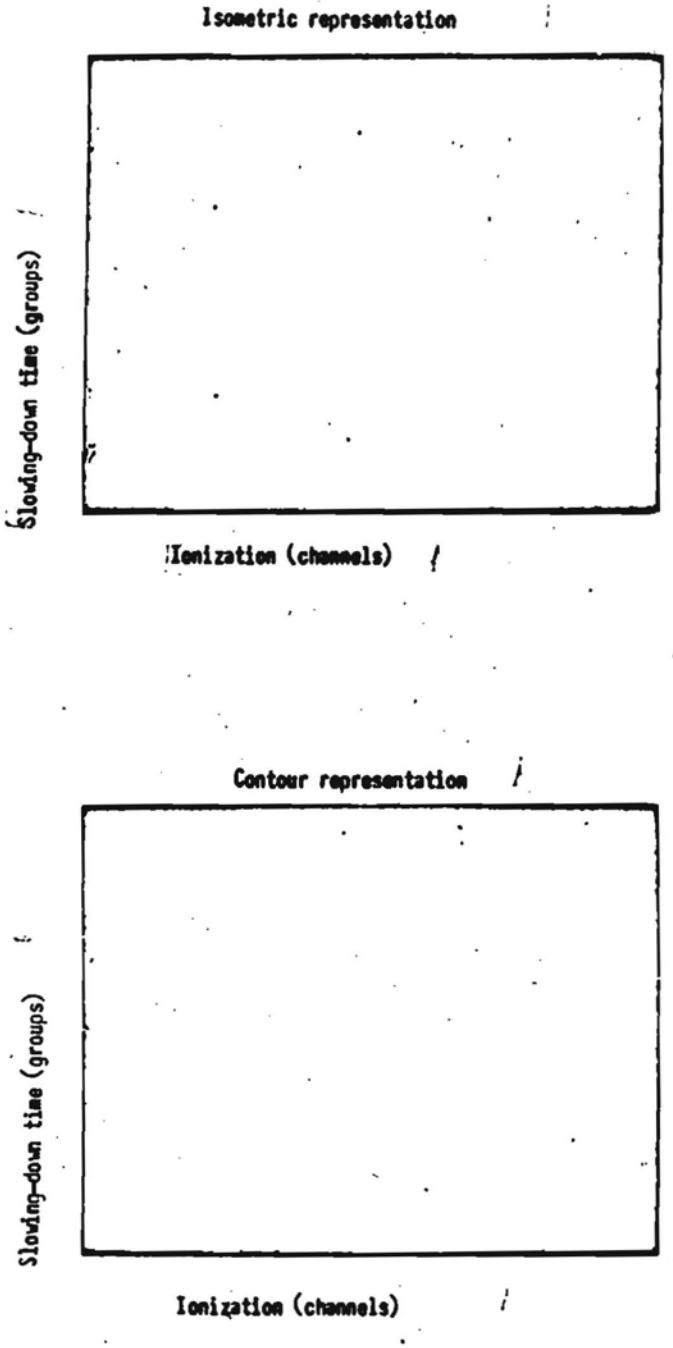

Fig. 12.--Two dimensional representation of the ionization spectra as a function of the slowing-down time.

The steep drop in the ionization spectra corresponds to the mean maximum ionization and thus to the mean neutron energy. The measured ionization spectra N(I) were analyzed by iteration in two steps in such a way that the position of the maximum in the neutron spectra was determined by means of the well-known relation:

$$\varphi(E) \sim \frac{dN(I)}{dI} \frac{E}{\sigma(E)} \tag{8}$$

Iterative analysis is necessary because a preliminary energy-ionization relation must be determined first for the final evaluation. Fig. 13 shows three ionization spectra and the analyzed neutron spectra. The ionization values corresponding to the maxima in the final neutron spectrum was used to establish the energy-ionization relation shown in Fig. 14.

The measurements were performed with a cylindrical counter (100 cm active length, 2.3 cm diameter, 0.5 atm hydrogen fill without quenching addition) and with a spherical counter (3.94 cm diameter, 2 atm hydrogen fill). No systematic differences could be observed in the results from the two counters. The linear relation

$$E = I + 0{,}41 \tag{19}$$

correctly represents the measuring results within the limits of error. A better fit is given by

$$E = I - 0{,}15 + \exp(-I/1{,}76) \; . \tag{20}$$

This relation also correctly reproduces the curvature occurring below 5 keV (E and I in keV).

For very low energies (< 1 keV), W = dE/dI should rise sharply [20]. However, the measurements show (Fig. 15) that below 5 keV, W first decreases with decreasing energy to about 70% of the asymptotic value at 1 keV. This means that the probability for ionizing processes is greater in the range of 1-5 keV than in the range of higher proton energies. It can be estimated that the remaining uncertainties in the energy-ionization relation no longer significantly impair the accuracy of spectral measurements above 5 keV. The results obtained here are in good agreement with those of Bennett [20] but the deviations from proportionality are somewhat more pronounced here.

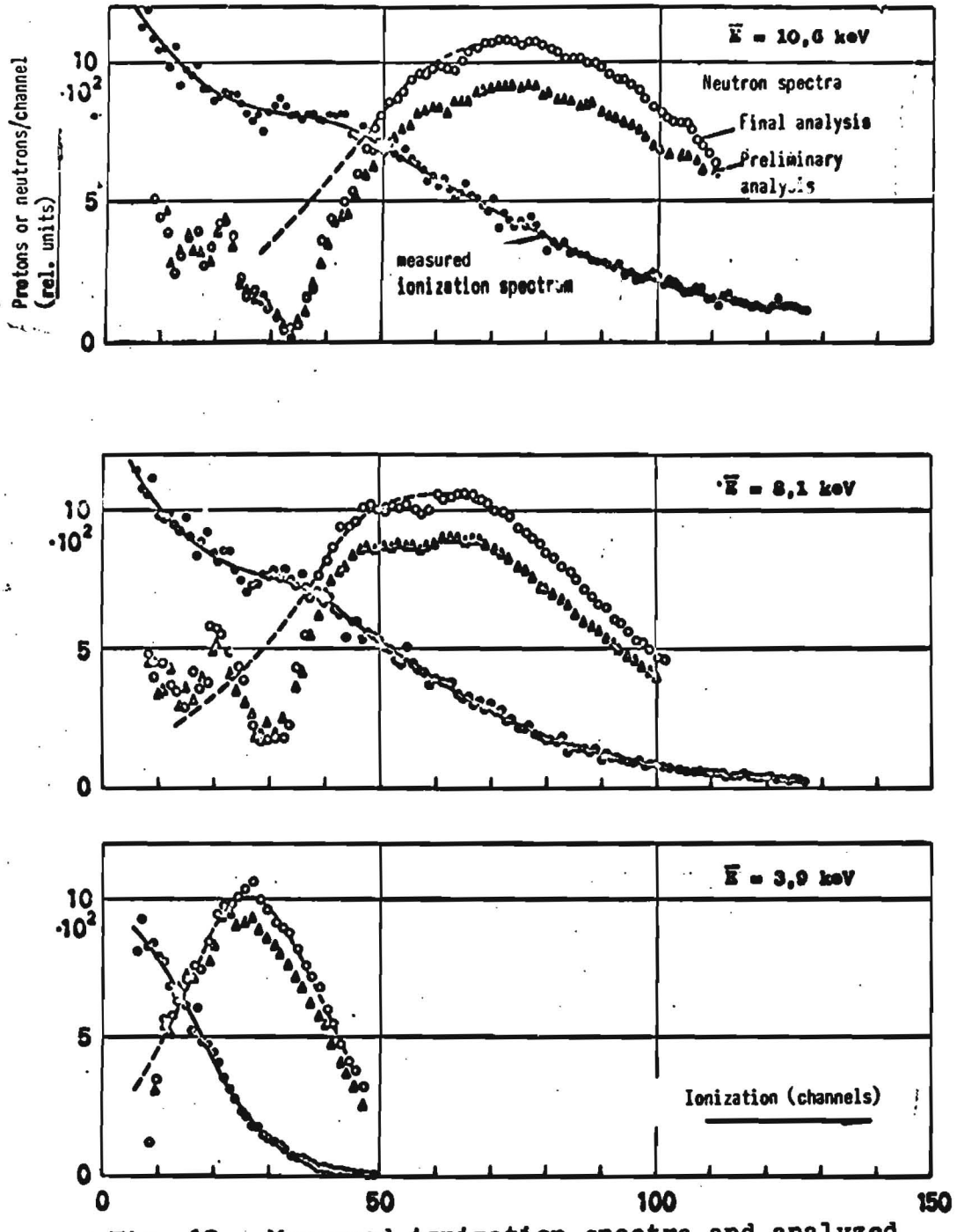

Fig. 13.--Measured ionization spectra and analyzed neutron spectra.

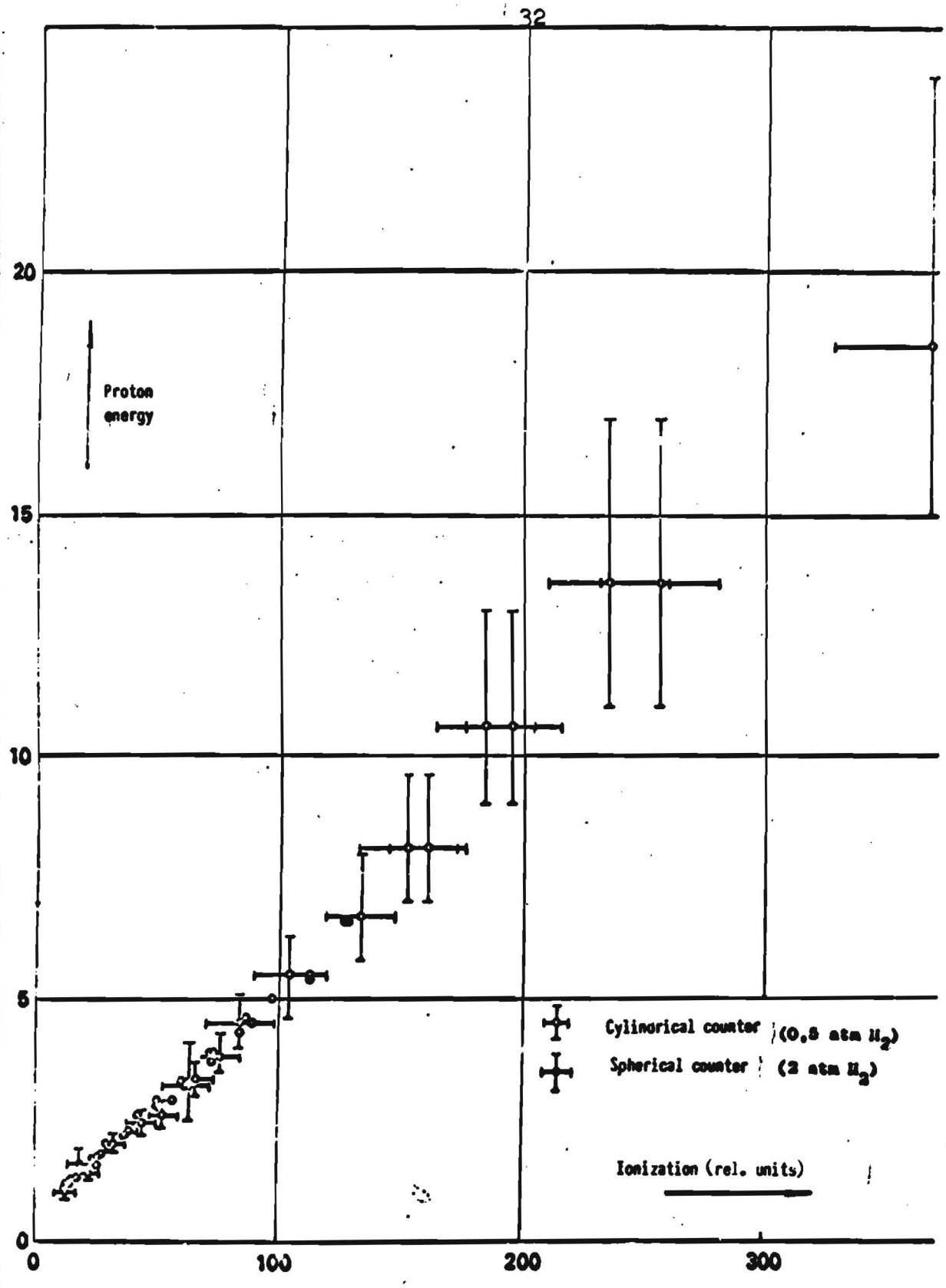

Fig. 14.--Dependence of ionization on the proton energy.

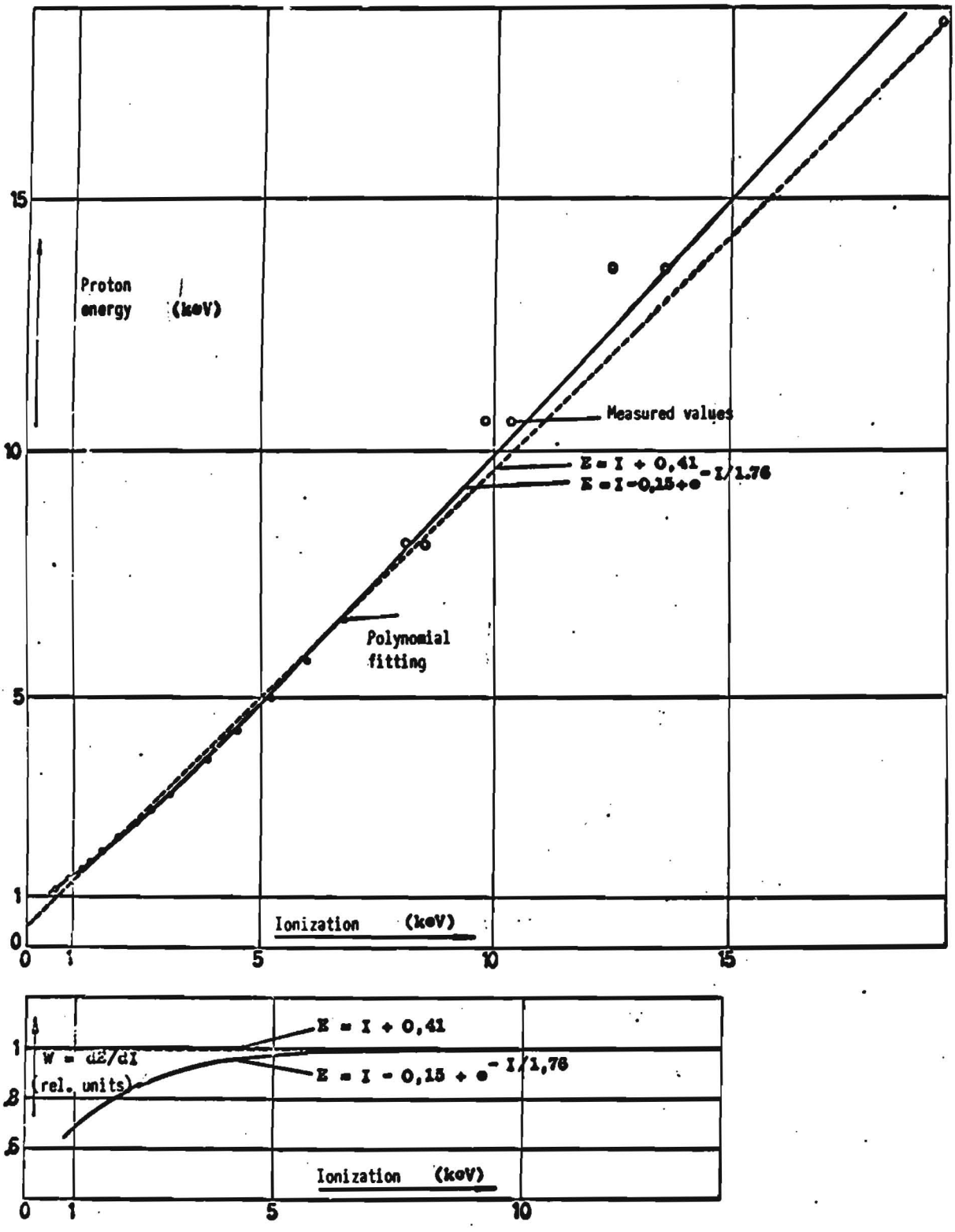

Fig. 15.--Different forms of fitting to the measured ionization-energy dependence.

Above approximately 10 keV, we can assume proportionality between proton energy and ionization in hydrogen [27]. This was verified with monoenergetic neutrons in the range of 30 keV to 1 MeV for the counters utilized here. The neutrons were produced by the $Li^7(p,n)Bo^7$-reaction with a 3 MeV Van de Graaff accelerator. These measurements at the same time served to verify the calculated wall effects, the energy calibration lines and energy resolution. The 764 keV protons from the $He^3(n,p)T$-reaction produced by thermal neutrons served as calibration lines for the cylindrical counters and the 5 MeV-a-particles of a very weak Pu^{239}-specimen mounted in the center of the counting wire serve for the spherical counters. As a result of the spherical symmetry, a sharp line is obtained even when the α-particles are not completely slowed down in the counter. The results of these measurements are shown in Fig. 16 and 17 for two spherical counters. The neutron energies were determined by time-of-flight measurements.

Methane: Allen and Ferguson [27] found a linear relationship between proton energy E and ionization I in methane above 250 keV. Extrapolation of the values to above 250 keV furnished an intersection with the energy axis between 20 and 40 keV. We verified these measurements with a number of different counters and methane pressures of 1 and 3 atm. The pulse height distributions of recoil protons produced by monoenergetic neutrons and the monoenergetic proton distribution from the $He^3(n,p)T$-reaction were measured. Monoenergetic neutrons with energies of 3.035 and 2.55 MeV were produced by the $D(D,n)He^3$-reaction (angle between deuteron and neutron beam 0 and 100°) and below 1 MeV, monoenergetic neutrons from the $Li^7(p,n)Be^7$-reaction were used. The results shown in Fig. 18 confirm the measurements of Allen and Ferguson [27]. Consequently, we assumed that $E = I + 30$ (E and I in keV) for methane as the filling gas. The estimated uncertainty of ±10 keV in the position of the extrapolated intersection leads to errors of a maximum of 2% above 600 keV in the measured neutron spectrum and methane fills were used only in this energy region.

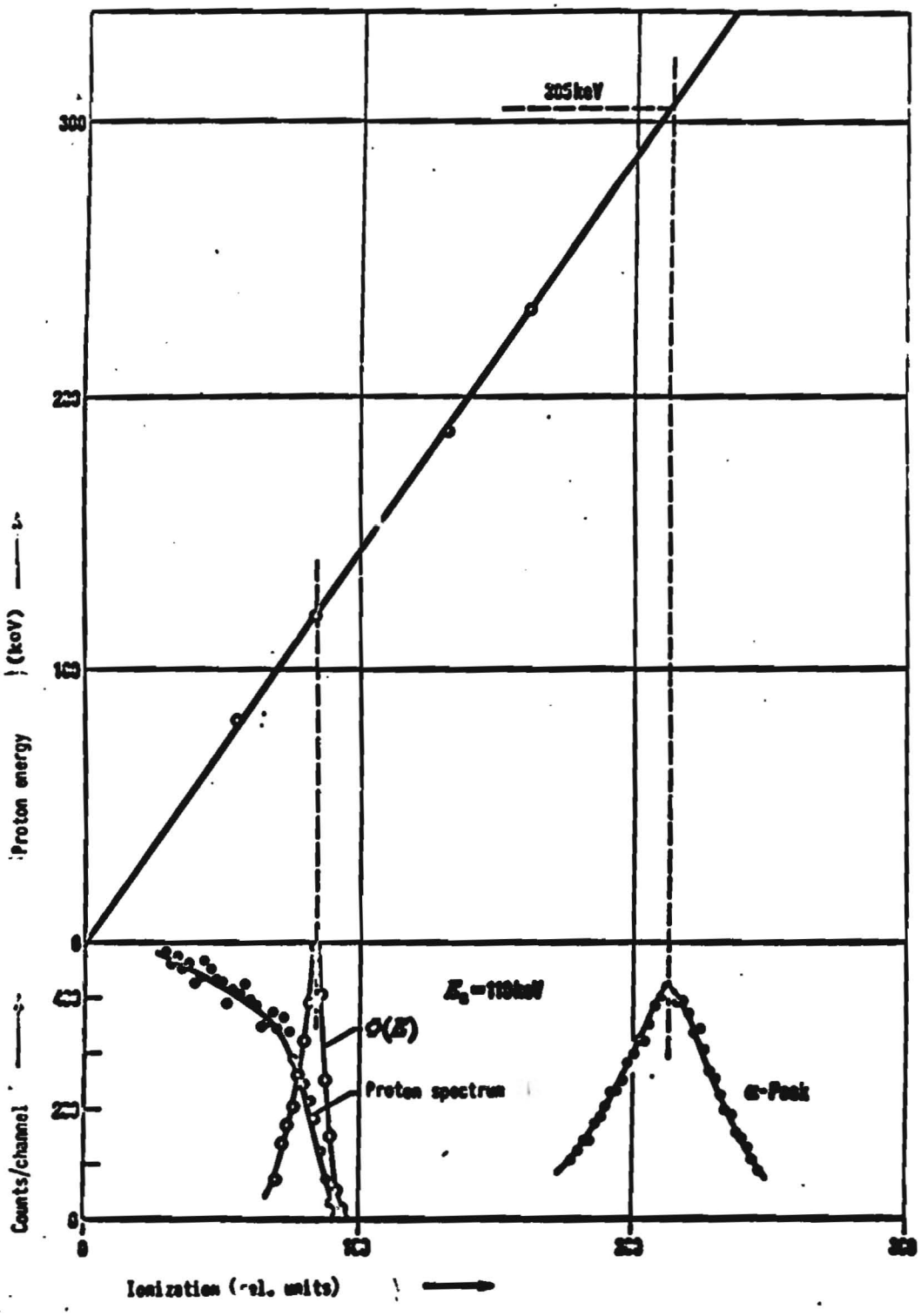

Fig. 16.--Dependence of ionization of the proton energy and energy calibration of a 1 atm H_2 spherical counter (3.94 cm diameter).

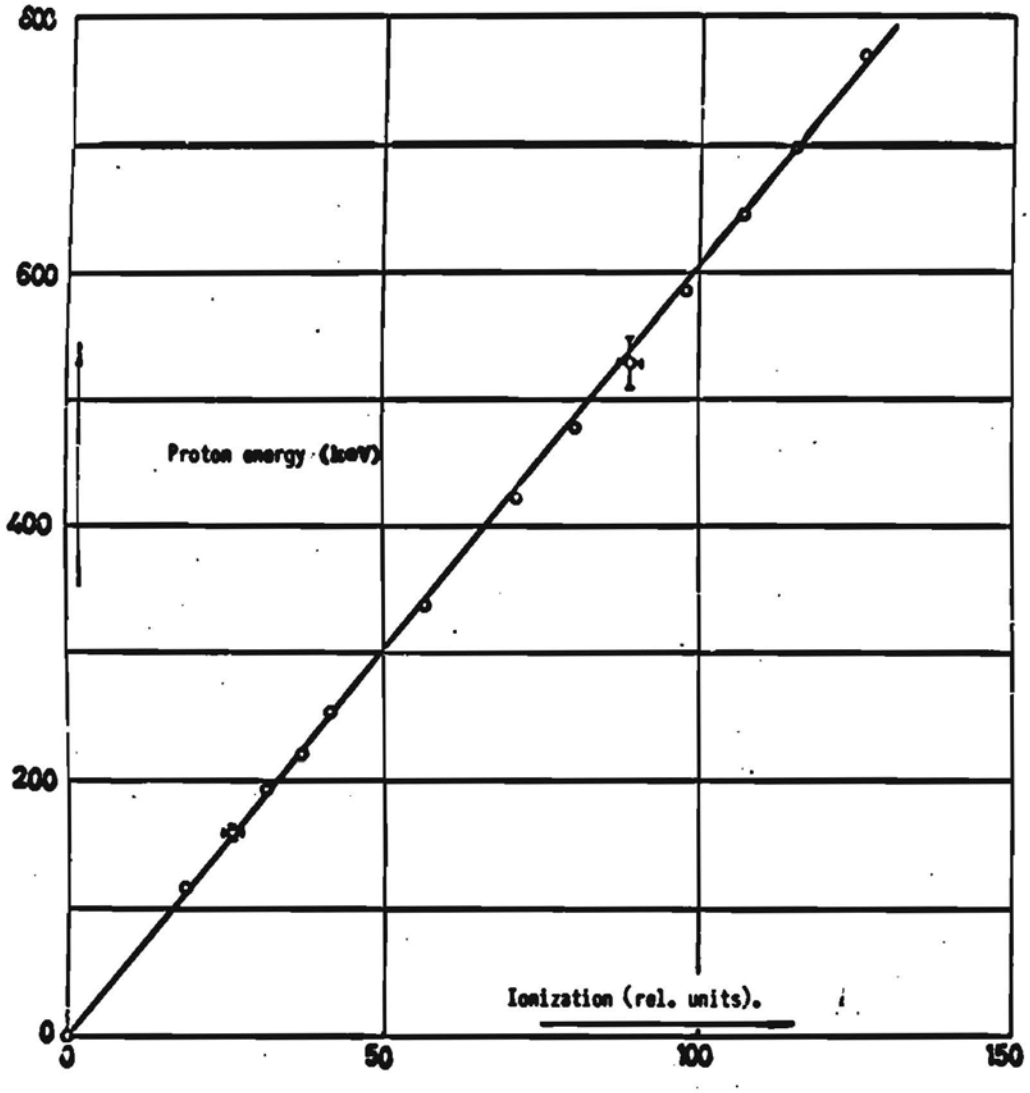

Fig. 17.--Dependence of ionization on the proton energy for a 4 atm H_2-spherical counter (3.94 cm diameter).

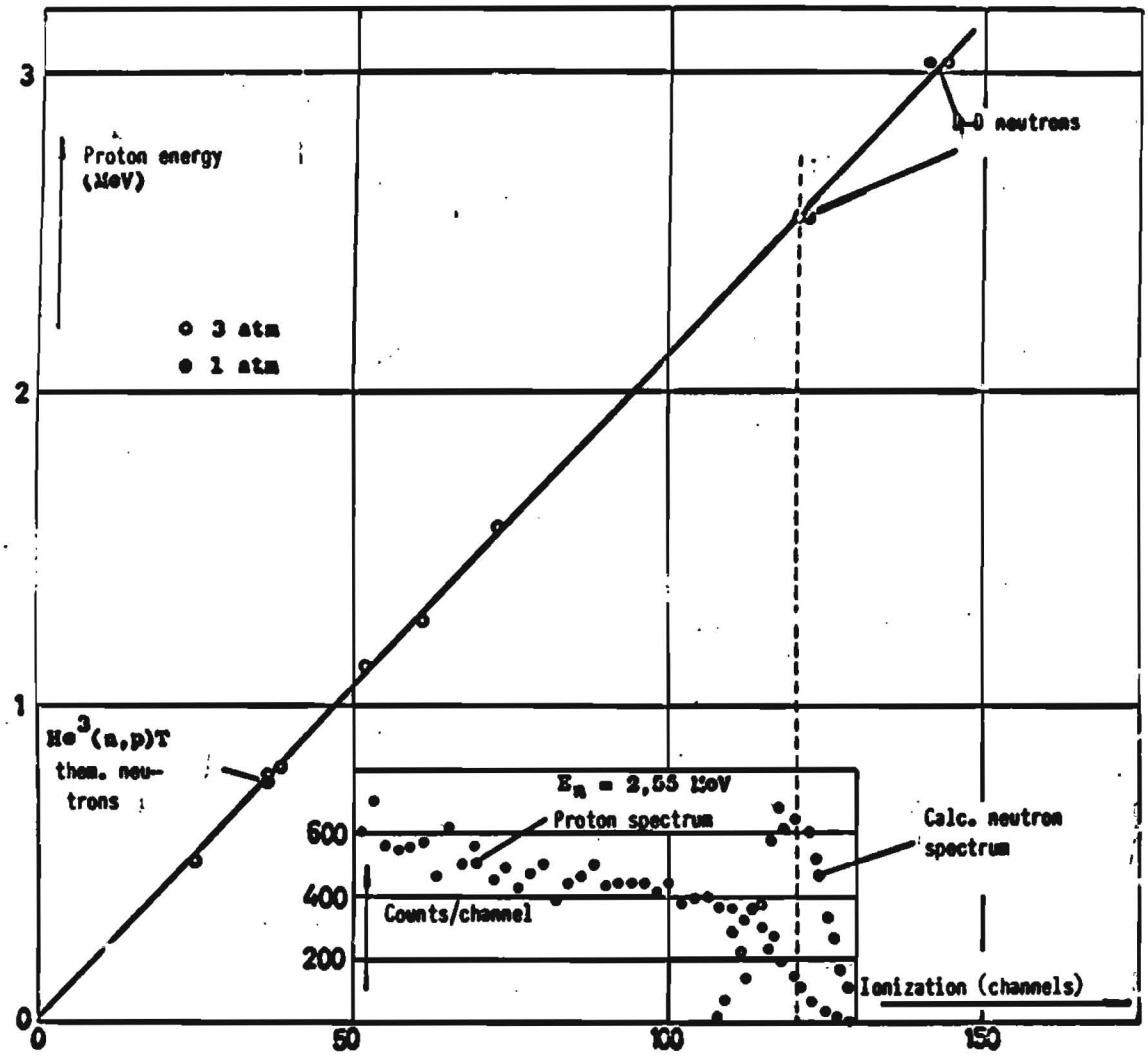

Fig. 18.--Energy calibration and dependence of ionization on the proton energy for methane counters.

Krypton-hydrogen and krypton-methane mixtures: Monoenergetic neutrons of 3 and 15 MeV from the $D(D,n)He^3$- as well as the $D(T,n)He^4$-reaction and 764 keV protons from the $He^3(n,p)T$-reaction were used to verify the relation between proton energy and ionization. The results shown in Fig.19 do not contradict the assumption of direct proportionality made in the evaluation of the proton spectra. It can be estimated that the errors in the neutron spectra produced by the deviations from proportionality beyond experimental accuracy are not greater than 3% in the energy regions utilized (> 1 MeV for $Kr-H_2$ and >3 MeV for $Kr-CH_4$).

3.2.4 Electronics with and without γ,n-discrimination: The γ,n-pulse shape discrimination developed by Bennett [20] is based on the fact that the specific ionization (ion pairs per cm of track) is considerably greater for protons than that of γ-induced electrons with the same energy. In the energy regions in which discrimination against the γ-background is necessary, the proton tracks therefore are small compared to the counter diameter, while the electron tracks are entirely within the order of magnitude of the diameter. Consequently, all primary electrons produced by a recoil proton arrive at the counting wire almost simultaneously and the voltage pulse produced rises very rapidly. The arrival of the primary electrons produced by fast electrons, in contrast, extends over a long period of time because of the finite drift velocity and the voltage pulse consequently rises slowly.

The electronic system for pulse shape discrimination is shown in Fig. 20. The detector signals are transmitted over a fast FET-preamplifier (rise time 50 nsec) and are fed in parallel into two main amplifiers. The fast amplifier (rise time 50 nsec, 200 nsec "delay-line" differentiation) furnishes an output signal, the amplitude A of which is proportional to the voltage increase per unit of time of the counter signal. The output amplitude B of the slow linear amplifier, in contrast, is proportional to the primary ionization. An analog pulse height computer [30] calculates the ratio A/B of the two amplitudes. A/B is proportional to the "radial" specific ionization of the produced track and therefore is considerably greater on the average for recoil protons than for γ-induced fast electrons. The ionization pulse B and the pulse A/B corresponding

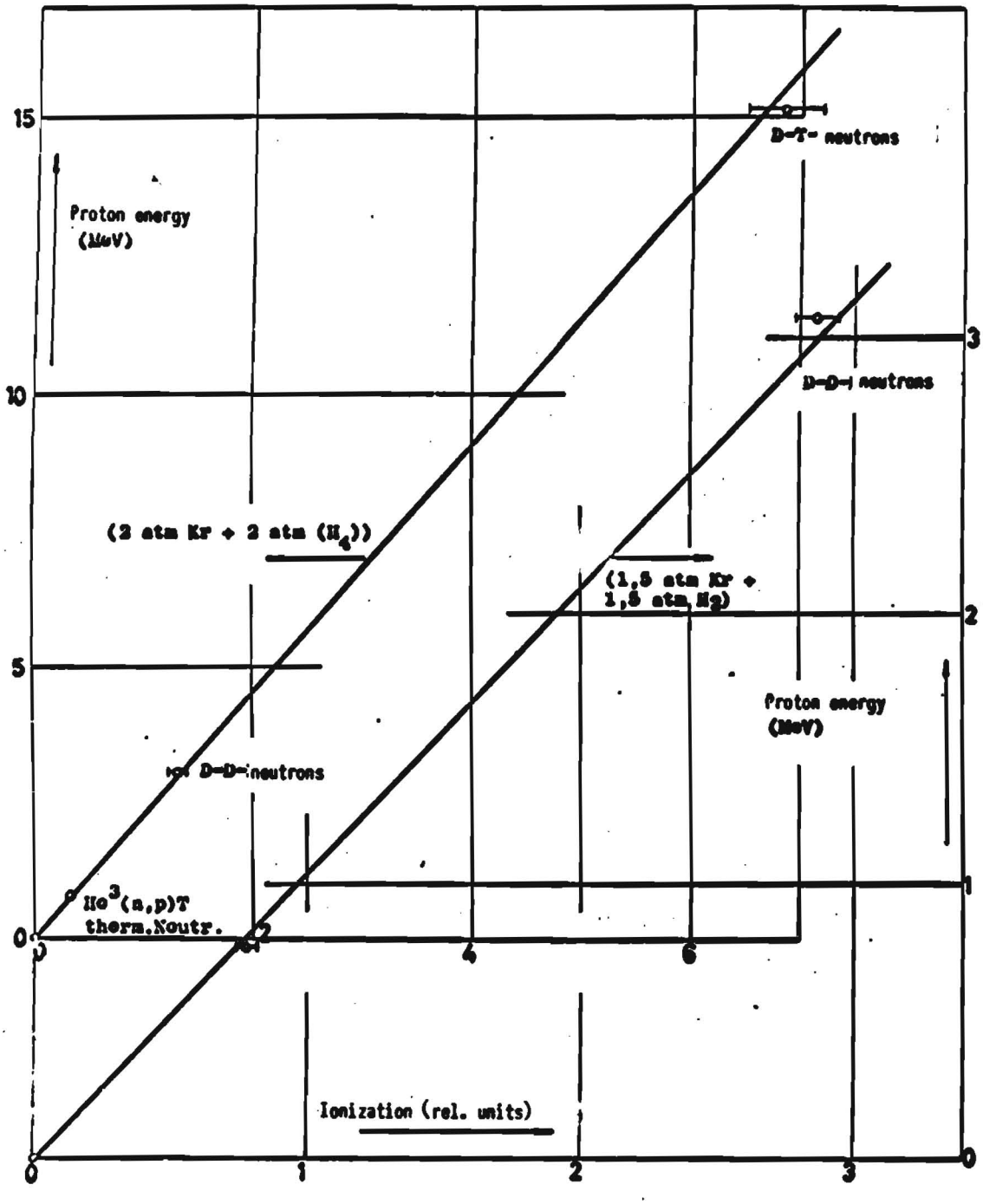

Fig. 19.--Energy calibration and dependence of ionization on the proton energy for a counter filled with (2 atm Kr + 2 atm CH_4) (counter No. 1, Table 6) and counter filled with (1.5 atm Kr + 1.5 atm H_2) (counter No. 3, Table 6).

without γ,n-discrimination

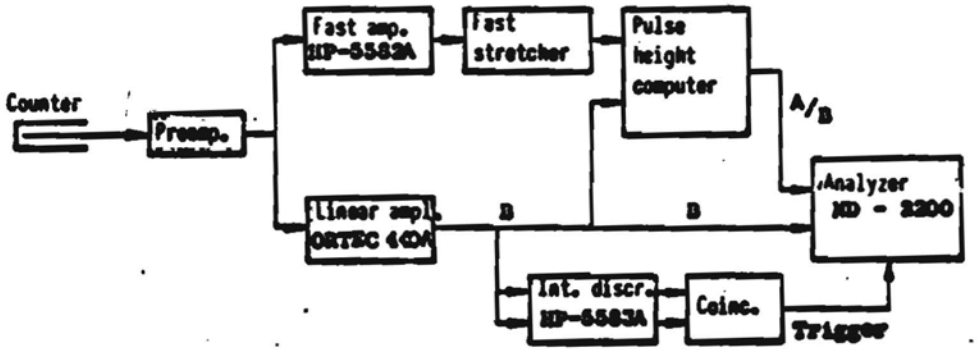

with γ,n-discrimination

Fig. 20.--Block diagram of the instrumentation.

to the specific ionization are recorded in coincidence in a two-parameter pulse height analyzer (128 ionization groups with 32 channels each in which the specific ionization spectrum is recorded). Fig. 21 shows such a two-dimensional spectrum. The events of identical total ionization stored in one energy group are resolved into two groups: the broad peak at small specific ionization values corresponds to the γ-counts, while the narrow peak at high specific ionization values originates from recoil protons.

Recoil protons and γ-induced electrons are not completely resolved, particularly at low energies as indicated by Fig. 21. To correct the contribution of γ-induced counts in the proton peak, the spectrum of a pure γ-source is recorded immediately before or after measurement in the mixed neutron-γ-field. Subsequently, in the range of low specific ionization, where no proton pulses are recorded any longer, the γ-spectrum is then fitted in groups to the mixed spectrum and subtracted from the latter. At higher proton energies, the proton peak in the specific ionization spectrum is no longer symmetrical but extends far into the range of lower specific ionization. Since an intense γ-field is usually connected with a neutron field, it is difficult to establish the exact shape of the proton peak which is of great importance for a correct γ-background correction. In the Pb-pile of the slowing-down-time spectrometer mentioned in 3.2.3, however, this is possible because of the very low γ-background, as shown in Fig. 22. The measurements were performed with the Am-Be(5C)-source which was at a distance of about 50 cm from the detector. Below about 40 keV, where the γ-background normally rises sharply (see Fig. 21), the proton peaks are symmetrical and make no contribution in the fitting range at low specific ionization. The small peaks at low specific ionization below 5 keV are γ-background.

In the Pb-pile above 5 keV, the γ-background is smaller than 1% as indicated by Fig. 22, and therefore the neutron spectra measured with and without γ,n-discrimination should be identical. As shown by Fig. 23, this is the case within the statistical errors. Therefore, it can be assumed that the relatively complicated γ,n-discrimination system is operating correctly.

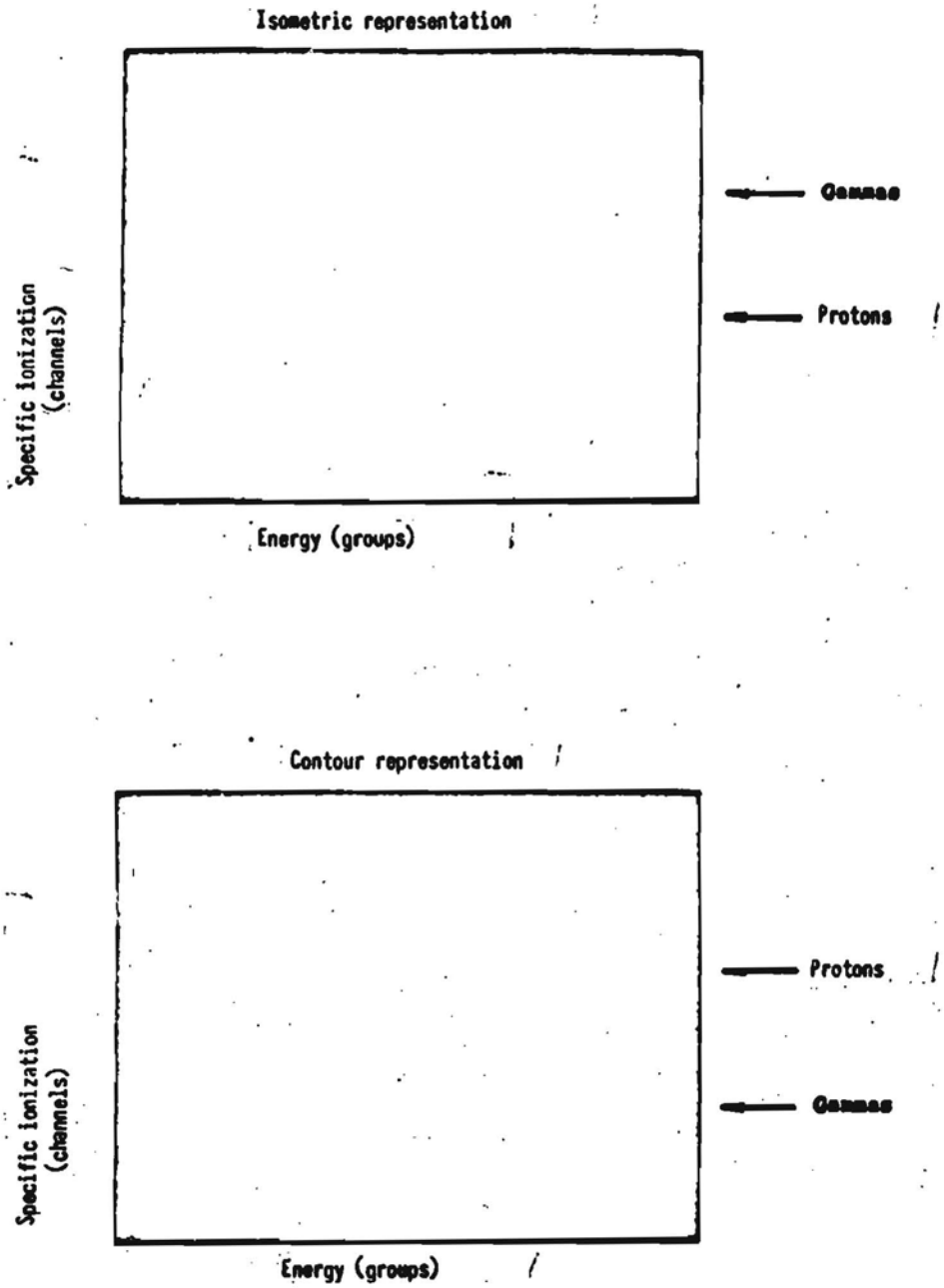

Fig. 21.--Two-dimensional recoil-proton spectrum measured with the γ,n-pulse shape-discrimination method.

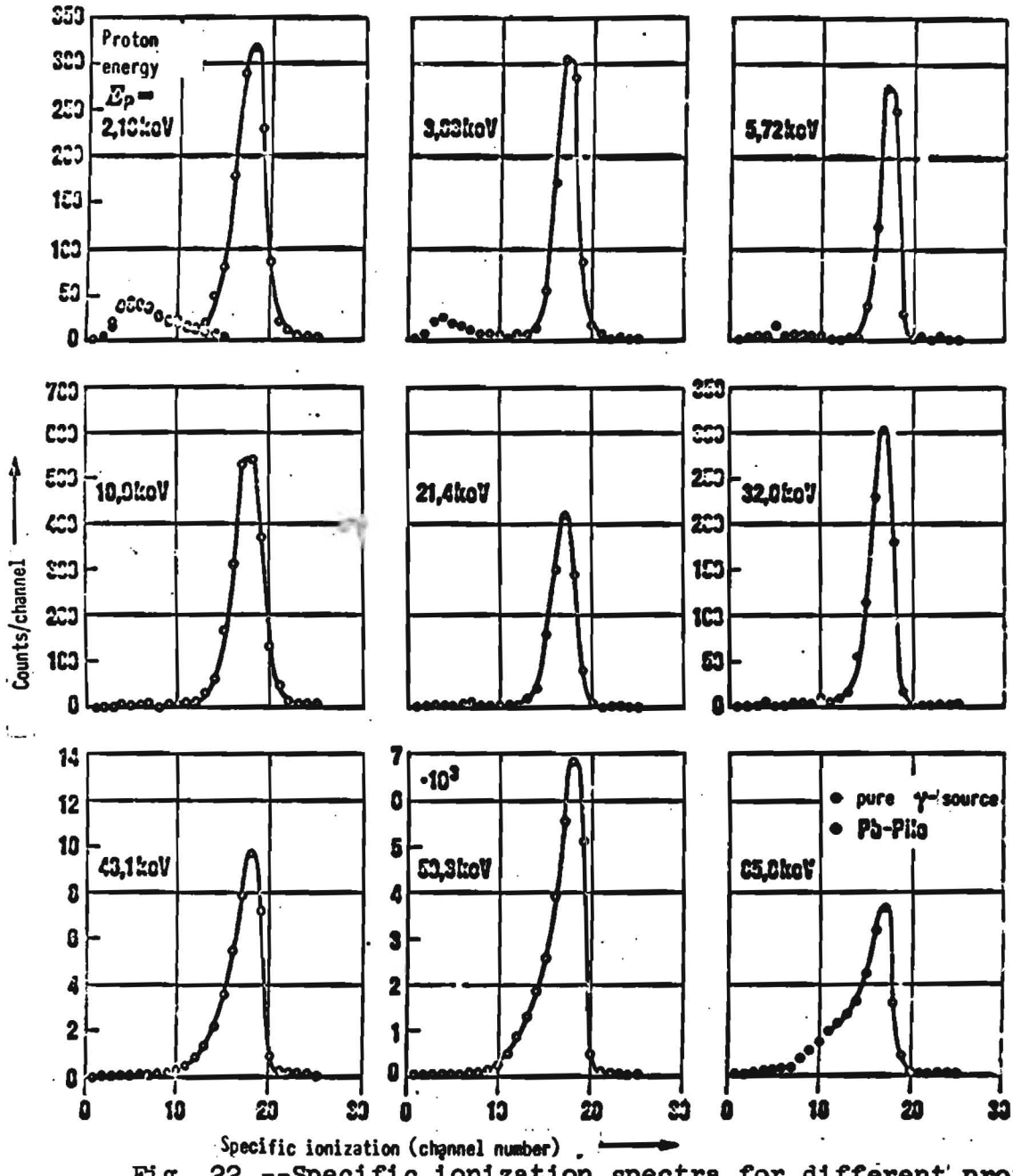

Fig. 22.--Specific ionization spectra for different proton energies Ep for the 2 atm H_2 spherical counter in the

- Pb-pile,
- pure γ-source.

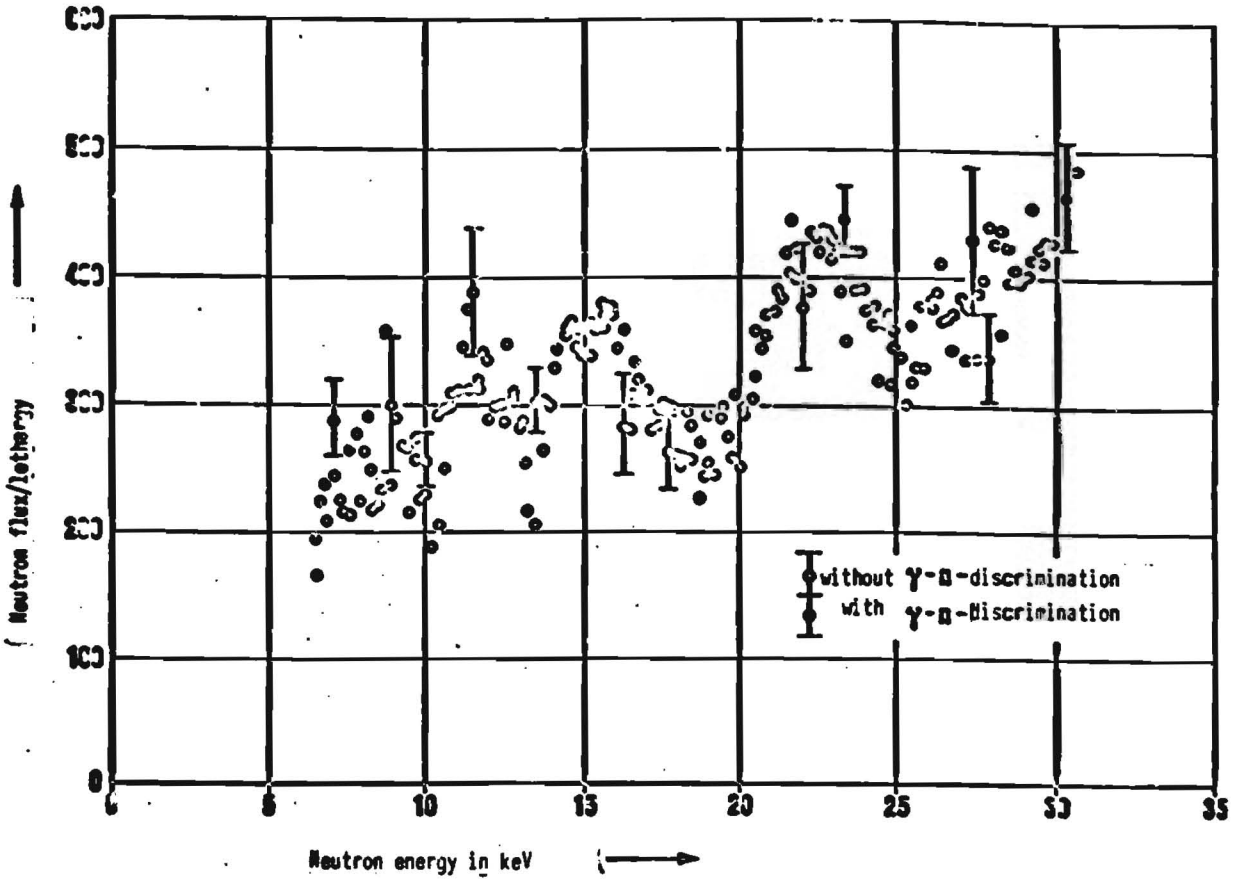

Fig. 23.--Neutron spectrum in the Pb pile.

The measuring system without pulse shape discrimination (Fig. 20) is very simple and is identical with the energy channel in the two-dimensional electronic system. It is important that the integration and differentiation times of the entire system be sufficiently long so that the different rise times of the counter pulses discussed in 3.2.2 do not falsify the proton spectrum. The important time constants, i.e. the largest integration and smallest differentiation time constants, are determined by the main amplifier. Two types of main amplifiers were used: an ORTEC 440 A active filter amplifier with a selectable time constant τ between 0.1 and 4 µsec, and a conventional RC-amplifier (HVL-120 modified) with time constants between 0.1 and 10 µsec. When the rise times of the counters permitted (see Table 5), the ORTEC 440 A amplifier was used, because as a result of the good pulse shaping, no counting rate effects such as those occurring in in-core measurements, were detectable even at higher counting rates.

3.2.5 Source-detector geometry and counters utilized: The γ,n-discrimination method was used only below 70 keV because the measurements and evaluations are quite complicated. Without γ,n-discrimination, the measurable energy range of a counter extends only up to a fairly well-defined lower limit E_1 and in the upper direction, to E_2 because of the increase in wall effects. It is known from experience that $E_2/E_1 \approx 8$ is independent of counter type, counter size and filling system. Consequently, at least three suitable counters must be used to measure the energy range from 100 keV to 10 MeV. With the use of hydrocarbons as the counter gas, the lower limit of the measurable energy region in spectra with high-energy neutrons can also be determined by the appearance of C-recoils.

The maximum energy which can be transferred from a neutron to a carbon nucleus, because of A = 12, is the following according to [2]:

$$E_{C_{max}} = 0{,}284 \cdot E_{p_{max}} . \tag{21}$$

However, the energy loss per ion pair is about 40% greater for carbon than for protons in hydrocarbons [4]. Therefore,

$$I_{C_{max}} \approx \frac{0{,}284}{1{,}4} I_{p_{max}} = 0{,}20\, I_{p_{max}} . \tag{22}$$

i.e. the maximum ionization of the C-recoil nuclei produced by monoenergetic neutrons amounts only to 20% of the maximum proton ionization. This value was confirmed by measurements with monoenergetic neutrons. The peak produced by C-recoils in the analyzed neutron spectrum is lower in ionization than the proton peak by a factor of about 5.

For the spectrum measurements of the radioactive sources, the five cylindrical counters specified in Table 6 were used primarily in the parallel geometry shown in Fig. 24. Other counters, including spherical counters, and other geometries were used only for control measurements and measurements below 100 keV. The detection probability in the parallel geometry is small but has the following advantages:

1. The source strength can be determined absolutely with good accuracy.

2. The partial intervals of an extended spectrum measured with different counters can be referred to each other without arbitrary normalization constants. This is done by multiplying the neutron spectra obtained with the factor $d_1 \cdot d_2$, where d_1 and d_2 are the spacings shown in Fig. 24.

3. A calculation of the response matrix is relatively simple.

The distance d_1 was four times as large as the counter diameter. Errors in the neutron spectrum due to non-parallelity fall within the statistical accuracy of the spectrum measurements of about ±5%. This is shown in Fig. 25 in which neutron spectra of the Am-Be(5C)-source measured with counter No. 2 (Table 6, 9 cm diameter) as well as d_1 = 10, 30 and 50 cm. Systematic differences appear only below about 2.5 MeV and these are caused by the different contribution of spatially scattered neutrons.

The closest walls were at a distance of 2 m from the source and detector. Nevertheless, with the large counters (9 cm diameter), the background of spatially scattered neutrons of 10% is so high that it requires correction. This correction was made by subtraction of the spectrum measured with a shadow cone (Fig. 24) from that obtained without a shadow cone. The shadow cone consisted of steel and had a length of 15 cm. The probability that neutrons with energies below 10 MeV penetrate the shield without scattering is smaller than 2%. (The spectra shown in Fig. 25 and only these have not been corrected with respect to spatially scattered neutrons.)

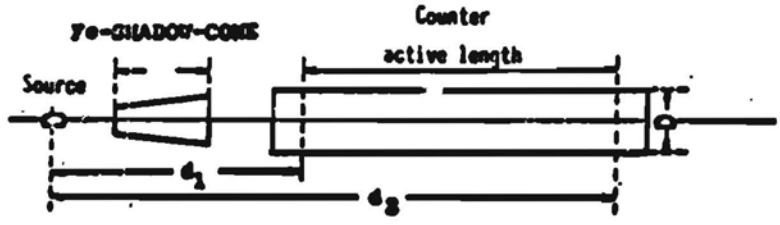

Fig. 24.--Source-detector geometry for the radioactive neutron sources.

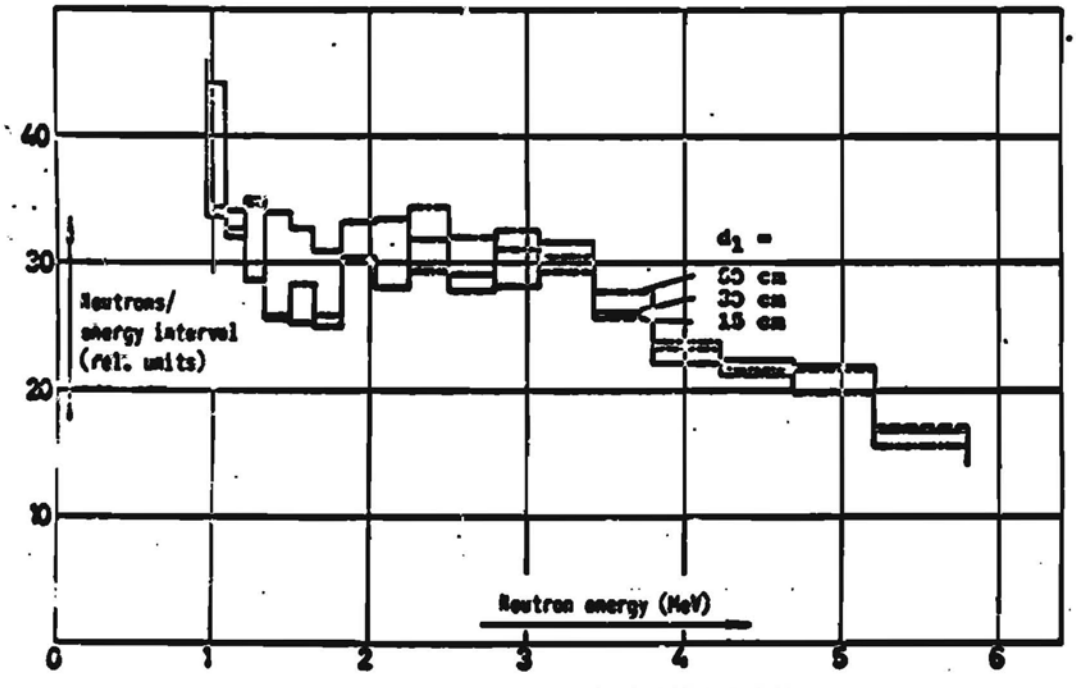

Fig. 25.--Dependence of the neutron spectrum on the source-detector distance (Am-Be(5C), counter No. 2, Table 6).

Table 6.--Counters used for measurements of the radioactive source spectra.

No.	Type	Dimensions (cm)					Filling	High-voltage	Gas ampl. factor	Max. rise time	Measuring range
		ε	a	b	H	T	(atm)	(V)		ΔT_{max} (/usec)	(MeV)
1	cyl.	$2,5 \cdot 10^{-3}$	0,2	4,5	83,5	4,05	$2Kr+2CH_4$	3600	8	6	1,5 -10
2	cyl.	$2,5 \cdot 10^{-3}$	0,2	4,5	83,5	4,05	$3CH_4$	3800	7	3,5	0,8 - 6
3	cyl.	$2,5 \cdot 10^{-3}$	0,1	2,1	33,5	2,8	$1,5Kr+1,5H_2$	2000	10	5	0,6 - 4
4	cyl.	$2,5 \cdot 10^{-3}$	0,1	2,1	33,5	2,8	$2H_2+0,1CH_4$	2500-3120	20-150	4,5	0,15- 1
5	cyl.	$2,5 \cdot 10^{-3}$	0,1	2,4	105,0	3,0	$3CH_4$	3800	10	0,9	0,5 - 3

a = wire radius
ε = wall thickness of counter housing
b = radius of counter housing
H = length of counter
T = length of inactive zone at each counter end.

3.3 Analysis of the Proton Spectra

3.3.1 Monoenergetic neutrons: The reliability of the neutron spectra obtained depends essentially on how accurately the response functions are known, i.e. the pulse height distributions produced in a counter by monoenergetic neutrons. The total of the response functions forms the response matrix by means of which the neutron spectrum is determined from the measured recoil proton distribution by unfolding. In general and also in this study, the calculated response matrixes are used. The absolutely necessary experimental verification is made most simply by comparison with measured recoil proton spectra of monoenergetic neutrons.

A number of programs for the calculation of proton spectra is already available for spherical counters. The calculations are based on a locally constant and isotropic neutron flux in the counter. In fact, however, the trend of the proton spectra in spherical counters depends little on the angular and position distribution of the neutron field because of the symmetry and absence of dead space. This fact as well as the agreement of measured and calculated proton spectra of monoenergetic neutrons in the energy region below about 1 MeV has been confirmed in earlier studies [19,31]. Fig. 26

shows the measured and calculated proton spectra of monoenergetic neutrons for spherical counters. The $Li^7(p,n)Be^7$-reaction served for the production of monoenergetic neutrons. The distance between target and detector amounted to 20 cm. The measured proton spectra were not corrected for spatially scattered neutrons. Aside from the differences caused by the finite energy resolution of the counters, the measured and calculated [32] proton spectra are in good agreement. The neutron spectra determined from the measured proton spectra by unfolding with the use of calculated response matrixes [32] are monoenergetic, i.e. above the sensitivity limit for gammas, the spectrum has a peak and is otherwise equal to zero within the indicated statistical accuracy and certain systematic errors.

Response matrixes calculated with a Monte Carlo code [33] served for unfolding of the proton spectra measured with cylindrical counters. A locally constant flux in the counter and neutrons with a parallel incidence to the counting wire or isotropic incidence from all sides were assumed for the calculation. Verification of the response functions calculated with the code in the entire measuring range up to 10 MeV was not possible, since only monoenergetic neutrons with energies of less than 1 MeV ($Li^7(p,n)Be^7$), with 3.05 and 2.55 MeV (D-D-reaction in direction of the incident ions and below 100°) and 15 MeV neutrons (D-T-reaction) were available.

On the other hand, the course of the proton spectra in a given counter is determined not by the neutron energy but by the range distribution of the protons. Consequently, when the same counter is irradiated with monoenergetic neutrons of different energy, nearly identical proton spectra are obtained when provision is made by a suitable counter gas that the maximum proton range will be the same in both cases; i.e., if the calculated and measured proton spectra agree for all reasonable values of the ratio of maximum proton range to counter dimensions (essentially diameter), it can be assumed that the calculations are correct.

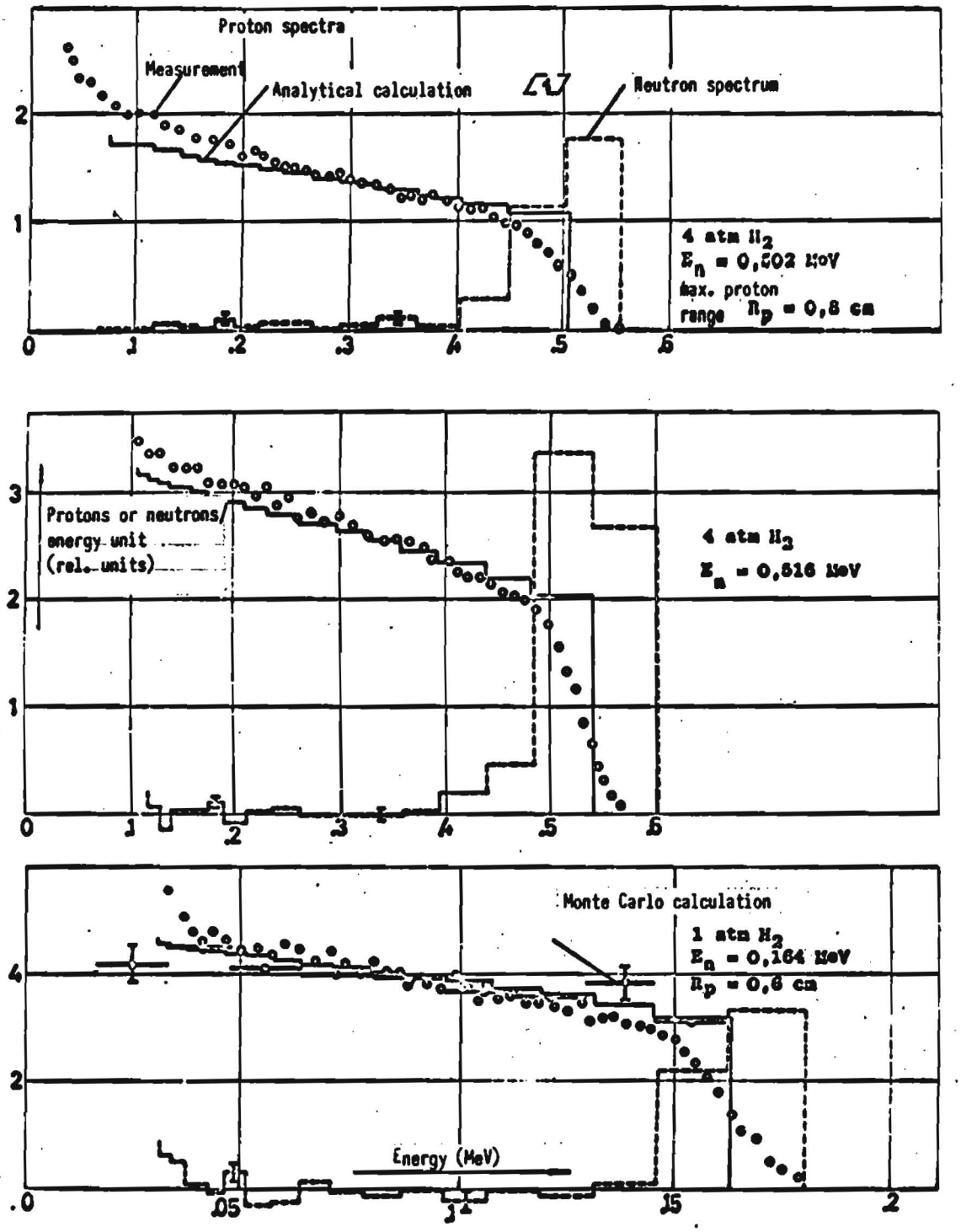

Fig. 26.--Proton and neutron spectra of monoenergetic neutrons from the $Li^7(p,n)Be^7$ reaction in different spherical counters; (3.94 cm diameter).

Figs. 27-31 show measured and calculated proton spectra as well as the neutron spectra determined from the measured proton spectra with the use of calculated response matrixes for a number of different counters and counter gases. As in the spectral measurements with radioactive sources, the distance between target and front face of the counter was four times as large as the counter diameter and for counters with a diameter larger than 4 cm, the scattering background was corrected by a shadow cone measurement. In most measurements, monoenergetic neutrons of 3.05 and 2.55 MeV from the D-D-reaction were used (counter below 0 and 100° with respect to the incident ion beam). The agreement between calculated and measured proton spectra is good, particularly with strong deformation by wall effects.

The relatively large discrepancies in the spectra with small effects probably are caused by the inexact correction of the low-energy neutrons. Fig. 31 for 15.14 MeV neutrons from the D-T-reaction shows that the calculation correctly reproduces the measured proton spectrum even with extreme wall effects. Oblique incidence from a neutron point source cannot be treated with the code utilized here. Spectra measured in such a geometry, however, do not deviate significantly from those calculated with the assumption of isotropic incidence as demonstrated by Fig. 30. Consequently, this geometry is entirely suitable at least for control measurements. The deviations of the neutron spectra determined from the monoenergetic curve are used in 3.3.3 to estimate the errors caused in the source spectra by the use of calculated response matrixes.

3.3.2 Analysis program: The analysis procedure will be explained on the basis of the example shown in Fig. 32, i.e. the spectrum of the Am-Be(5C)-source measured with counter No. 2 (Table 6):

After subtracting the proton spectrum measured with a shadow cone from that measured without a shadow cone, we obtain the spectrum corrected for spatially scattered neutrons which will be used for further analysis. The background spectrum of the spatially scattered neutrons drops very rapidly with increasing energy; in our case, it contributes about 25% to the total spectrum at 1 MeV but only 3% at 5 MeV. In measurements with spherical counters and small cylindrical counters, this correction is not made, since the contribution of spatially scattered neutrons is very small because of the small source-detector distance.

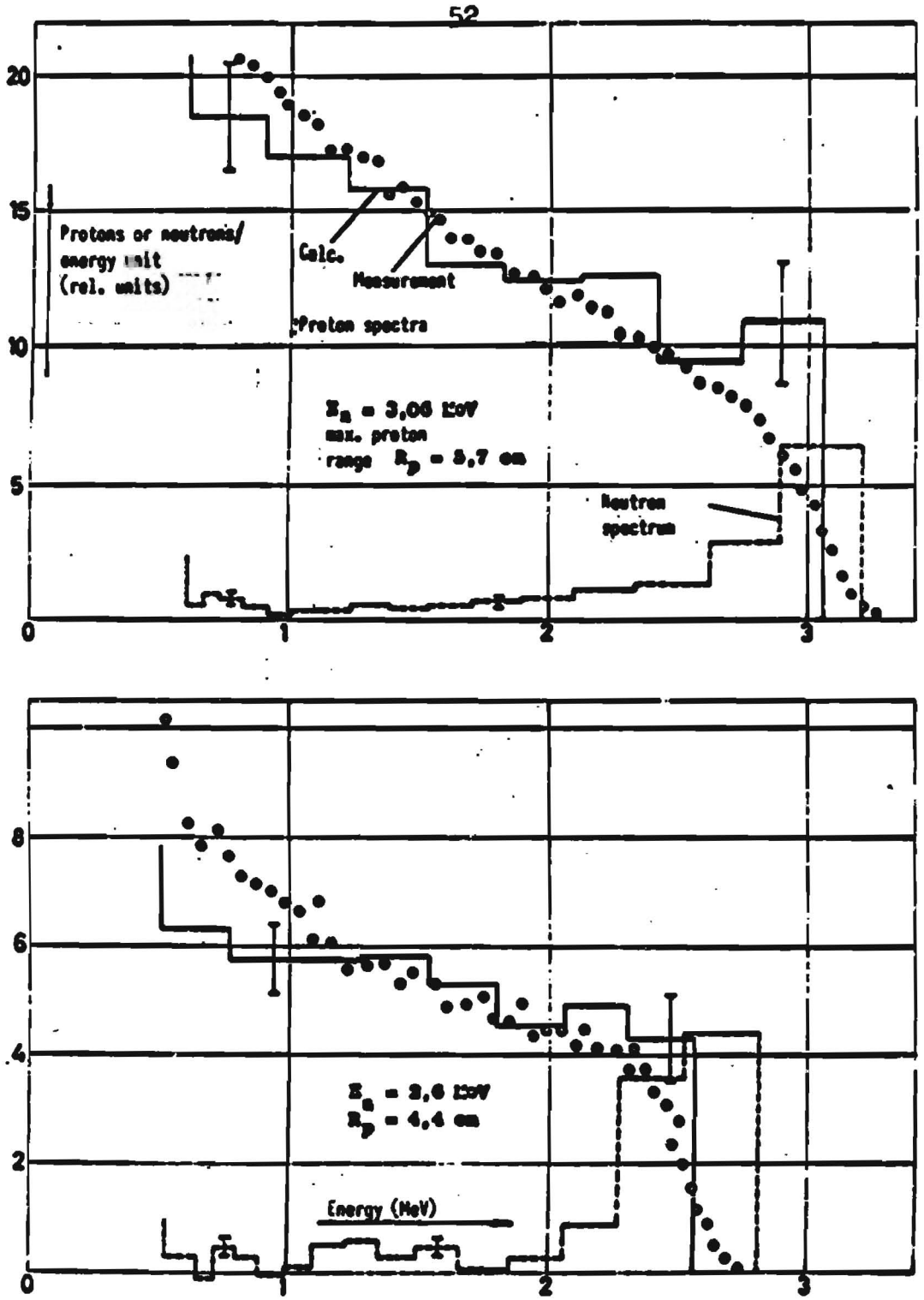

Fig. 27.--Proton and neutron spectrum of monoenergetic neutrons from the D-D reaction in a cylindrical counter (83.5 cm height, 8.9 cm diam., 3 atm CH_4 fill) Parallel incidence.

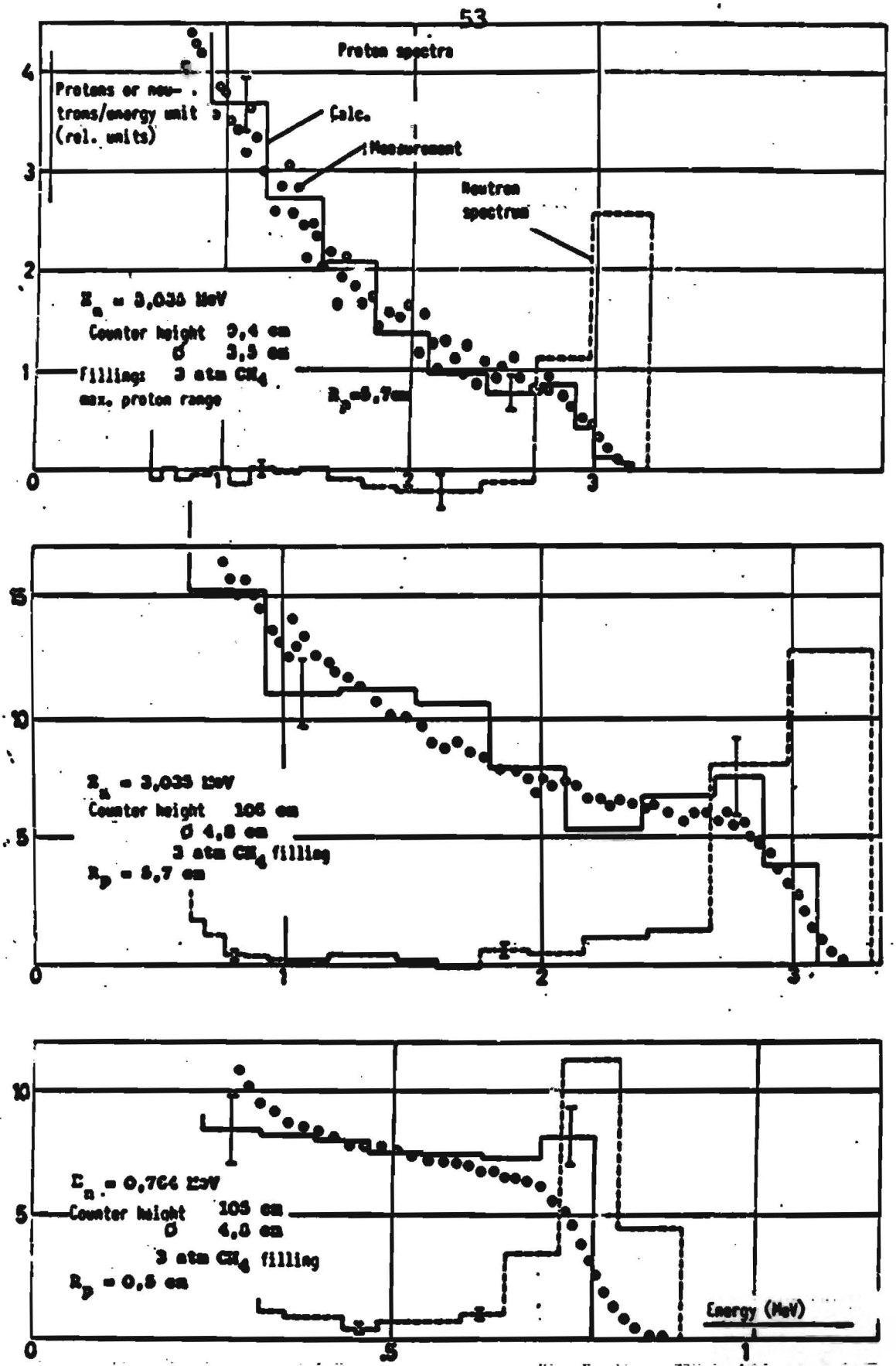

Fig. 23.--Proton and neutron spectra of monoenergetic neutrons (D-D, Li (p,n) I in different cylindrical counters. Parallel incidence.

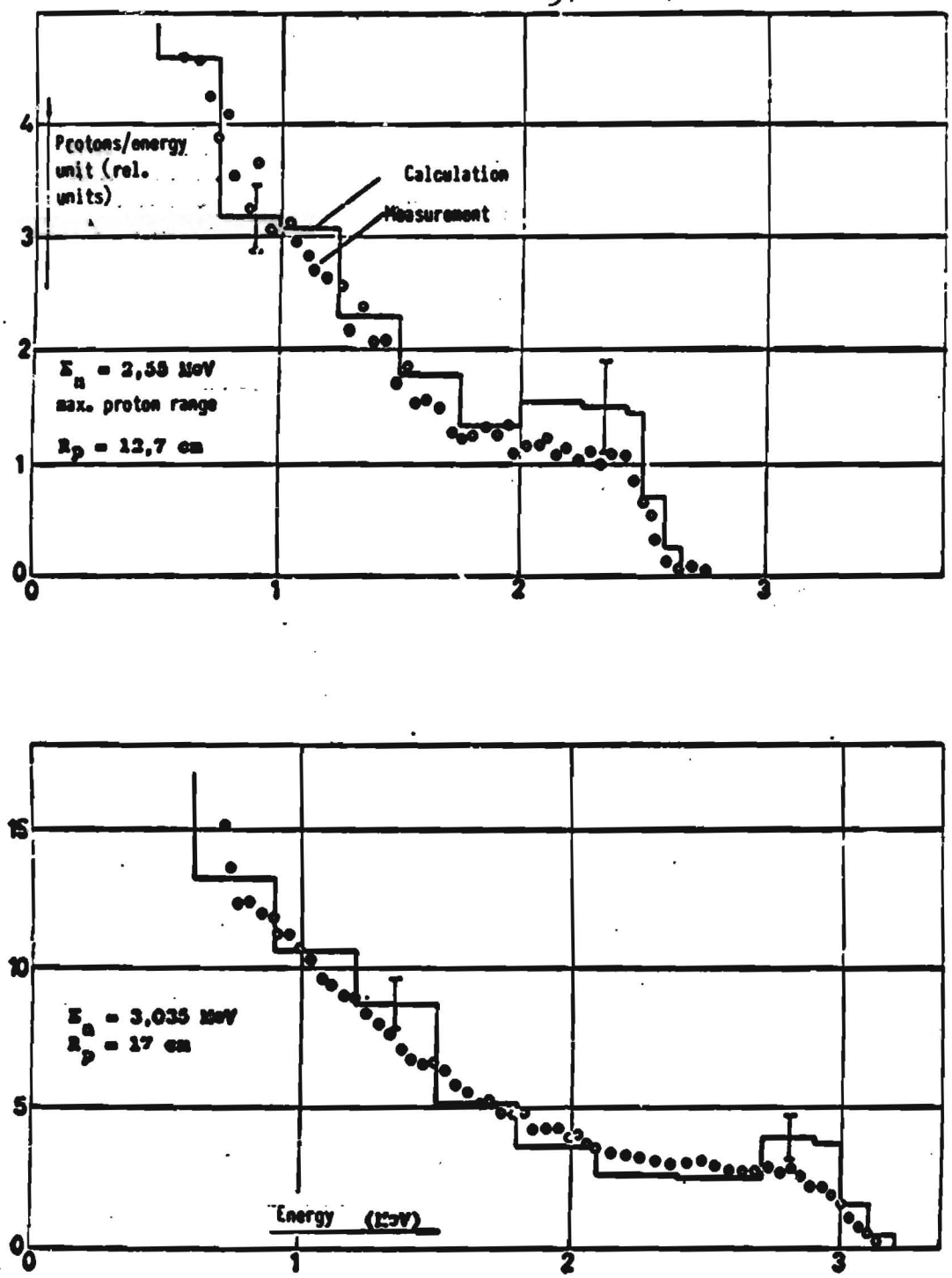

Fig. 29.--Proton spectra of monoenergetic neutrons (D-D-reaction) in a cylindrical counter (83.5 cm height, 8.9 cm diam., 1 atm CH_4 filling). Parallel incidence.

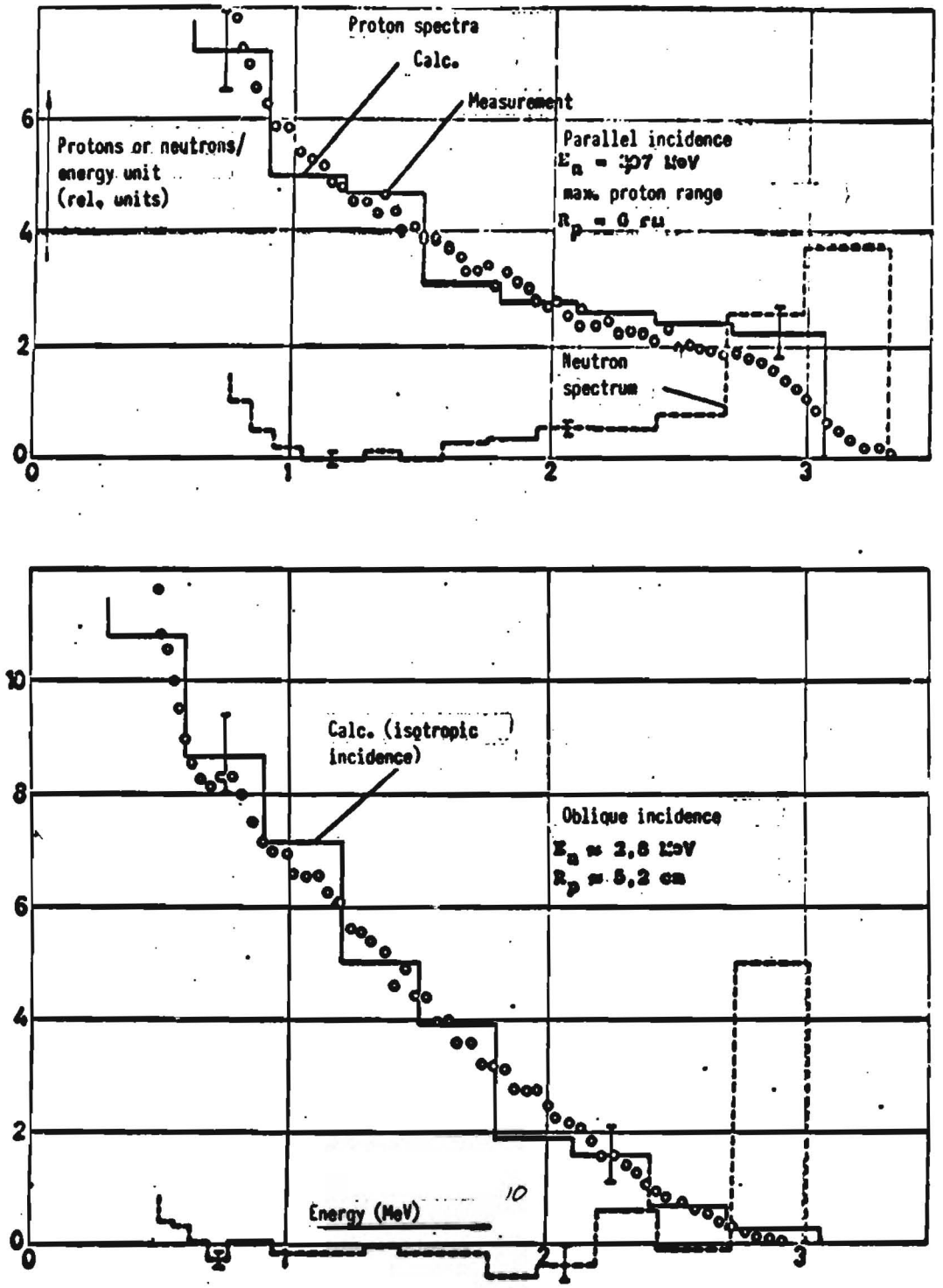

Fig. 30.--Proton and neutron spectra of monoenergetic neutrons (D-D reaction) in a cylindrical counter (33.5 cm height, 4.2 cm diameter, 1.5 atm Kr + 1.5 atm H_2 filling).

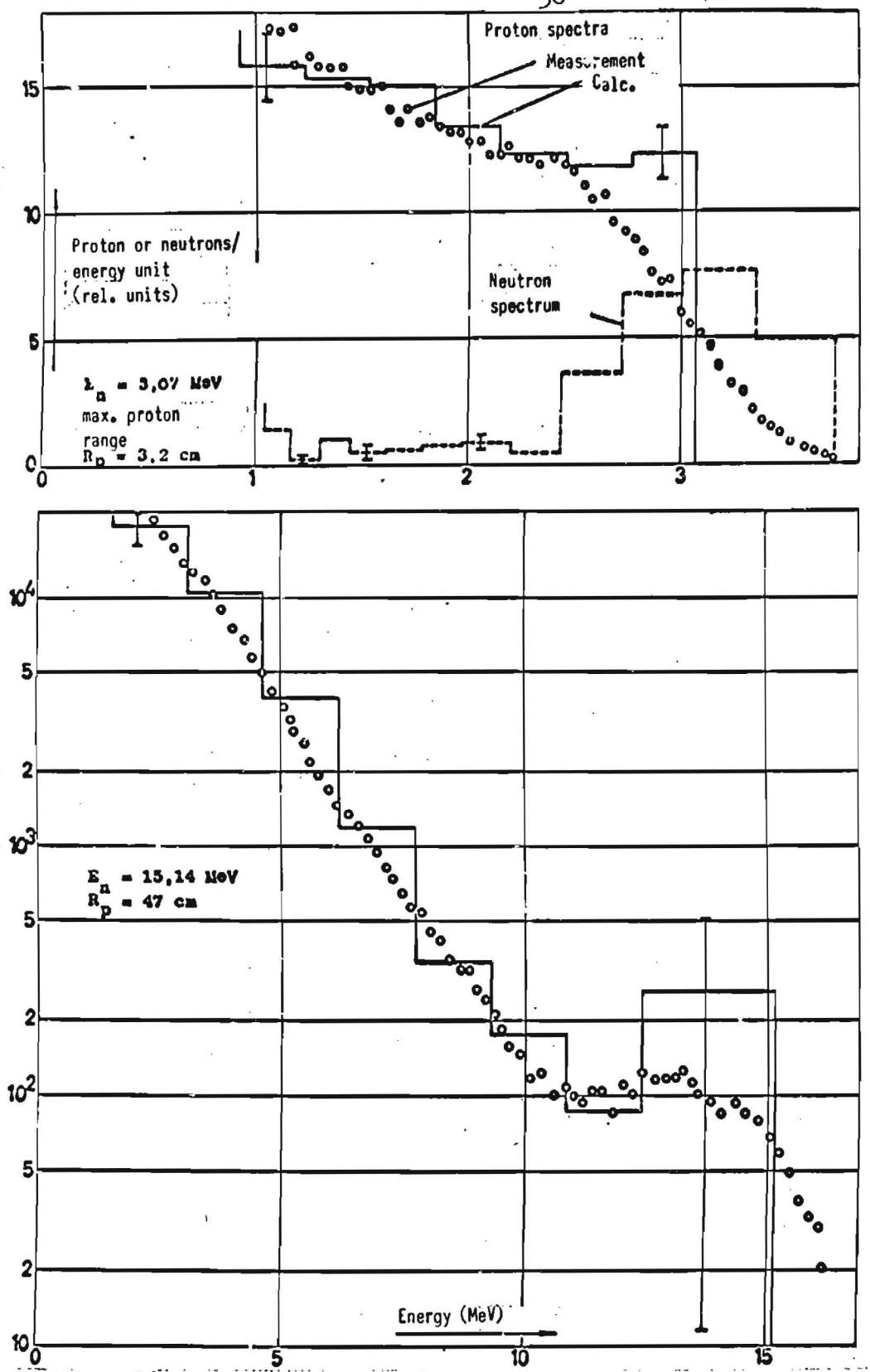

Fig. 31.--Proton and neutron spectra of monoenergetic neutrons (D-D- and D-T reactions) in a cylindrical counter (83.5 cm height, 8.9 cm diameter, 2 atm Kr + 2 atm CH_4 filling). Parallel incidence.

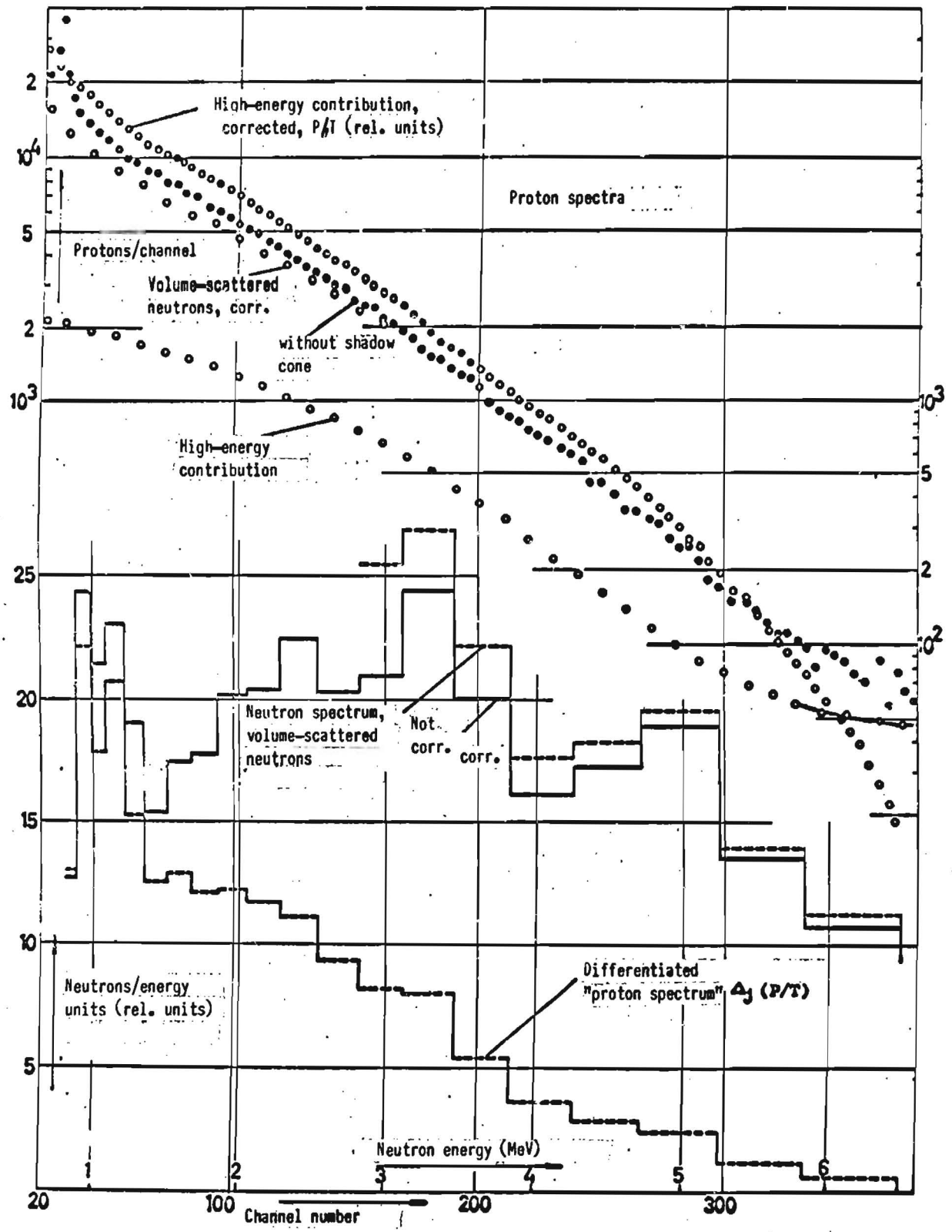

Fig. 32.--Analysis of the measured proton spectra.

Subsequently, the contribution to the measured proton spectrum originating from neutrons with an energy greater than E_{max}, i.e. 6.5 MeV in this example, is subtracted. E_{max} is defined by the fact that the level of the corresponding response function is approximately twice as high at $E_{max}/2$ than at E_{max}. The reason for the limitation of the analysis range is that if wall effects become very great, possible systematic errors in the response functions become very prominent in the neutron spectrum obtained and the statistics become very poor above E_{max}. To calculate the high-energy contribution, it is necessary to know the neutron spectrum above E_{max} and the response matrix. The neutron spectrum above E_{max} is measured with suitable counter and the response matrix is calculated with the Monte Carlo program [33]. After subtracting the high-energy contribution, the proton spectrum originating from neutrons with energies below E_{max} remains from which the neutron spectrum is determined by means of unfolding. The method proposed by Benjamin, Kemshall and Brickstock [34] is used in which the differentiated proton spectrum is unfolded by means of the "differential" response matrix. As shown in [34], unfolding of the proton spectrum tends to instability already at moderate wall effects, while the method used here is inherently stable even with large wall effects. This is a consequence of the well-known fact for all unfolding problems, i.e. the unfolding process becomes more unstable the more the response functions deviate from delta-functions.

To explain the unfolding process proper, we transform (7) in such a way that the form of the response function which has been modified by wall effects is taken into account:

$$p(E) = N \cdot T \int_{E}^{\infty} \frac{\sigma(E_n)}{E_n} p(E_n, E) \, \varphi(E_n) \, dE_n \, . \tag{23}$$

$\frac{p(E_n,E)dE}{E_n}$ is the probability that a recoil proton produced by a neutron of energy E_n releases an energy of between E and E+dE in the counter and $p(E_n,E)/E_n$ is the response function. Differentiation for E, followed by transformation and substitution of the differential by a finite interval and of the integral by a summation, furnishes the following:

$$\varphi(E_j)\,\Delta E_j = -\frac{E_j}{N\sigma(E_j)\,p(E_j,E_j)}\left(\Delta_j\left(\frac{P(E)}{T}\right) - \sum_{E_{n_i} > E_j}\frac{N\,\sigma(E_{n_i})}{E_{n_i}}\cdot\Delta p(E_{n_i},E_j)\,\varphi(E_{n_i})\cdot\Delta E_{n_i}\right). \tag{24}$$

The width of the energy intervals is chosen such that $\Delta E_j = \epsilon \cdot E_j$ with ϵ = const--in this example, $\epsilon = 0.1$--corresponds approximately to the counter energy resolution. We call the matrix,

$$p'(E_n,E) = \frac{N\,\sigma(E_n)}{E_n}\cdot\left\{\begin{matrix} p(E_n,E_n) \\ \Delta p(E_n,E) \end{matrix}\right\} \tag{25}$$

the differential response matrix. It has been plotted for some E_n-values in Fig. 33 for counter No. 2 (Table 6) used in this example. $\Delta(P(E)/T)$ and $\Delta p(E_n,E)$ are the changes of the proton spectrum referred to the unit of energy and time and of the response function over the energy interval ΔE. If the corresponding group indices are also used instead of the energy values, (24) can be rewritten with (25) as follows:

$$\phi_j = -\frac{1}{p'_{j,j}}\left(\Delta_j\left(\frac{P}{T}\right) - \sum_{i>j} p'_{i,j}\cdot\phi_i\right). \tag{26}$$

where $\phi_j = \varphi(E_j)\Delta E_j$ is the integral flux in group j. This relation is the basis for the numerical evaluation. If index n designates the uppermost energy group, then, according to (26), we have:

$$\begin{aligned} \phi_n &= -\frac{1}{p'_{n,n}}\cdot\Delta_n\left(\frac{P}{T}\right) \\ \phi_{n-1} &= -\frac{1}{p'_{n-1,n-1}}\left(\Delta_{n-1}\left(\frac{P}{T}\right) - p'_{n,n-1}\cdot\phi_n\right), \text{ etc.} \end{aligned} \tag{27}$$

i.e., the lower the group, the more correction terms are necessary to calculate the neutron spectrum. The neutron flux per unit of energy φ^E and of lethargy φ^u is obtained from (26),

$$\varphi_j^E = \phi_j / \Delta E_j \quad \text{and} \quad \varphi_j^u = \phi_j / \Delta u_j\ . \tag{28}$$

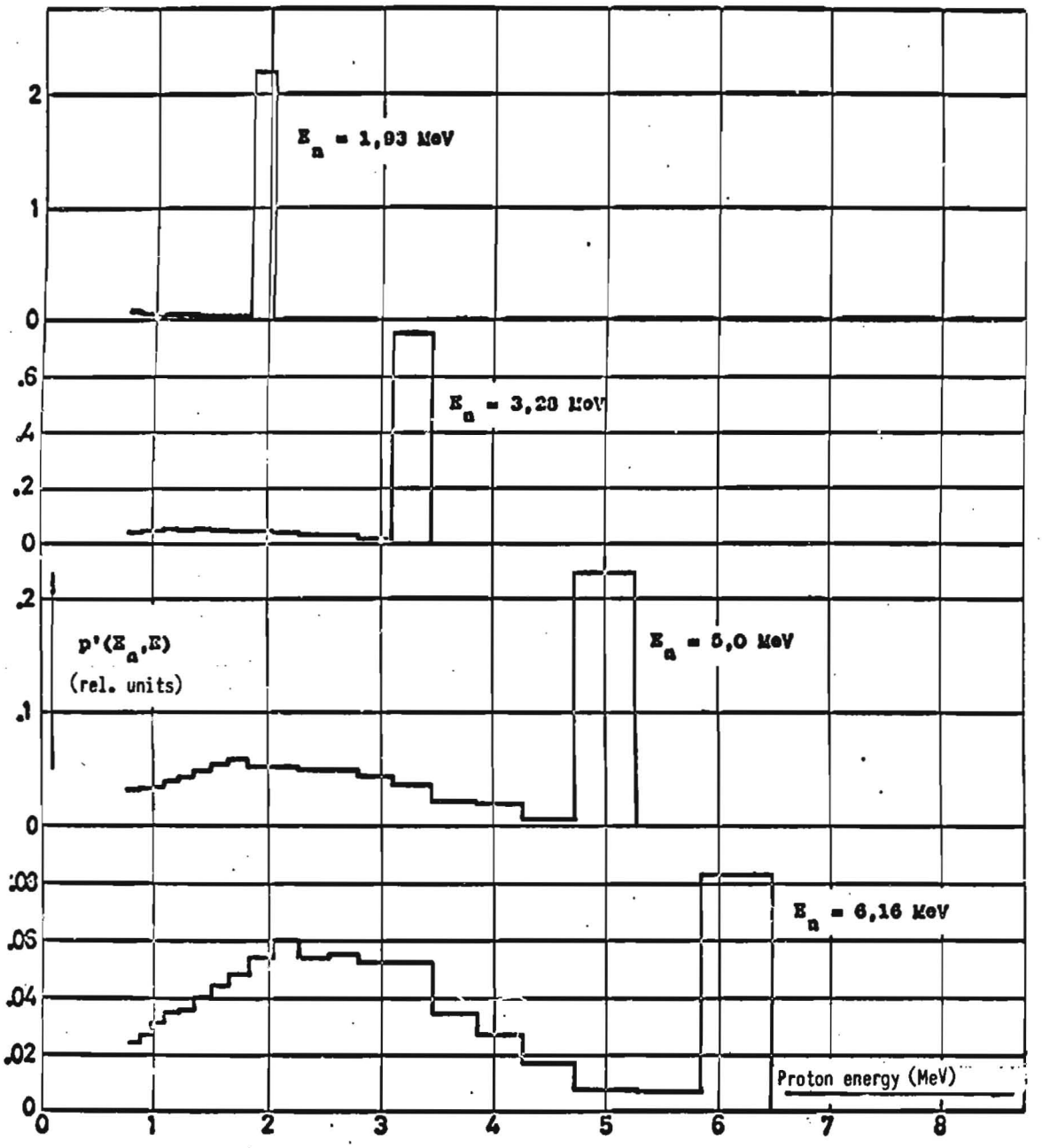

Fig. 33.--Differential response functions for counter No. 2 (Table 6)

where ΔE_j and Δu_j is the energy and lethargy interval corresponding to group j, respectively. For the calculation of the quantities $\Delta_j(\frac{P}{T})$ we should still note that this is done by a line fit and multiplication of the slope by the group width in order to benefit from the full information content of the proton spectrum.

The numerical evaluation of the series of proton spectra belonging to a neutron spectrum is made in one run on a 7074 IBM computer. The spectrum of the counter which measures the uppermost energy region is analyzed first. This result then permits a determination of the high-energy correction for the counter, the measuring range of which follows directly.

In connection with the spectrum measurements with radioactive neutron sources, we should still briefly note the relation between the neutron flux φ_j^E (per energy interval) determined according to (28) and the source strength N_j^E (per energy interval) which is otherwise usually given. If d is the distance between the source and a (point-shaped) detector, we have:

$$\varphi_j^E = \frac{N_j^E}{4\pi d^2} . \tag{29}$$

For cylindrical counters in the parallel geometry (Fig. 24) used here, if the counter diameter is small compared to d_1 and d_2, we have:

$$\varphi_j^E = \frac{N_j^E}{4\pi d_1 \cdot d_2} . \tag{30}$$

3.3.3 Estimate of systematic errors: The influence of the following errors on the determined neutron spectrum was investigated:

1. Systematic errors in the response matrix,
2. Deformation of the measured proton spectrum by differences in counter pulse rise times,
3. Background of spatially scattered neutrons or their inexact correction,
4. Errors in the neutron spectrum used for calculation of the high-energy contribution,

5. Energy calibration errors,

6. Fitting errors of the partial regions of a broad spectrum measured with different counters as a result of inaccuracies in the gas pressure and in the geometry factor (Section 3.2.5).

The error in the values $p(E_n,E_n)$ (23) which correspond to the diagonal elements of the response matrix (Point 1), was estimated at 0.03 on the basis of measurements with monoenergetic neutrons and from a series of suitable measurements (Figs. 35-37) of the same neutron spectrum with different counters, i.e. since the diagonal elements are directly contained in the determined neutron spectrum according to (26), the relative error caused thereby in the neutron spectrum increases with increasing energy and increasing deformation due to wall effects, and for $p(E_n,E_n) = 1$, 0.5 and 0.3, it amounts to about 3, 6 and 10%. Errors caused by different counter rise times (Point 2), are included in this information.

The error $\delta_M(\varphi_j^E)$ in the neutron flux determined (per energy interval) as a result of errors in the non-diagonal elements $p'_{i,j}(i>j)$ of the response matrix (Point 1), according to (26) and (28), is given by:

$$\delta_M(\varphi_j^E) = \frac{1}{p'_{j,j}\cdot\Delta E_j}\sum_{i>j}\varepsilon\, p'_{i,j}\,\phi_i \approx \frac{10\,\varepsilon}{\sigma_j\, p_{j,j}}\sum_{i>j}\frac{\sigma_i}{E_i}\Delta p_{i,j}\,\phi_i \approx C_M\, E_j \sum_{i>j}\frac{\phi_i}{E_i^2}\,. \tag{31}$$

if we assume that ϵ is constant in $\delta(p'_{i,j}) = \epsilon p'_{i,j}$ and if we let $\sigma_j\, p_{j,j} \sim 1/E_j$ and $\sigma_i,\ \Delta p_{i,j} \sim 1/E_i$, which is justified within the range of this error estimate. The relation is reasonable and essentially states that $\delta_M(\varphi_j^E)$ becomes greater the larger the number of high-energy neutrons which are present and that the influence of high-energy neutrons decreases with increasing energy E_i. The constant C_M in (31) was estimated from the measurements with monoenergetic neutrons discussed in 3.3.1. It was assumed that the neutrons emitted by the target are actually monoenergetic and that the measured proton spectrum corresponds to the response function. The values in the determined neutron flux below the peak which differ from zero then are to be attributed to errors in the calculated response matrixes utilized. Accordingly, C_M is in the order of magnitude of 0.1-0.2. The error estimated according to (31) contains all errors--including

those of Points 2 and 3--which can result from the use of a calculated response matrix instead of the "correct" one.

Errors in the neutron spectrum utilized to calculate the high-energy contribution (Point 4), are a part of the error in the neutron spectrum determined in the same manner described by (31) but with a smaller weight. The reason for this is that because of normalization of the calculated high-energy contribution, only the relative trend of the neutron spectrum is contained in the range of E_{max} to $E_{max} \cdot 1.05$, on one hand, and that $p'_{i,j}$ (25) does not vary extensively with i when j is constant, on the other hand. The relatively small influence of the high-energy neutron spectrum is shown in Fig. 34, where the same proton spectrum was analyzed with two spectra which differ in their relative course by up to 50%. If an error of 10% is assumed in the high-energy neutron spectrum, this leads to an error in the order of magnitude

$$\sigma_{II}\left(\varphi_j^E\right) < 0{,}1\, E_j \sum_{i>j} \frac{\sigma_i}{E_i^2} \tag{32}$$

in the calculated neutron spectrum below E_{max}.

The energy calibration is obtained by the energy and analyzer channel number of the He^3-peak and by the channel number which corresponds to zero ionization as determined with a linear pulse generator. Errors in energy calibration (Point 5) are produced mainly by the finite width of the He^3-peak and by the uncertainty in the energy value E_o assigned to zero ionization (Section 3.2.3). The finite width of the He^3-peak has the result that an energy value falling only within a certain limit which corresponds to about one-third of the energy resolution can be assigned to a certain part of the spectrum. However, because of the relative constancy of the n,p-cross section, this essentially causes only a corresponding expansion of the spectrum referred to the unit of energy or a constant shift of the spectrum referred to the unit of lethargy. The errors in the spectra caused by uncertainties in E_o--they have already been discussed in 3.2.3--are small compared to the other systematic errors except in limited energy intervals at the lower end of a given measuring range.

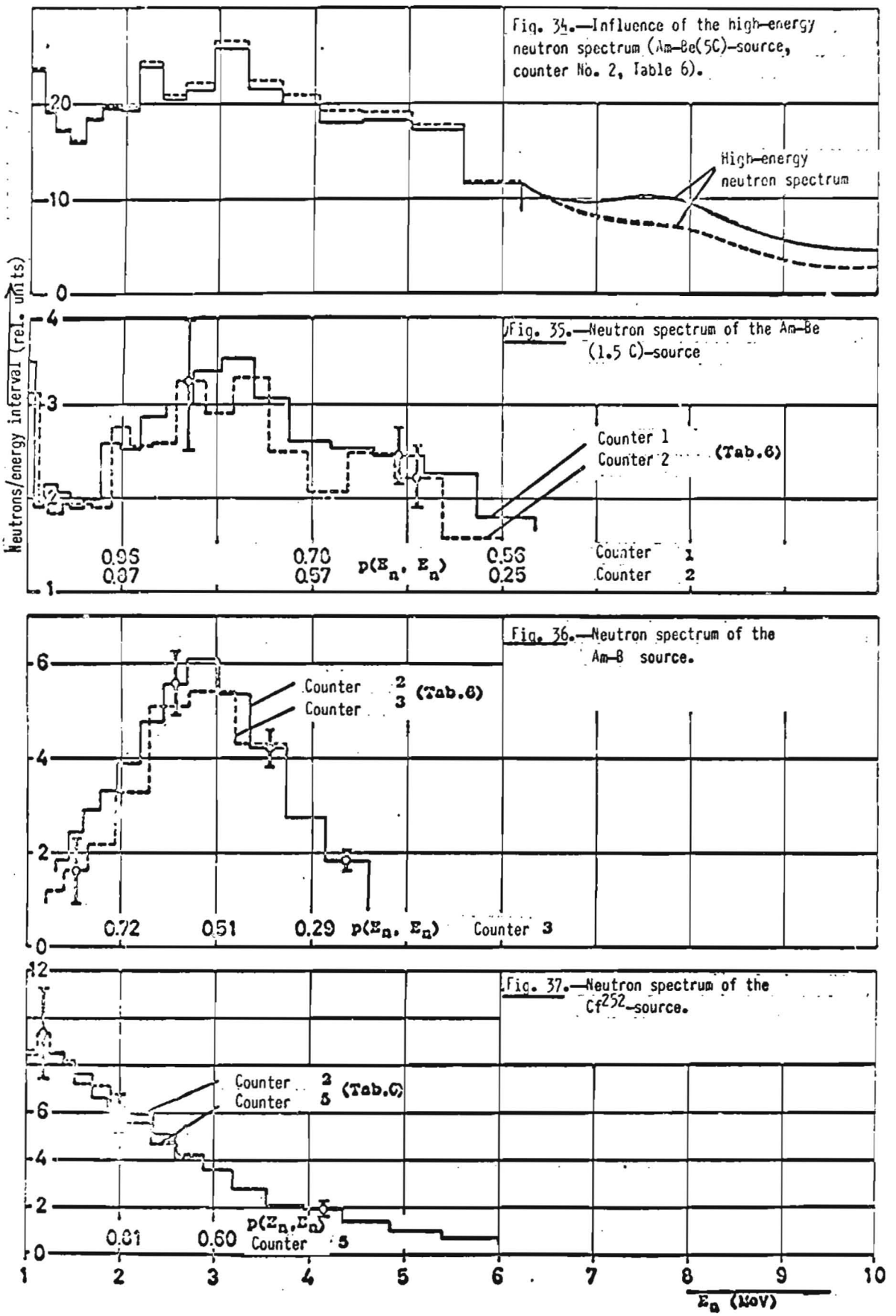
Fig. 34.—Influence of the high-energy neutron spectrum (Am-Be(5C)-source, counter No. 2, Table 6).
High-energy neutron spectrum
Fig. 35.—Neutron spectrum of the Am-Be (1.5 C)-source
Counter 1
Counter 2
(Tab.6)
0.95
0.87
0.70
0.57
p(E_n, E_n)
0.56
0.25
Counter 1
Counter 2
Fig. 36.—Neutron spectrum of the Am-B source.
Counter 2
Counter 3
(Tab.6)
0.72
0.51
0.29
p(E_n, E_n)
Counter 3
Fig. 37.—Neutron spectrum of the Cf252-source.
Counter 2
Counter 5
(Tab.6)
0.81
0.60
p(E_n, E_n)
Counter 5
Neutrons/energy interval (rel. units)
E_n (MeV)

The inaccuracy of the gas pressures amounting to a few atm (Point 6) amounts to about 2%. The error in the geometry factor (30), by means of which the partial intervals of a spectrum measured with different counters are referred to each other is caused by the finite extension of the sources and by the dead spaces at the counter ends, and amounts to about 5% for the small counters (4 cm diameter) and about 2% for the large counters (9 cm diameter).

In summary, the significant systematic errors can be described as follows:

1. Errors due to the diagonal elements of the response matrix: 3, 6 and 10% for $p(E_n,E_n) = 1$, 0.5 and 0.3. Because of the good overlapping of the partial intervals measured with different counters, this error is significant only in the high-energy region of a spectrum.

2. Errors due to high-energy neutrons.

$$\delta(\varphi_i^E)\ [1/\mathrm{MeV}] = \delta_M(\varphi_i^E) + \delta_H(\varphi_j^E) \approx 0.2\, E_j \sum_{i>j} \frac{\sigma_i}{E_i^2} \,. \tag{33}$$

3. Fitting errors of the partial intervals measured with different counters: 5%.

The estimated limits of error were verified by measuring the same spectra with different counters (different dimensions, different counter gases). Some of these measurements are shown in Figs. 35-37. The measurements are in agreement within the systematic errors (these are listed in the spectra) and the statistical errors (5%). The relatively large deviation below 2 MeV in the Am-B-source spectra (Fig. 36) originates from the C-recoils in the methane-filled counter.

4. Spectrum Measurements

4.1 Comparison Measurements with other Methods in SUAK

The fast subcritical assembly SUAK, which is described in [35], has served in recent years mainly to improve the various experimental methods for the determination of neutron spectra of fast multiplying media. In addition to the proton recoil method, the time-of-flight method and Li^6-sandwich-semiconductor spectrometer have been used in particular in the energy region above 10 keV. In the following, the recoil proton measurements will be briefly described and the results obtained will be compared with those of the other methods.

The spectra were measured in the center of the assemblies. Below 1.4 MeV, small spherical and cylindrical counters were used, located in a cavity in the center of the assembly. A collimated neutron beam incident on a large cylindrical counter (No. 2 in Table 6) which was extracted from the center and was incident on a large cylindrical counter (No. 2 in Table 6) parallel to the counting wire served to measure the spectrum above 0.8 MeV, similar to time-of-flight measurements. The counter was at a distance of about 3 m from the assembly and was shielded from spatially scattered neutrons by means of a paraffin layer of about 50 cm thickness on all sides. The remaining background of spatially scattered neutrons was corrected by measurements with and without a shadow cone as in the source spectrum measurements.

Fig. 38 shows the spectrum measured in assembly U1B. The 46 l-core consists of pure uranium metal enriched with 20% U^{235} and therefore has a very hard spectrum permitting measurements up to 2 MeV with the time-of-flight method. The latter measurements as well as the multigroup spectrum calculations were performed by Wattecamps and the measurements with the Li^6 spectrometer in SUAK UHC were made by Bluhm [36]. In the common energy region between 40 keV and 2 MeV, the deviations between the proton recoil and time-of-flight measurements are smaller than 20%. The accuracy of the time-of-flight method in this energy region is reported to be 15% [36].

The UHC core is identical to the VERA 7A core which was investigated in detail in Aldermaston and Harwell [37]. As shown by Fig. 39, the proton recoil measurements are in agreement with the Li^6-measurements within 20% in the common energy region between about

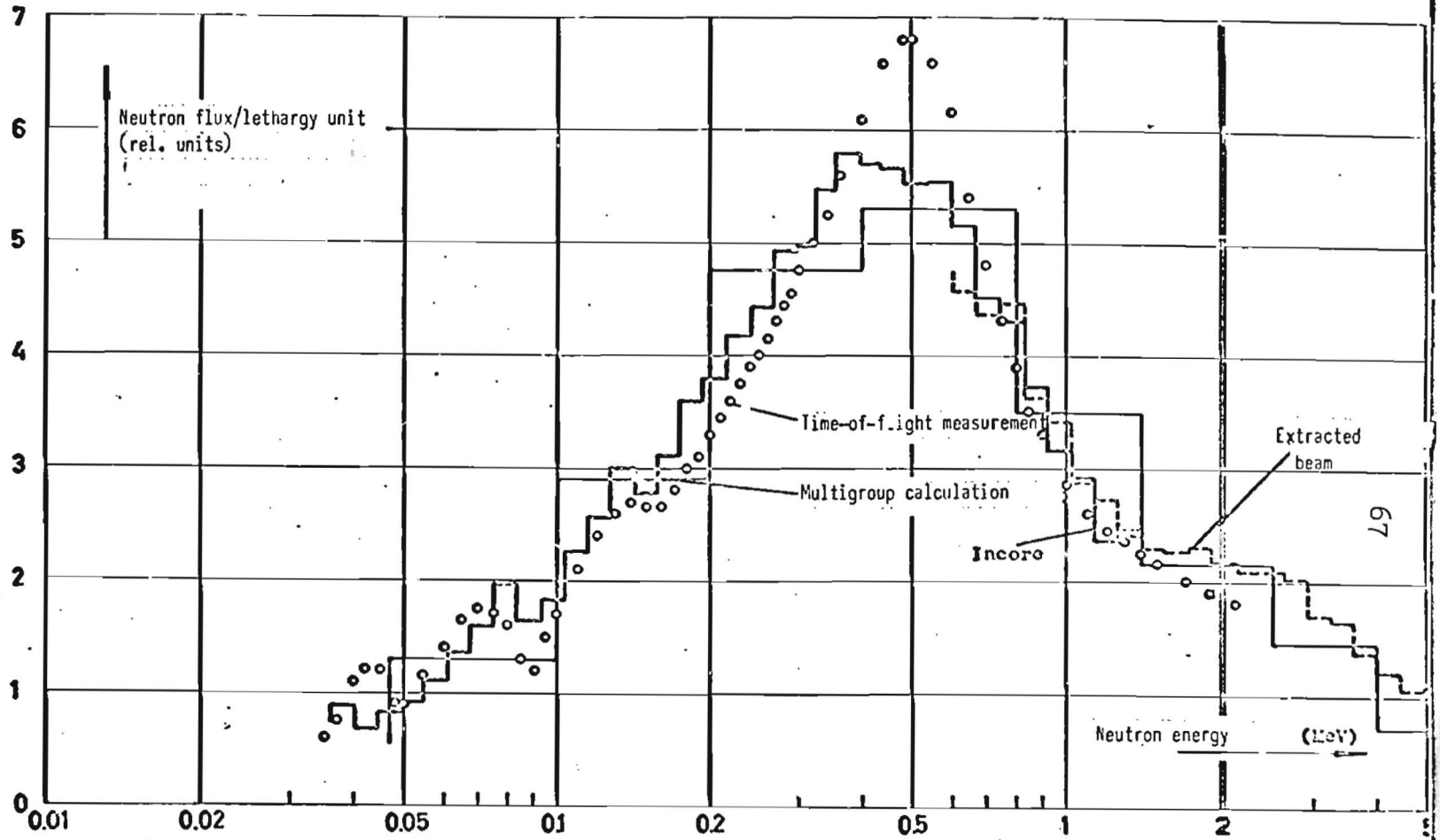

Fig. 38.--Neutron spectrum in the center of SUAK U1B.

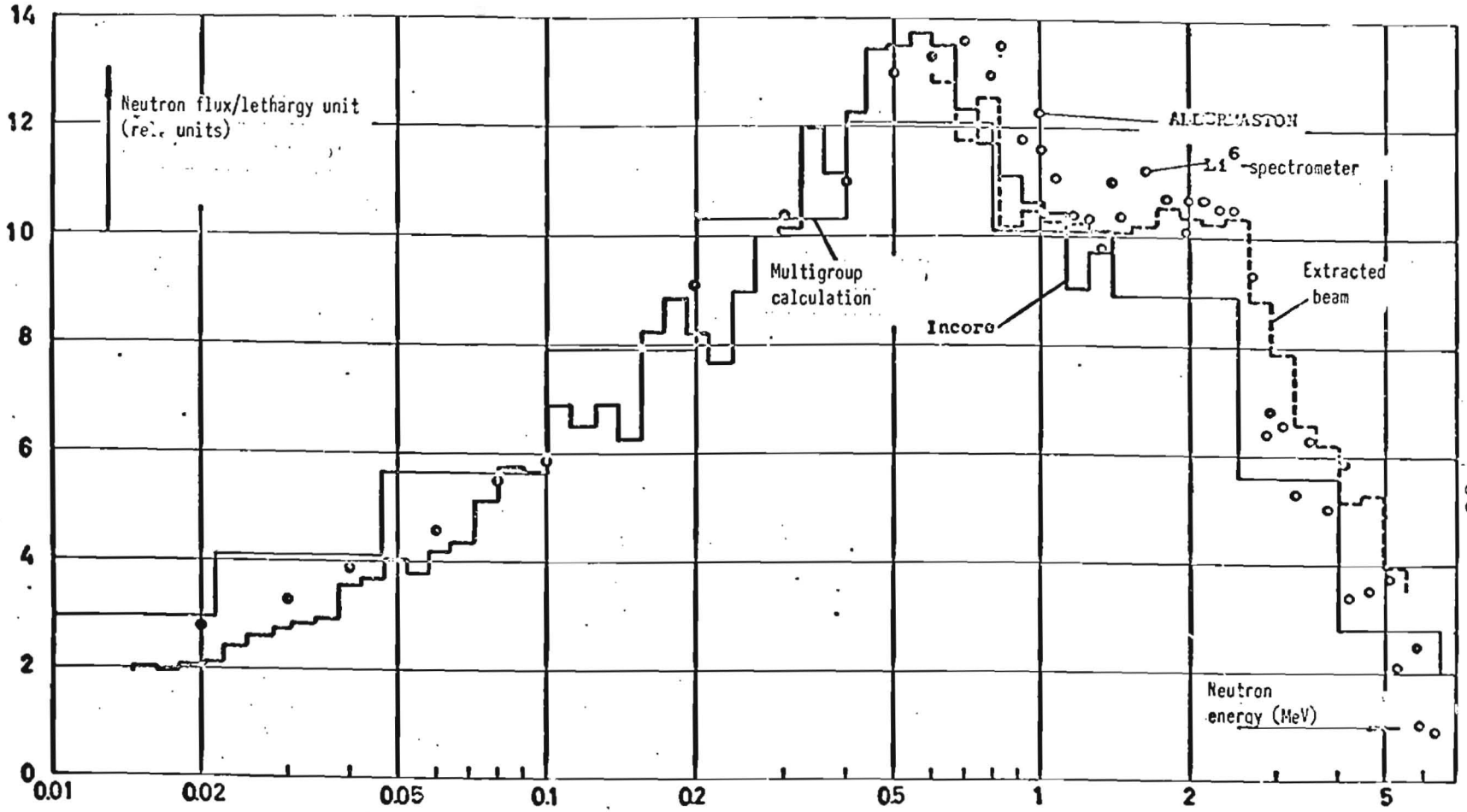

Fig. 39.--Neutron spectrum in the center of SUAK UHC (VERA 7A).

1 and 5 MeV. The accuracy of the Li^6-measurements is reported to be about 10% below 2 MeV and about 20% above 2 MeV [36]. The measurements made in Aldermaston in which recoil proton counters were also used below 1 MeV, while nuclear emulsions were employed above 1 MeV, are in agreement with our measurements within 15% in the entire energy region between 30 keV and 6 MeV, while the Harwell results above about 200 keV show a marked deviation.

The conclusions from this experiment are as follows:

1. With the use of an extracted neutron beam, the proton recoil method can also be used above 1.5 MeV for the measurement of fast reactor spectra and there is no reason to doubt the reliability of results in this energy region. Compared to the other two methods usually used in this energy region, i.e. the Li^6-semiconductor spectrometer and nuclear emulsions, it has the following advantages:

The lifetime of proton recoil counters is practically unlimited in contrast to Li^6-semiconductor detectors which normally can be used only once. The measuring time is shorter by a factor of about 10 than that of the Li^6-spectrometer.

Evaluation is simpler and more rapid than that of nuclear emulsions.

2. The discrepancies between individual measurements are considerably smaller than the sum of indicated systematic errors. This leads to the assumption that the estimate of the systematic error made in 3.3.3 is too pessimistic.

4.2 Sb-Be(γ,n)-Source

In contrast to α,n-sources, γ,n-sources furnish monoenergetic neutrons and are therefore still frequently used for cross section measurements in addition to importance measurements. The following relation exists between the neutron energy E_n, γ-energy E_γ the atomic weight a of the target nucleus and the threshold energy Q for the γ,n-reaction [18]:

$$E_n = \frac{A-1}{A}(E_\gamma - |Q|) \pm E_\gamma \left(\frac{2(A-1)\,(E-|Q|)}{931\ \mathrm{MeV}\cdot A^3}\right)^{1/2} . \qquad (34)$$

The most common γ,n-source is the Sb-Be-source and a number of studies have been published in which the mean neutron energy was determined. Measurement of the differential neutron spectrum is difficult because of the very high γ-activity. In cloud chamber measurements of Hughes and Eggler [38], the statistical accuracy is very poor (≈50%). Hanson [39] recorded the pulse height spectrum generated by a Sb-Be-source in a recoil proton counter and compared it with those of monoenergetic neutrons. Because of the high γ-background, however, it was impossible to obtain detailed information on the neutron spectrum and only an upper limit could be given for the Sb-Be-neutron energy.

For the measurement of the differential neutron spectrum, the counter must be shielded from the intense γ-radiation. However, if the γ,n-discrimination method is used, the quantity of shielding material can be reduced to a point where the energy distribution of the source neutrons is no longer markedly changed.

Reliable γ-corrected proton spectra are obtained only if the γ/n-ratio is not too high. The limit with the discrimination system used here is found at about 100. Consequently, as shown in Fig. 40, the lead shield between source and detector must have a thickness of 10, 15 and 20 cm to permit a reliable determination of the neutron spectrum down to 15, 12 and 8 keV.

The source consisted of a homogeneous mixture of 23 g Sb and 6.6 g Be powders placed in an Al-cylinder (3.6 cm height, 2.3 cm diameter) and had a source strength of about 5.10^4 n/sec). The measurements were performed with a cylindrical counter (25 cm active length, 4.2 cm diameter) filled with 2 atm H_2 and 0.1 atm CH_4 (No. 4 in Table 6). From a comparison of the He^3-energy calibration with the resonance structure of an iron transmission spectrum, an error of 0.8 keV was estimated for the energy determination in the region between 10 and 30 keV.

Below 30 keV, no wall effects occur and (8) can therefore be used to determine the neutron spectrum. The dependence between proton energy E (keV) and ionization I (keV) discussed in 3.2.3 was taken into account in the evaluation by using the relation $E = I + 0.4$.

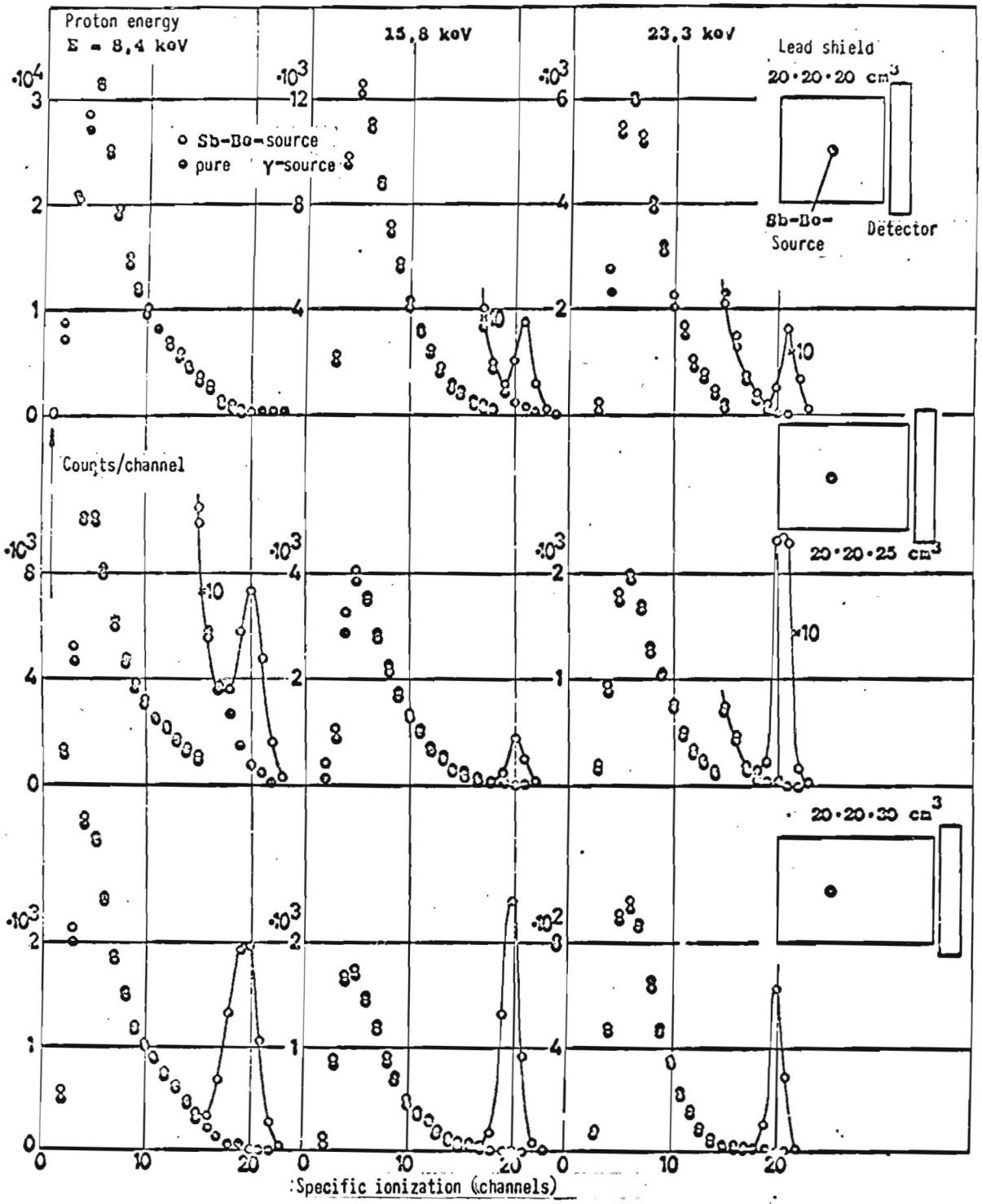

Fig. 40.--Specific ionization spectra of the Sb-Be source for different lead shields.

Fig. 41 shows the three quadratic lead shields utilized and the corresponding neutron leakage spectra as well as a γ-corrected proton spectrum in the energy region below 30 keV. The maximum of the neutron distribution shifts from 24 to 22.5 and to 21 keV when the lead shield thickness between source and detector is increased from 10 to 15 and finally to 20 cm.

In addition to the determination of the differential spectrum of the primary neutron group produced by the intense 1.691 MeV γ-radiation, an attempt was made to detect directly the higher neutron groups produced by the gammas of higher energy and, if possible, to determine their intensities. Above approximately 150 keV, no γ-background occurs any longer in the counter utilized and it is therefore possible to make measurements without γ,n-discrimination. The proton spectrum above 150 keV is also shown in Fig. 41. At 363 ± 15 keV, a neutron group can be clearly recognized, and at 550 keV, a neutron group is indicated although the statistics are already very poor here. For the three spectra below 30 keV, about 10 h of measuring time were used each and the measurement of the proton spectrum above 150 keV required 50 h.

The proton spectrum measured above 150 keV was compared with a theoretical spectrum calculated as follows: The neutron leakage spectrum produced by monoenergetic neutrons of 363 keV energy was determined with the Monte-Carlo neutron transport code MONTE [40]. The corresponding proton spectrum was then determined from this by means of the Monte Carlo proton recoil code [33]. It was assumed that the high-energy neutron background originated from the 550 keV neutron group. From the good agreement between measured and calculated proton spectra, we can conclude that if neutrons between 150 and 350 keV are present at all, their total intensity is at least 1/5 of that of the 363 keV-group. The area below the proton spectra of the 26 keV and 363 keV groups was used to determine their intensity ratio, i.e. I(363 keV)/I(26 keV) = (5.1 ± 1)%.

With a given photoneutron spectrum, the neutron leakage spectra modified by scattering on the source and shielding material can be directly calculated by means of the MONTE neutron transport code. Consequently, this code can also be used inversely to determine the photoneutron spectrum from the measured leakage spectra. This was

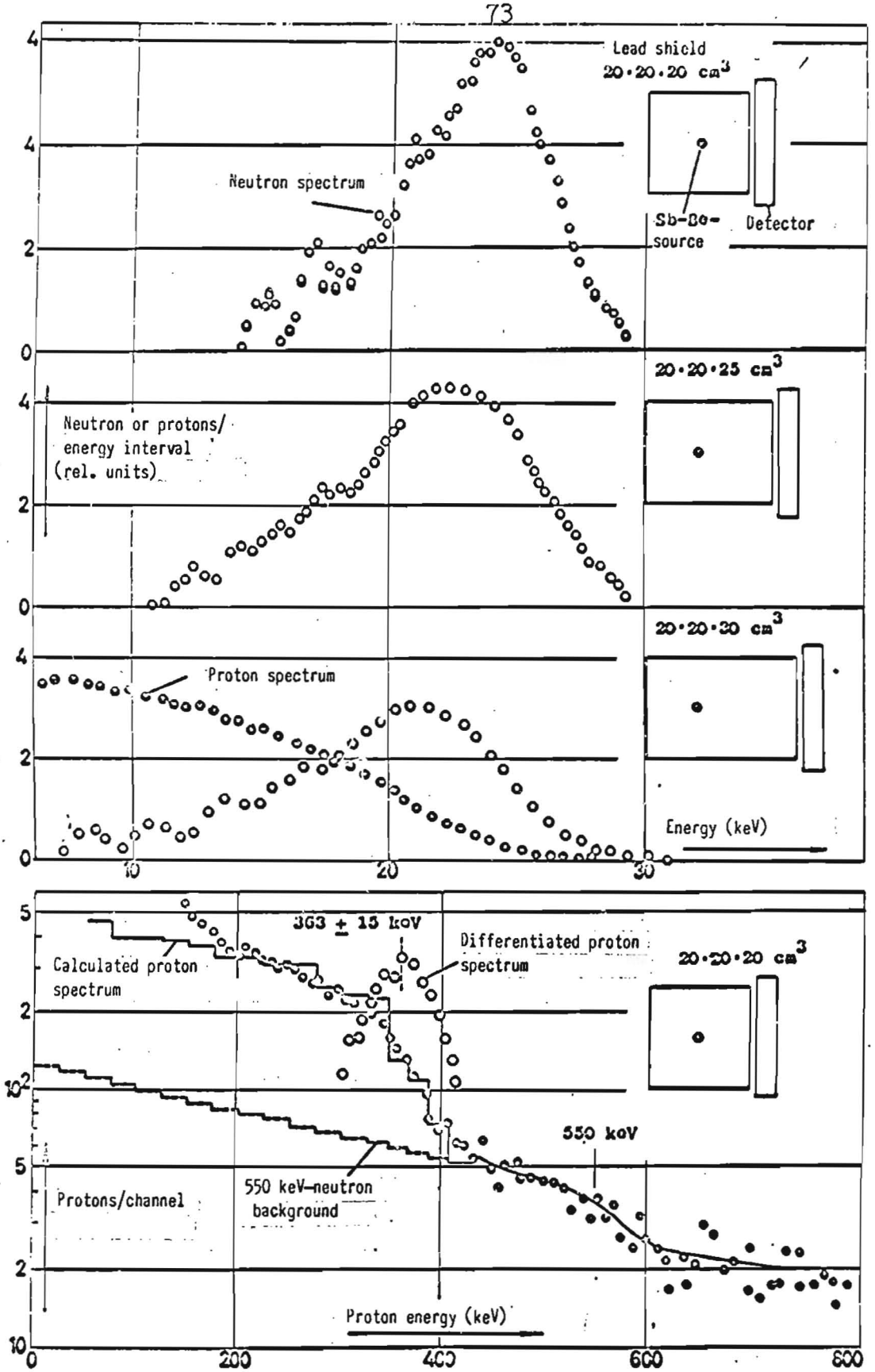

Fig. 41.--Neutron leakage spectra below 30 keV and proton spectrum above 150 keV.

Table 7.--Determination of the photoneutron spectrum.

Energy group (keV) i ↓ / E_j (keV) j →	1 23	2 24	3 25	4 26	5 27	6 28	7 29	Least-Square-Fit $\sum_{j=1}^{7} a_j \varphi_{i,j}$	Experiment φ_i
1 10 - 14	0,0123	0,0003	0,0000	0,015	0,0000	0,0003	0,0040	0,0093	0,0
2 14 - 17,5	0,0341	0,0314	0,0200	0,020	0,0174	0,0001	0,0160	0,0240	0,020
3 17,5-21,5	0,0934	0,0743	0,0000	0,040	0,0320	0,0320	0,0200	0,0540	0,064
5 21,5-22	0,0230	0,171	0,100	0,070	0,0500	0,0500	0,0440	0,105	0,103
6 22 - 23	0,100	0,107	0,110	0,107	0,0700	0,0000	0,0370	0,118	0,117
7 23 - 24	0,0	0,104	0,100	0,120	0,0047	0,0700	0,0620	0,137	0,138
8 24 - 25		0,0	0,194	0,204	0,123	0,103	0,0740	0,138	0,138
9 25 - 26			0,0	0,104	0,177	0,130	0,115	0,105	0,106
10 26 - 27				0,0	0,177	0,164	0,114	0,0004	0,066
11 27 - 28					0,0	0,174	0,100	0,0341	0,034
12 28 - 29						0,0	0,175	0,0164	0,0165
Least-Square-Fit-coefficients a_j	0,0512	0,1600	0,2330	0,2[illegible]	0,2160	0,1070	0,0937		

done as follows: The leakage spectra $\varphi_{i,j}$ of monoenergetic neutrons which had started in the source with energies E_j of between 23 and 29 keV were first calculated for the smallest lead cube. Subsequently, on the basis of the method of least squares, it was demanded that

$$\sum_{j=1}^{7} a_j \, \varphi_{i,j} = \varphi_i \, . \qquad i = 1, 12 \, . \tag{35}$$

φ_i is the measured leakage spectrum of the smallest lead cube divided into groups. Consequently, the coefficients a_j determined with (35) represent the photoneutron spectrum. The results of this calculation are compiled in Table 7.

The leakage spectra for the larger lead cubes were calculated with this photoneutron spectrum a_j, determined from the measured leakage spectrum of the smallest lead cube. Fig. 42 shows that the measured and calculated leakage spectra are in good agreement and this proves the reliability and consistency of the measurements and calculations. The errors in the mean energies $\bar{E}_n$ (measured) of the

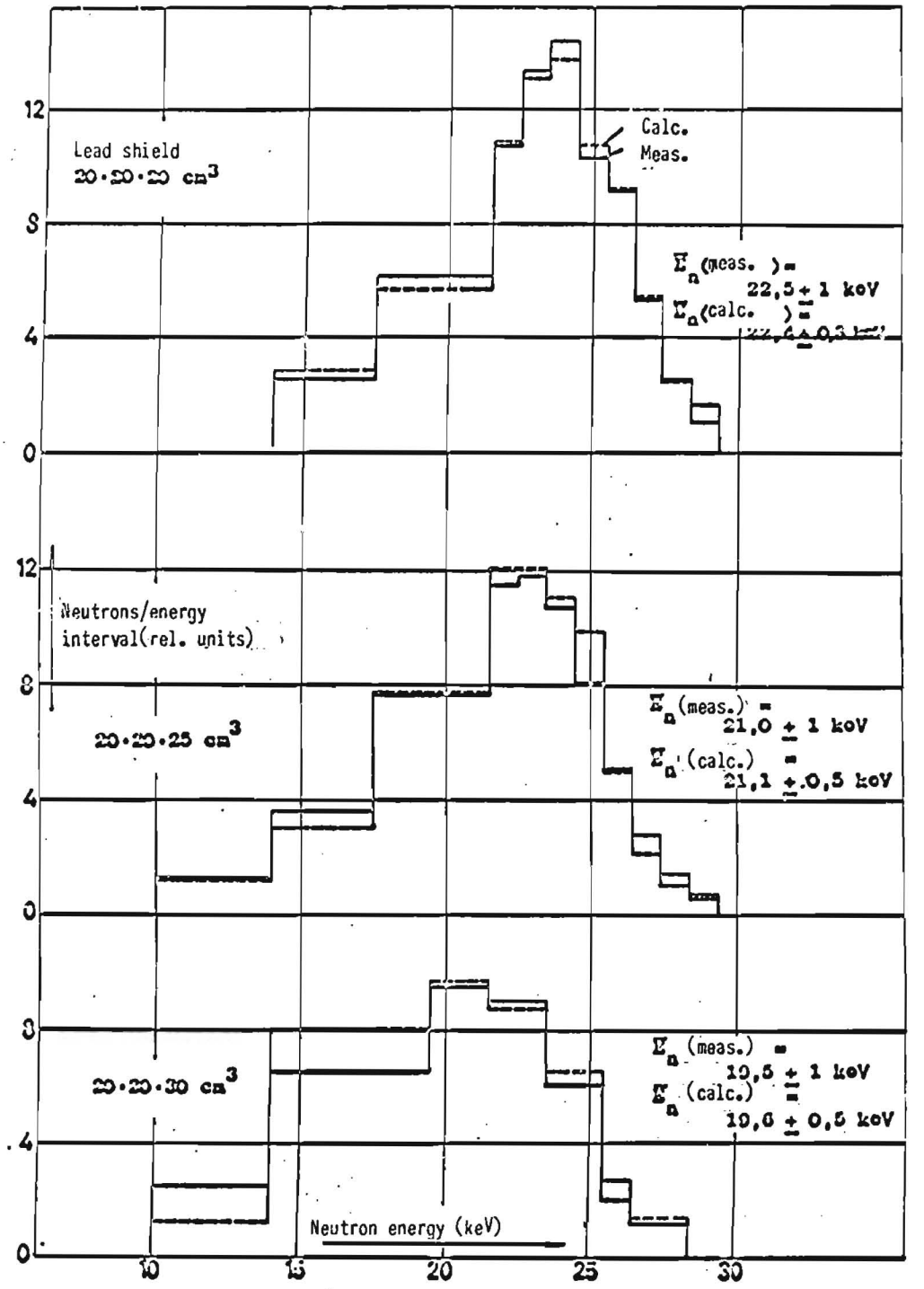

Fig. 42.--Measured and calculated leakage spectra for the three lead cubes.

measured leakage spectra amount to 1 keV if the error of 0.8 keV in the energy calibration is taken into account and an error in the flux values of 30% below 20 keV and of 10% above 20 keV, originating mainly from the γ-background, is taken into consideration.

The influence of some important parameters in the ph toneutron spectrum on the leakage spectra was investigated. The results can be summarized as follows:

The leakage spectra are very insensitive to changes in the form of the photoneutron spectrum, provided the mean energy and width are not modified. In particular, for example, for a symmetrical distribution, the same leakage spectra are obtained within the limits of error.

Leakage spectra are also relatively insensitive to changes in the photoneutron distribution width. The width must be changed by about ±1.5 keV to produce noticeable changes in the leakage spectra.

In contrast, every change in the mean photoneutron spectrum energy results in nearly the same changes in the mean leakage spectrum energies.

In Fig. 43, the photoneutron spectrum a_j, source spectrum and leakage spectrum of the smallest lead cube are compared. The mean energy of the photoneutron spectrum is 26.0 ± 1.3 keV and the width amounts to 3.5 ± 1.5 keV. These values should be compared with that of 22.8 ± 1.0 keV calculated according to (34) from the γ-energy of 1690.7 ± 0.4 keV [41] and the threshold energy of 1665.1 ± 0.6 keV [42], and with that measured by Schmitt [43] of 24.8 ± 2.4 keV for the mean photoneutron energy and the theoretical width of the photoneutron distribution of ±1.4 keV due to the center-of-mass displacement of the (Be^9+γ)-system, calculated according to (34).

The mean energy of the neutrons emitted by the source used here amounts to 24.4 ± 1.3 keV (the source spectrum was calculated from the photoneutron spectrum a_j by means of MONTE). Earlier published values of mean source neutron energies of 35 ± 10 keV [38], 24 ± 3 keV [39], 24.0 ± 2.4 keV [43] thus can be compared only conditionally because the energy losses caused primarily by beryllium are different.

The values of 363 ± 15 keV and (5.1 ± 1)% for the energy and intensity of the second neutron group confirm the values of 375 keV and 5.4% calculated by Tuttle [44]. The neutron group indicated at about 550 keV probably originates from the very weak 2.26 meV-Sb^{124}-γ-line which according to (34) would lead us to expect neutrons of 530 keV energy.

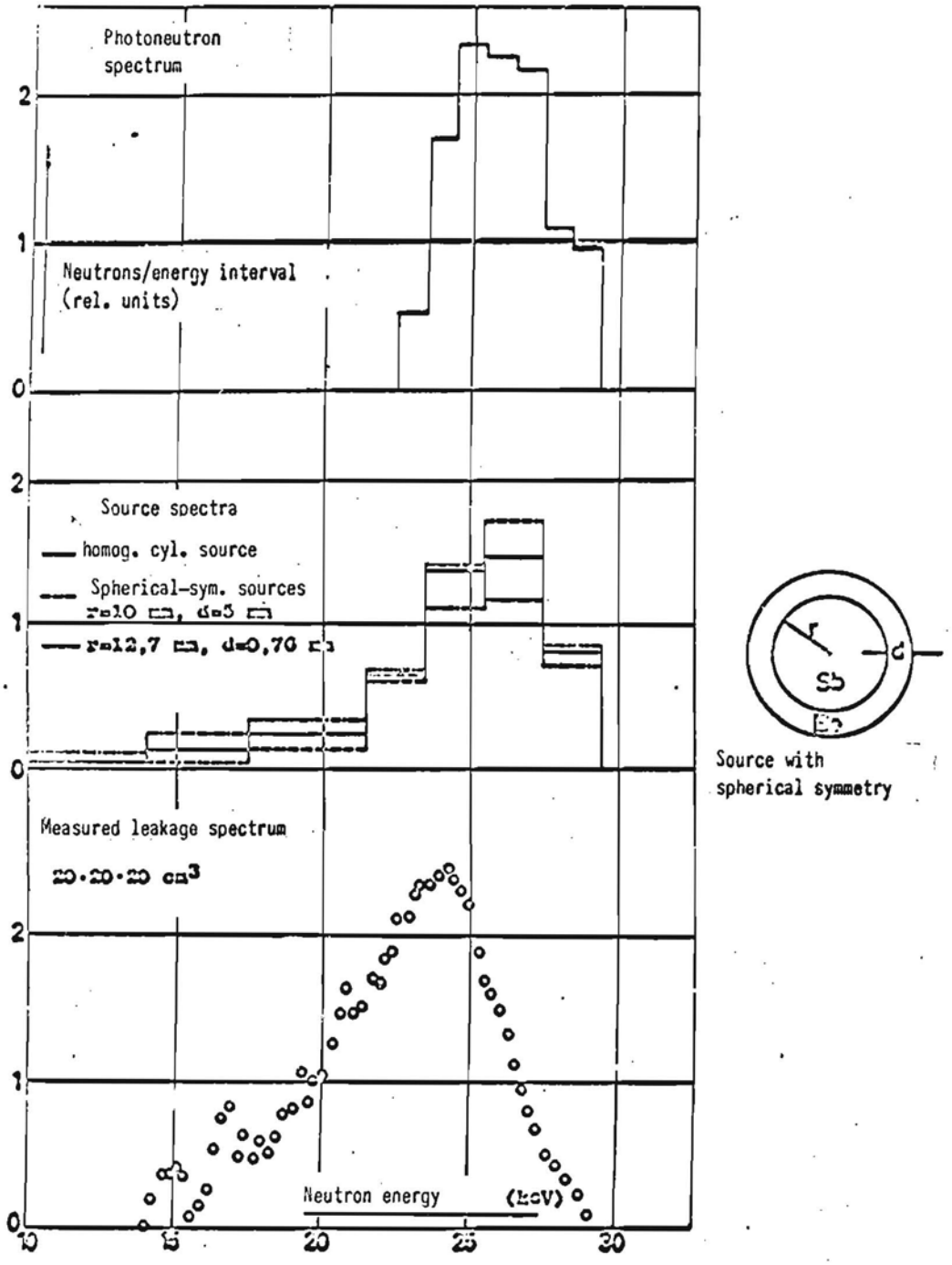

Fig. 43.--Comparison of photoneutron, source, and leakage spectrum.

4.3 Cf^{252}-Source

Since Cf^{252} has been available in sufficient quantities for some time, its γ-background is very insignificant and the neutron spectrum, in contrast to α,n-sources does not depend on secondary effects, such as the particle size of the powders used for the mixture, this spontaneously splitting isotope has become a convenient standard in neutron spectroscopy.

A number of spectrum measurements above about 1 MeV exists [9,10, 45,46] but they deviate by up to 50% from each other. More precise measurements below 500 keV were made by Meadows [47] with the time-of-flight method.

The source utilized here consisted of 1 µg Cf^{252} located in a small steel capsule (18 mm height, 7 mm diameter, 0.6 mm wall thickness, 90% of the interior filled with platinum) and at the time of the measurements, it had a source strength of about $1.7 \cdot 10^6$ n/sec. The spectrum was measured in the region of 60 keV to 6 MeV and is shown in Fig. 44. As in the case of the α,n-sources, the spectrum is plotted with respect to the unit of energy as well as of lethargy and the systematic errors discussed in 3.3.3 are indicated. The spectra of other authors have been normalized to the same area in the common energy region. Counter No. 2 was used above 1 MeV and counters No. 3 and 4 were used below this value (Table 6). The measuring time amounted to a total of about 7 h. The average statistical accuracy is about 5% as for the α,n-sources.

The spectrum determined here (per energy unit) drops somewhat more rapidly with increasing energy above 1 MeV than in most other studies [9,10,45,47], but in this range is in excellent agreement with the trend measured by Conde and During [46] (below 1 MeV, the errors of the spectrum measured by Conde and During are very large). In the tracing referred to the lethargy unit, the maximum of the spectrum measured here is about 0.3 MeV lower and in the energy region between about 200 keV and 1 MeV, there are more neutrons than in the spectrum reported by Meadows [47]. This leads to a mean neutron energy of about 2 MeV which is in good accord with the values of 2.12 and 2.05 MeV reported by Conde and During [46] as well as by Bonner [48], respectively, but is about 0.3 MeV lower than the values of other authors [45,47,49].

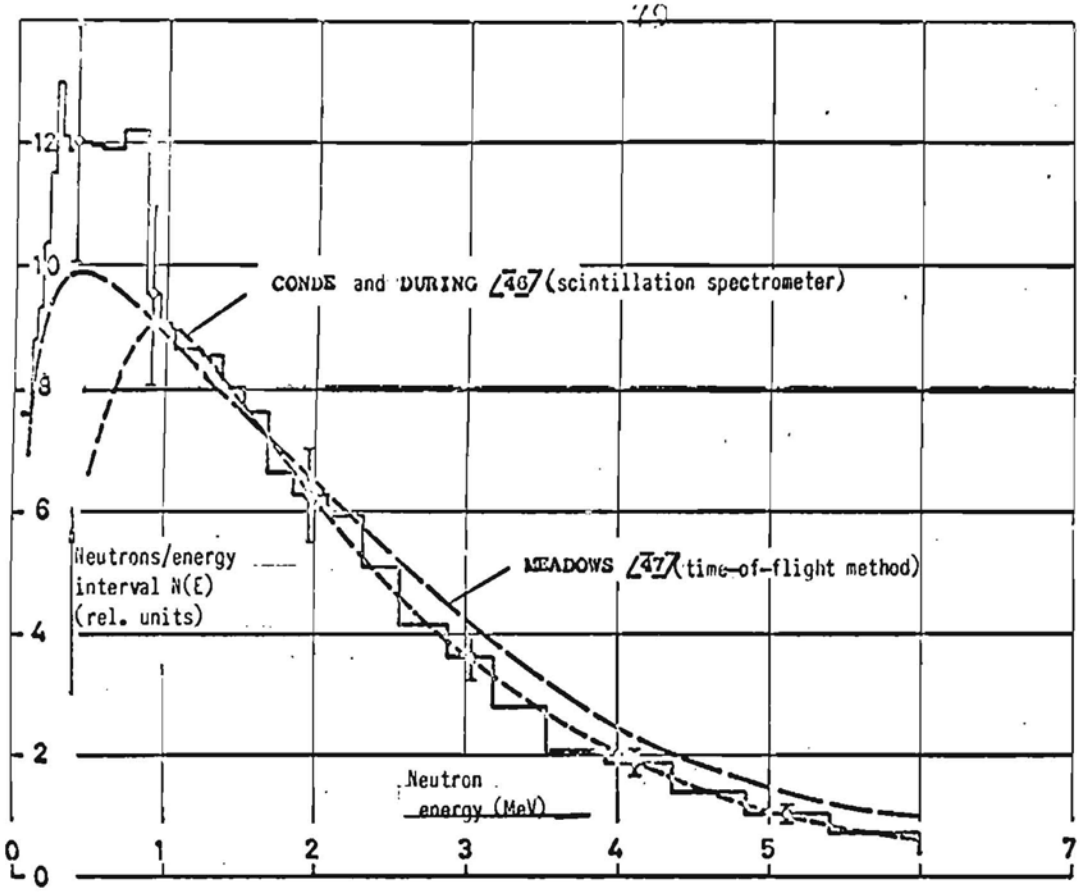

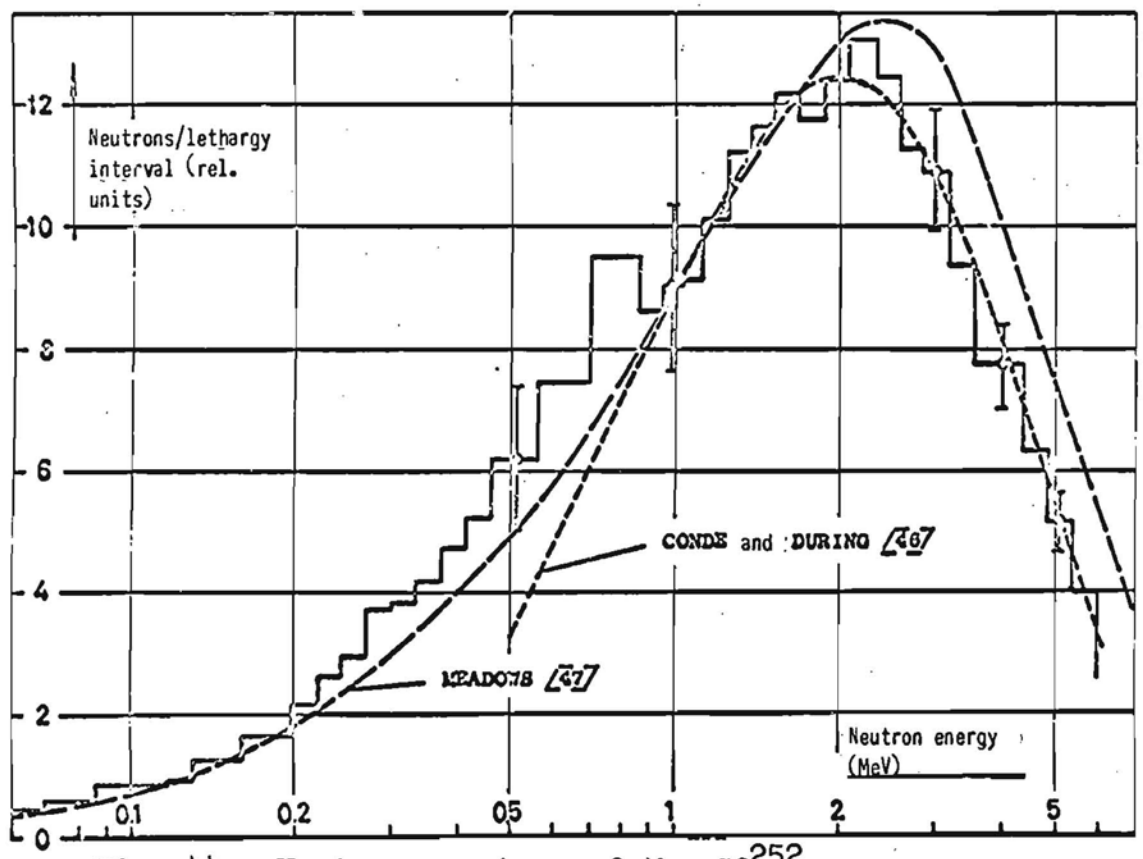

Fig. 44.--Neutron spectrum of the Cf^{252}-source.

Terell [50] showed that the fission spectrum at higher energies can be described by the relation:

$$N(E) \sim E^{1/2} \exp(-E/T) \tag{36}$$

As shown by Fig. 45, the experimental values above 1 MeV are in excellent agreement with this relation for T = 1.4 MeV. Conde and During [46] found T = 1.39 MeV, while the value of Meadows [47] with T = 1.592 MeV is clearly higher. Below 1 MeV, the experimental values are clearly above the theoretical curve, an effect which was also observed by Meadows but not in the measurements of Conde and During.

4.4 α,n-Sources

4.4.1 Theoretical background: Reactions of the type

$$^{A}_{Z}X + \alpha \longrightarrow {}^{A+3}_{Z+2}X + n + Q \tag{37}$$

are observed in many nuclei. The excitation energy occurring by absorption of a α-particle amounts to about 10 MeV and the energy of the (monoenergetic) α-particles of the radioactive isotopes used for neutron sources is about 5 MeV; since the binding energy of the last neutron of the compound nuclei varies between 2 and 20 MeV, exothermic (Q > 0) as well as endothermic (Q < 0) reactions occur.

Only the isotopes with the highest neutron yields are practically useful as targets for neutron sources. Table 8 lists the yields of the most common target materials measured with Po-α-particles [4].

Beryllium has the highest yield, followed by boron, fluorine and lithium. The yield of most other α,n-reactions is considerably smaller.

The neutrons produced by monoenergetic α-particles, referred to the CM-system, are also monoenergetic. Their energy is given by [1]:

$$E_n' = \frac{M_P}{M_P + M_n} \cdot E_\alpha \left(\frac{M_T}{M_T + M_\alpha} + Q \right). \tag{38}$$

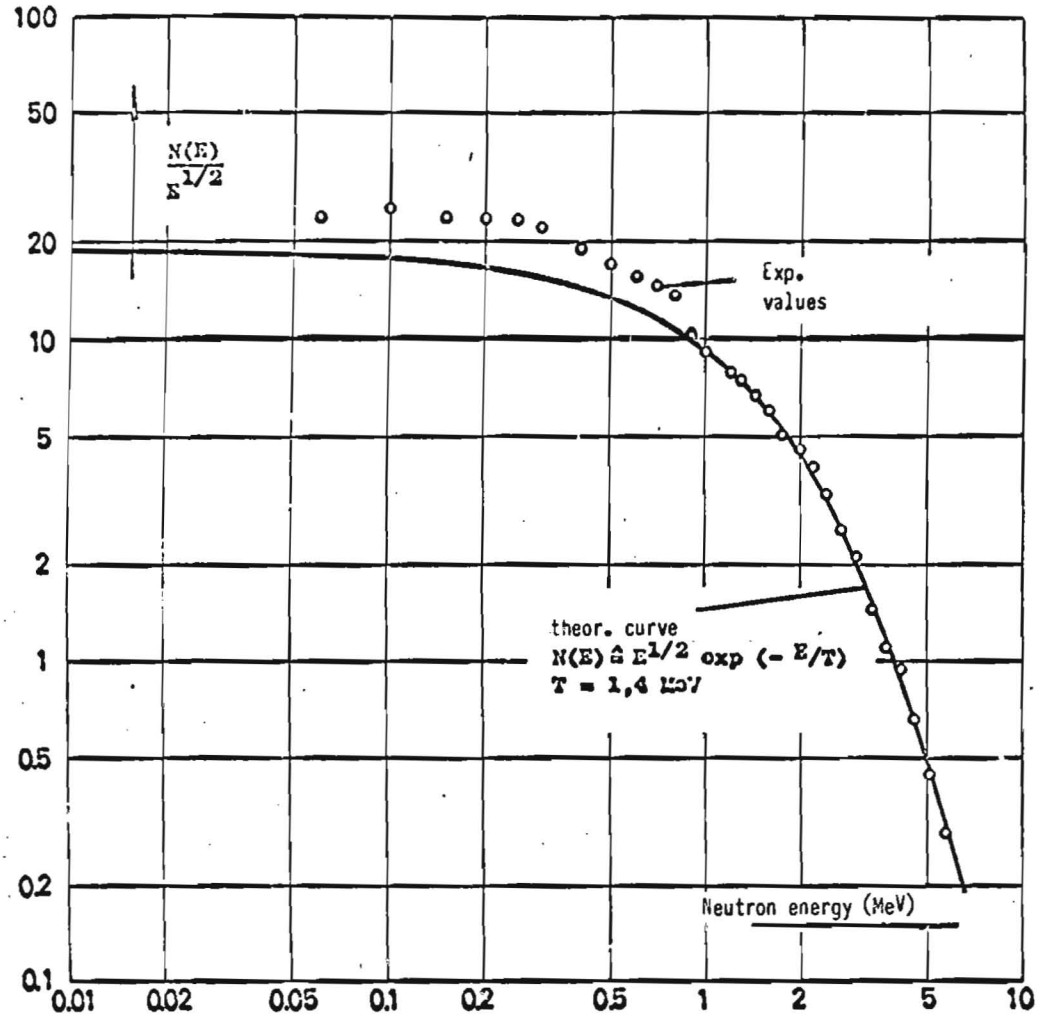

Fig. 45.--Comparison of the experimental Cf^{252}-spectrum with a theoretical spectrum (36).

Table 8.--Measured yields for common α,n-sources (Po-α-particles, thick targets); from [4].

Target	Reaction	Yield (neutrons/10^6 α-particles)
Be	$Be^9 + \alpha \rightarrow C^{12} + n + 5{,}7$ MeV	80
B	$B^{10} + \alpha \rightarrow N^{13} + n + 1{,}07$ MeV $B^{11} + \alpha \rightarrow N^{14} + n + 0{,}158$ MeV	24
CaF_2	$F^{19} + \alpha \rightarrow Na^{22} + n - 1{,}03$ MeV	5
Li	$Li^7 + \alpha \rightarrow B^{10} + n - 2{,}79$ MeV	2,6

M_T, M_F and M_n are the masses of the target nucleus, product nucleus and of the neutron, E_α is the α-particle energy and Q is the reaction energy. In contrast, the (measured) energy in the laboratory system depends on the angle between neutron and α-particle and can be calculated from (38) by an angular transformation. If the angular distribution is known, the energy distribution in the laboratory system can therefore be calculated.

The α-particles of the radioactive isotopes used for neutron sources are practically monoenergetic. Most α-particles of a radioactive neutron source lose their entire energy by ionization. Very few (Table 8) produce a α,n-reaction during this slowing-down process. The neutron spectrum generated as a result can be calculated with a knowledge of the (energy-dependent) α,n-cross section $\sigma_{n,\alpha}(E_\alpha)$, the specific α-particle energy loss $dE_\alpha(E_\alpha)/dx$ in the source material and of the disintegration mechanism of the compound nucleus forming by absorption of the α-particle. Hess [1] has made such calculations for a few important α,n-sources. The agreement of the spectra calculated in this manner with measured spectra is very mediocre in most cases, however, because the data necessary for the calculation are not known with sufficient accuracy and neutron scattering processes can modify the spectrum noticeably, particularly with large sources.

Since the energies of the α-particles of the radioactive isotopes used most commonly (Am^{241} 5.46 MeV, Po^{210} 5.3 MeV, Pu^{239} 5.13 MeV) differ little, the neutron spectra for the same target material generally are entirely comparable.

4.4.2 Am-Li-source: Most of the neutrons of this source are furnished by the Li^7 present with an abundance of 92.5% by the reaction:

$$Li^7 + \alpha \longrightarrow B^{10} + n - 2{,}79 \text{ MeV} , \qquad (39)$$

which represents the back-reaction of the well-known $B^{10}(n,\alpha)Li^7$-reaction. This reaction has a very well defined threshold at 4.379 MeV and the ground state is the only one energetically possible for the residual nucleus B^{10}. The threshold of the $Li^6(\alpha,n)$-reaction amounts to about 6.64 MeV, and this reaction therefore furnishes no neutrons [4].

The Am-Li source (fabricated by Amersham, Buckinghamshire, England) consisted of a homogeneous mixture of AmO_2(3C) and LiH (10 g) and had a source strength of $1.1 \cdot 10^5$ n/sec. The source material was placed into a cylindrical steel capsule (22.4 mm diameter, 48.5 mm height, 2.4 mm wall thickness).

The measured neutron spectrum is shown in Fig. 46. Above 500 keV, we used counter No. 5 and below this value, counter No. 4 (Table 6) as well as a hydrogen-filled spherical counter. The total measuring time amounted to about 5 h.

The spectrum measured here is in excellent agreement with that of an Am-Li-source determined by Bennett [50] also with proton recoil counters, but it differs considerably from the spectrum of a Po-Li-source determined with a cloud chamber by Barton [51] and that calculated by Hess [1] for a Po-Li-source. The energy of the Am-α-particles is higher by about 180 keV than that of the Po-α-particles. Accordingly, the spectrum measured here extends to about 1.6 MeV, while according to the calculation of Hess, no neutrons can be expected any longer above 1.3 MeV for a Po-Li-source. The theoretical spectrum of Hess as well as the measurements of Bennett and the spectrum measured here result in a mean neutron energy of 500 keV which is in good agreement with the value of 480 keV determined experimentally by Hess for a Po-Li-source, while a mean neutron energy of 250 keV was measured for the source utilized by Barton [52].

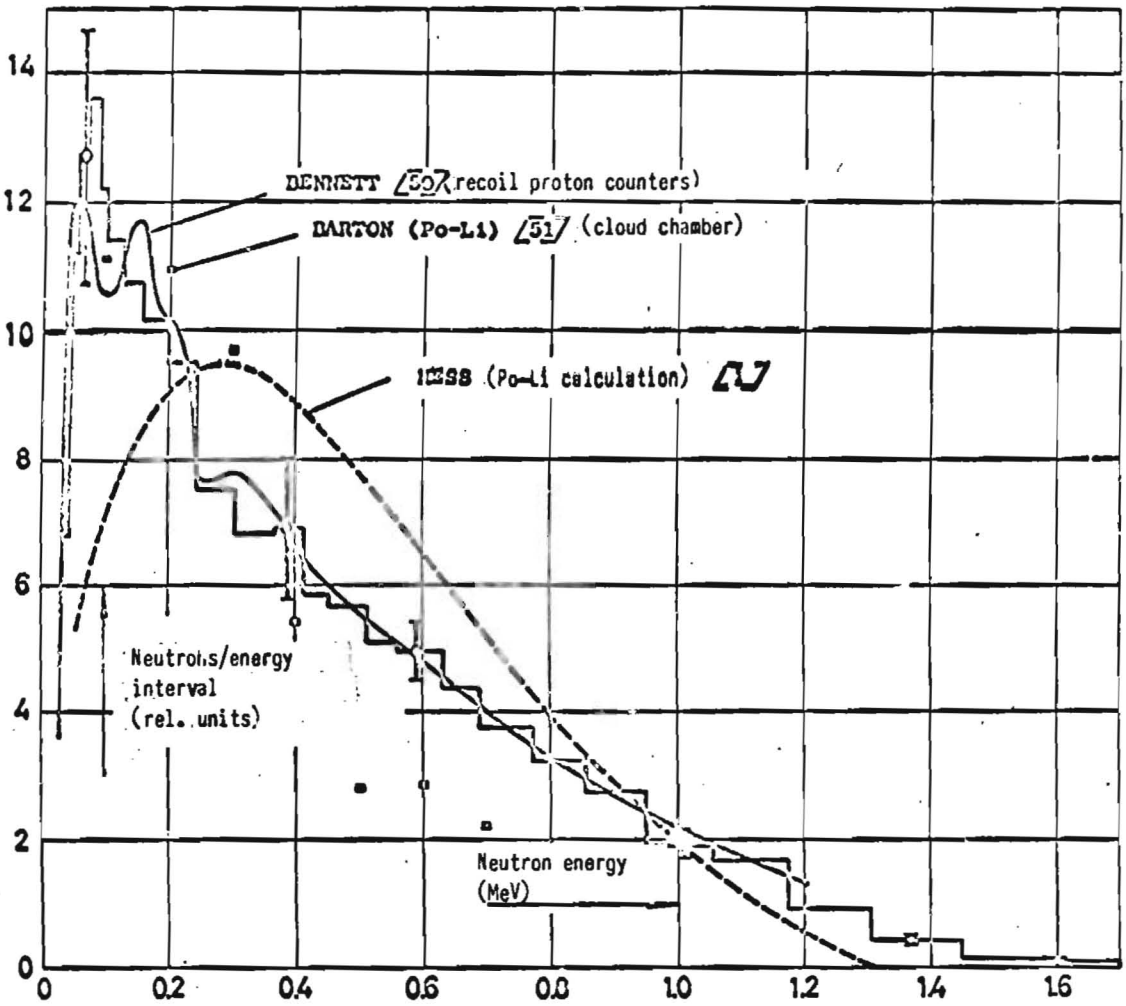

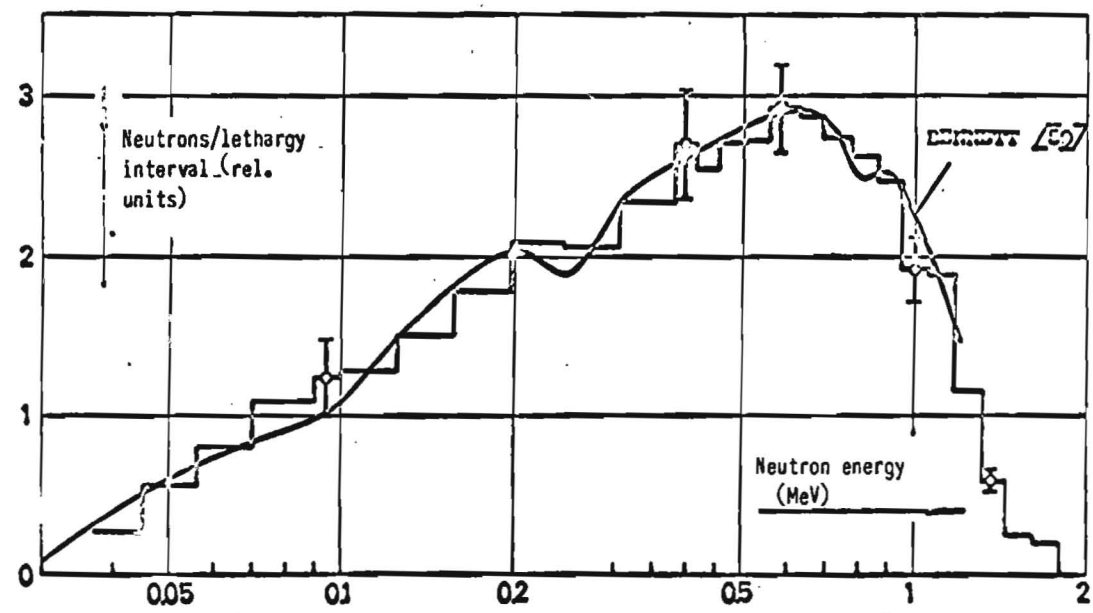

Fig. 46.--Neutron spectrum of the Am-Li source.

4.4.3 Am-F-source: This source is based on the following reaction:

$$F^{19} + \alpha \longrightarrow Na^{22} + n - 1{,}020 \text{ MeV} . \qquad (40)$$

The neutron spectrum is simple and considerably softer than that of Am-Be-sources and since the yield is relatively high, Am-F-sources are frequently used when high-energy neutrons are undesirable.

Spectrum measurements of Am-F-sources have not been published thus far, although a number of measurements concerning PuF_4- and Po-F-sources are available but only in the energy region above 500 keV.

The Am-F-source (fabricated by Amersham, Buckinghamshire, England) consisted of a homogeneous mixture of AmO_2(3C) and CaF_2(19 g) and had a source strength of about $4.6 \cdot 10^5$ n/sec. The source material was placed into a cylindrical steel capsule (22.4 mm diameter, 48.5 mm height, 2.4 mm wall thickness).

The measured neutron spectrum in the region of 50 keV to 3.2 MeV is shown in Fig. 47. Counter No. 2 was used above 800 keV, while counter No. 4 (Table 6) and a hydrogen-filled spherical counter was used below this value. The total measuring time amounted to about 10 h.

The spectrum of the Am-F-source is in good agreement with the measurements of Szilvasi, Geiger and Dixon [53] for a Po-F-source, but deviates noticeably from the spectrum of a Pu-F_4-source measured by Lehman [54]. In accordance with the different α-energies (Am-α 5.48 MeV, Po-α 5.30 MeV, Pu-α 5.12 MeV), the high-energy neutron contribution is somewhat greater in the Am-F-source than in the Po-F-source and considerably greater than in the Pu-F_4-source. The maximum in the neutron spectrum measured here at 1.35 MeV falls between the values of the Po-F-source (1.2 MeV) and the PuF_4-source (1.5 MeV). The neutron peak found at about 900 keV by Lehman is not present in the other two spectra, but in the Am-F-spectrum, a peak can be clearly recognized at about 400 keV which contradicts the assumption of a continuous drop below 500 keV of Lehman. The high low-energy neutron contribution confirms the results of n-γ-coincidence measurements with the Po-F-source [53] indicating that a considerable part of all transitions in the Na^{22}-residual nucleus leads to excited levels.

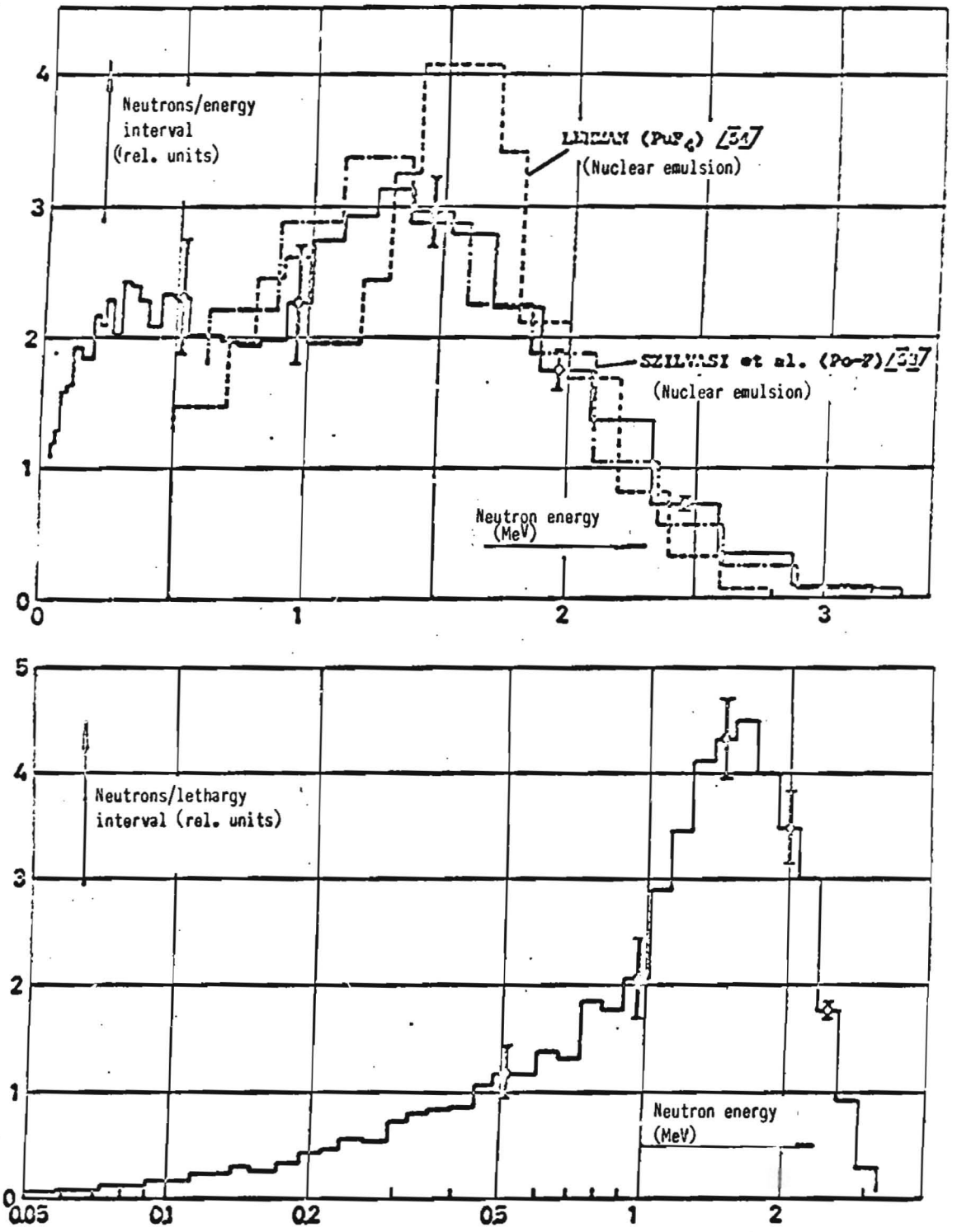

Fig. 47.--Neutron spectrum of the Am-F source.

4.4.4 Am-B^{10}-source: The Am-B^{10}-source is based on the reaction:

$$B^{10} + \alpha \longrightarrow N^{13} + n + 1{,}07 \text{ MeV} \qquad (41)$$

Geiger and Jarvis [15] determined the spectrum of a Po-B^{10}-source above 400 keV; measurements for Am-B^{10}-sources have not been published thus far.

The source (fabricated by Amersham, Buckinghamshire, England) consisted of a homogeneous mixture of AmO_2(2C) and B^{10} (13.2 g, 96%) and had a source strength of about $4.3 \cdot 10^5$ n/sec. The source material was placed into a cylindrical steel capsule (22.4 mm diameter, 48.5 mm height, 2.4 mm wall thickness).

Fig. 48 shows the measured neutron spectrum of the Am-B^{10}-source. Counter No. 2 was used above 1 MeV and counters No. 3 and 4 (Table 6) as well as a hydrogen-filled spherical counter was used below this value. The total measuring time amounted to about 20 h.

Above about 600 keV, the Am-B^{10}-spectrum is in good agreement with that of Po-B^{10}-sources [15], although the maximum at about 3 MeV is somewhat more pronouced in the Po-B^{10}-spectrum. Below 600 keV, the spectrum measured here clearly indicates more neutrons than would be expected by an extrapolation of the Po-B^{10}-spectrum.

Hess [1] calculated the spectrum of a Po-B^{10}-source with the assumption that all transitions lead to the ground state of the N^{13}-nucleus and accordingly, he obtained a very simple neutron spectrum with a maximum at 4 MeV. The measurements of Geiger and Jarvis [15] as well as those made here show, however, that the neutron spectrum is considerably more complicated and that transitions to higher excited states of the N^{13}-residual nucleus also occur. Geiger and Jarvis concluded from the shape of the neutron spectrum measured by them that about one-third of all transitions leads to the ground state and to the next two excited levels of the N^{13}-nucleus; it is true that the estimate for the occupation of the second excited level is essentially based on the course of the neutron spectrum below 1 MeV where its measurement undoubtedly is no longer very reliable. It follows from the spectrum measured here that about 40-50% of all transitions lead to the second excited level and the rest is approximately equally distributed over the ground state and the first excited state in agreement with the findings of Geiger and Jarvis.

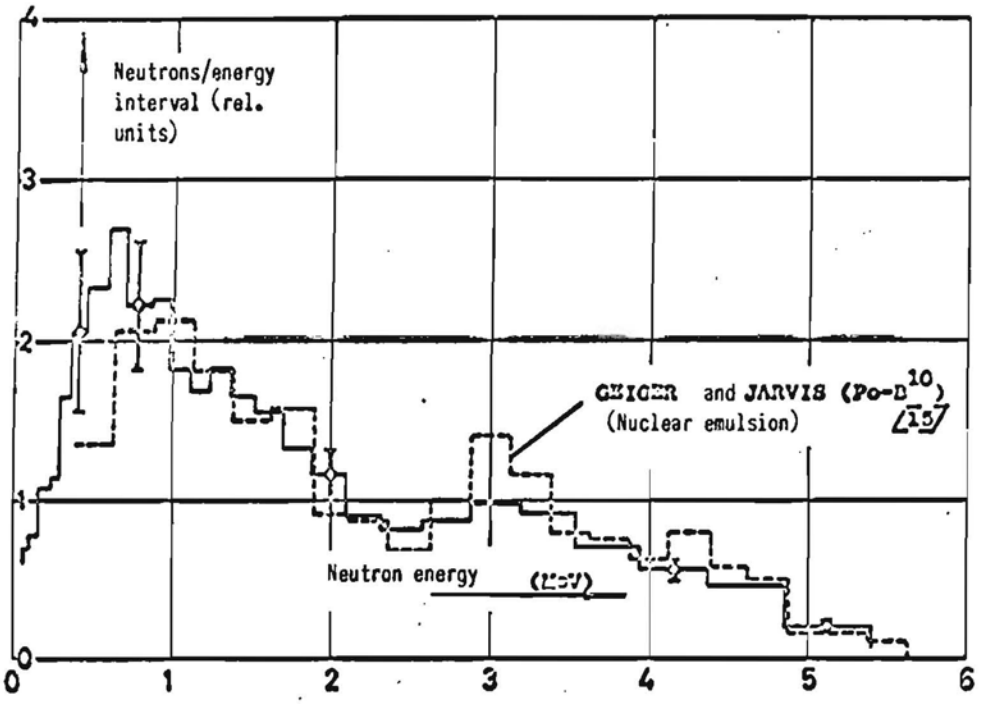

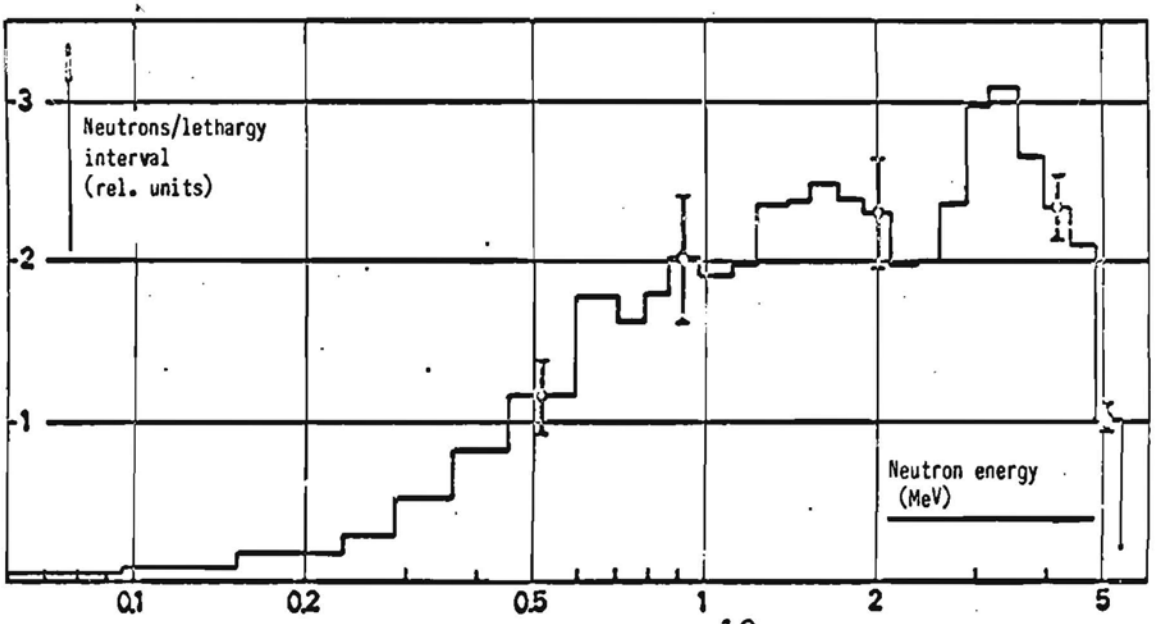

Fig. 48.--Neutron spectrum of the Am-B^{10} source.

4.4.5 Am-B-Source: Approximately 95% of all neutrons of Am-B-sources with a natural boron composition (19% Be^{10}, 81% B^{11}) originate from the reaction:

$$B^{11} + \alpha \longrightarrow N^{14} + n + 0{,}158 \text{ MeV} . \qquad (42)$$

The spectra of B (natural composition) and of B^{11}-sources consequently differ little. A number of spectrum measurements exist for Po-B-sources above about 500 keV and one measurement has been made by Bluhm and Stegemann [13] for the Am-B-sources utilized here by means of a Li^6-semiconductor spectrometer, but also only in the energy region above 500 keV. All authors found that the spectrum above 500 keV essentially consists of one peak with a maximum between 2.5 and 3.0 MeV, although the measured widths of this neutron distribution vary between 1.5 and 3 MeV, particularly in the older studies.

The source utilized here (fabricated by Amersham, Buckinghamshire, England) consisted of a homogeneous mixture of AmO_2(2C) and B(14.2 g) of natural composition and had a source strength of $1.2 \cdot 10^6$ n/sec. The source material was contained in a cylindrical steel capsule (22.4 mm diameter, 48.5 mm height, 2.4 mm wall thickness). The total measuring time amounted to about 20 h.

Fig. 49 shows the measured neutron spectrum together with the measurements of Bluhm and Stegemann [13] and those of Geiger and Jarvis [15] for a Po-B-source. The measurements of Geiger and Jarvis are in good agreement with those made here; the maximum of the neutron distribution is found at about 3 MeV in both. The spectrum measured by Bluhm and Stegemann, in contrast, is considerably harder and the maximum of the spectrum and mean neutron energy are about 0.5 MeV higher than in the other two measurements. Since the difference in the α-energies of Am and Po lead us to expect a difference in mean neutron energies of only about 100 keV, it may be assumed that the extremely high mean neutron energy of the spectrum measured by Bluhm and Stegemann compared to other measurements is attributable to uncertainties in energy calibration or in the sensitivity of the Li^6-spectrometer.

Measurements below 500 keV have not yet been published; the calculated spectra of Geiger and Jarvis [15] and of Hess [1] decrease continuously from 500 keV to zero energy. However, in this region,

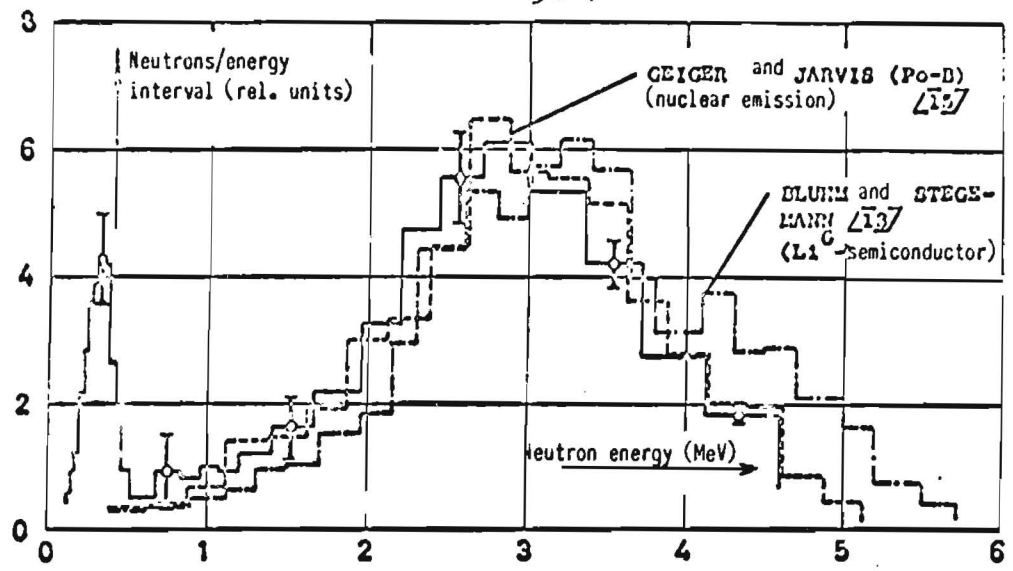

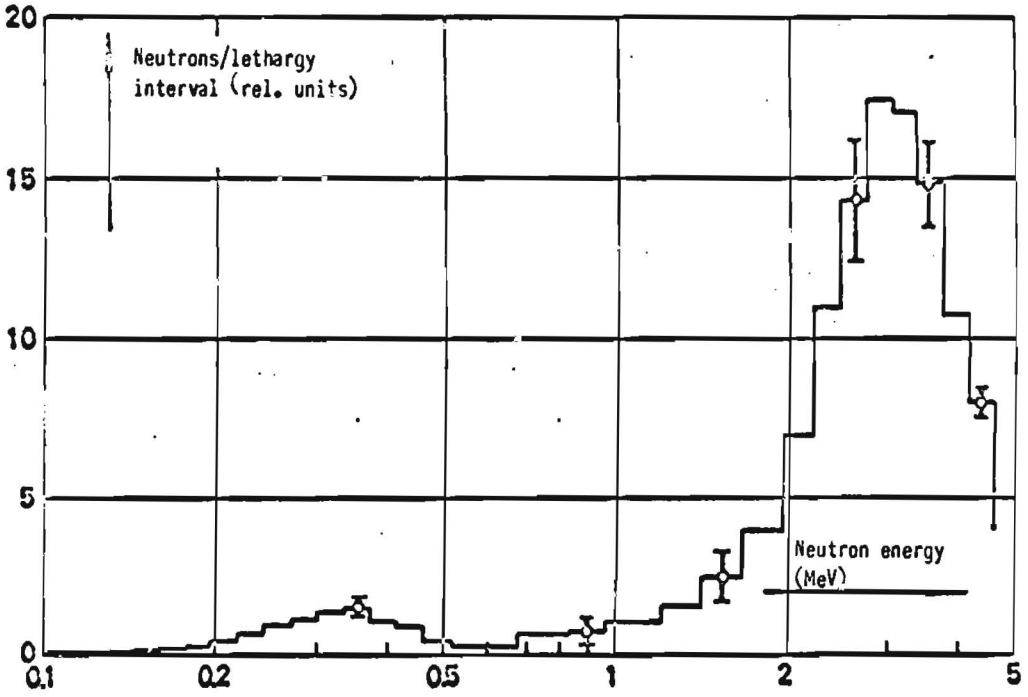

Fig. 49.--Neutron spectrum of the Am-B source.

the measurement shows a sharp peak with a maximum at about 340 keV, amounting to about 8% of the total neutron intensity. The disintegration mechanism on which this peak is based is still not clear. It is known from n,γ-coincidence measurements with Po-B-sources [15], that transitions to the first excited level (2.312 MeV) occur with a probability of about 5% in addition to the transitions into the ground state of the N^{14}-nucleus which lead to the maximum at about 3 MeV in the neutron spectrum. Transitions to this excited level, however, should result in a neutron distribution with a maximum at about 1 MeV according to the calculations of Geiger and Jarvis. It is true that the position of the maximum in the calculated spectrum depends on the nuclear data utilized which are still extensively unknown. Transitions to the second excited level of the N^{14}-nucleus (3.945 MeV) are energetically possible already with Po-α-particles, but could not be detected in the n,γ-coincidence measurements. Transitions to this level would lead to a neutron peak with a maximum corresponding approximately to the measured neutron peak energy.

4.4.6 Am-Be-sources: The reaction

$$Be^{9} + \alpha \longrightarrow C^{12} + n + 5{,}700 \text{ keV} \qquad (43)$$

is by far the most frequently used for neutron sources since it furnishes the highest neutron yield with radioactive α-emitters (Table 8). Until a few years ago, Po^{210}, Pu^{239} or Ra^{226} were usually used as α-emitters. However, Ra^{226} has a very intense high-energy γ-radiation, Po^{210} is very short-lived (138 d) and Pu^{239} has a very long half-life ($2.4 \cdot 10^{4}$ y) and therefore relatively large quantities are needed. Since Am^{241} is available in sufficient quantities, it is used most commonly since it has a convenient half-life (458 [?] y) and emits only low-energy gammas.

The trend of the neutron spectrum above approx. 2 MeV is fairly well known and has also been elucidated theoretically in its basic principles on the basis of nuclear data. Essentially, it consists of two peaks at 3 MeV and 4 MeV which are produced by transitions into the ground state and the first excited state (4.43 MeV) of the C^{12}-residual nucleus [1]. However, measurements with good resolution show that these two main peaks are again each composed of individual peaks. This fine structure has also been explained theoretically

by the anisotropic neutron emission of the C^{12}-residual nucleus [55]. However, this fine structure in particular depends highly on the energy losses of the α-particles in the radioactive material and on neutron scattering processes in the source material [1, 55] and is therefore manifested to a different degree for different sources. Below 1.5 MeV, no spectral measurements with $Be^9(\alpha,n)$-sources have been made as far as we know, although this energy region is of great interest for some applications, especially for importance measurements and Hess [1] has already suspected the presence of a neutron peak in it.

Geiger and Hargrove [56] determined a relative neutron contribution of 17% below 1.5 MeV from the source strength and the absolute measured spectrum above 1.5 MeV which is in good agreement with the value found by St. Romain et al. [57] with the counter ratio technique. The mean neutron energy of the postulated low-energy peak of 0.33 MeV determined experimentally by St. Romain et al. indicates that the low-energy neutrons originate primarily from the reaction:

$$Be^9 + \alpha \longrightarrow Be^{9*} + \alpha' \longrightarrow Be^8 + \alpha' + n \qquad (44)$$

Three different sources with the following specifications were used:

Am-Be(5C) (Fabricated by Amersham, Buckinghamshire, England): Homogeneous mixture of AmO_2 (5C) and Be (40 g) in a steel capsule (30 mm diameter, 60 mm height, 2.4 mm wall thickness); source strength of 10^7 n/sec.

Am-Be (0.4 C) (Fabricated by Amersham, Buckinghamshire, England): Homogeneous mixture of AmO_2 (0.4 C) and Be (4.4 g) in a steel capsule (22.4 mm diameter, 48.5 mm height, 2.4 mm wall thickness); source strength of $1.1 \cdot 10^6$ n/sec.

Am-Be (1.5 C) (Fabricated by Institute for Transuranium Elements, Gesellschaft für Kernforschung mbH, Karlsruhe): (Inhomogeneous) mixture of (coarse) AmO_2 (1.5 C) and Be (2g) in a steel capsule (12 mm diameter, 20 mm height, 1 mm wall thickness; source strength of $1.3 \cdot 10^6$ n/sec. We intentionally dispensed with homogeneity.

The three measured spectra are shown in Figs. 50-52 together with the results of Geiger and Hargrove [56] and of Cloth and Hecker [9]. Above 3 MeV, measurements were made with counter No. 1 and below it, with counters Nos. 3 and 4 (Table 6). The measuring time amounted to about 20 h for the Am-Be(5C)-source and to about 60 h each for the two weak sources.

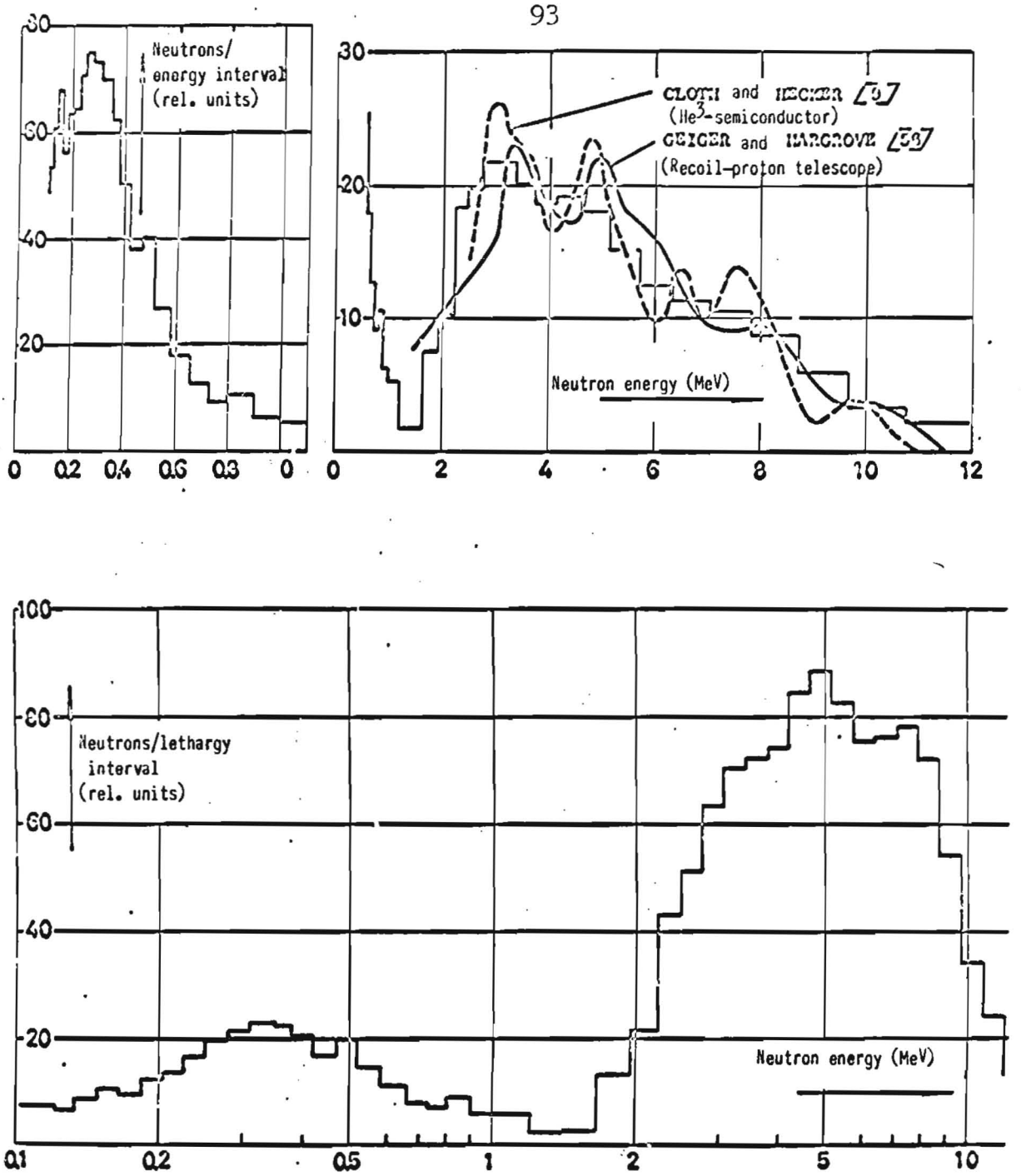

Fig. 50.--Neutron spectrum of the Am-Be(50)-source.

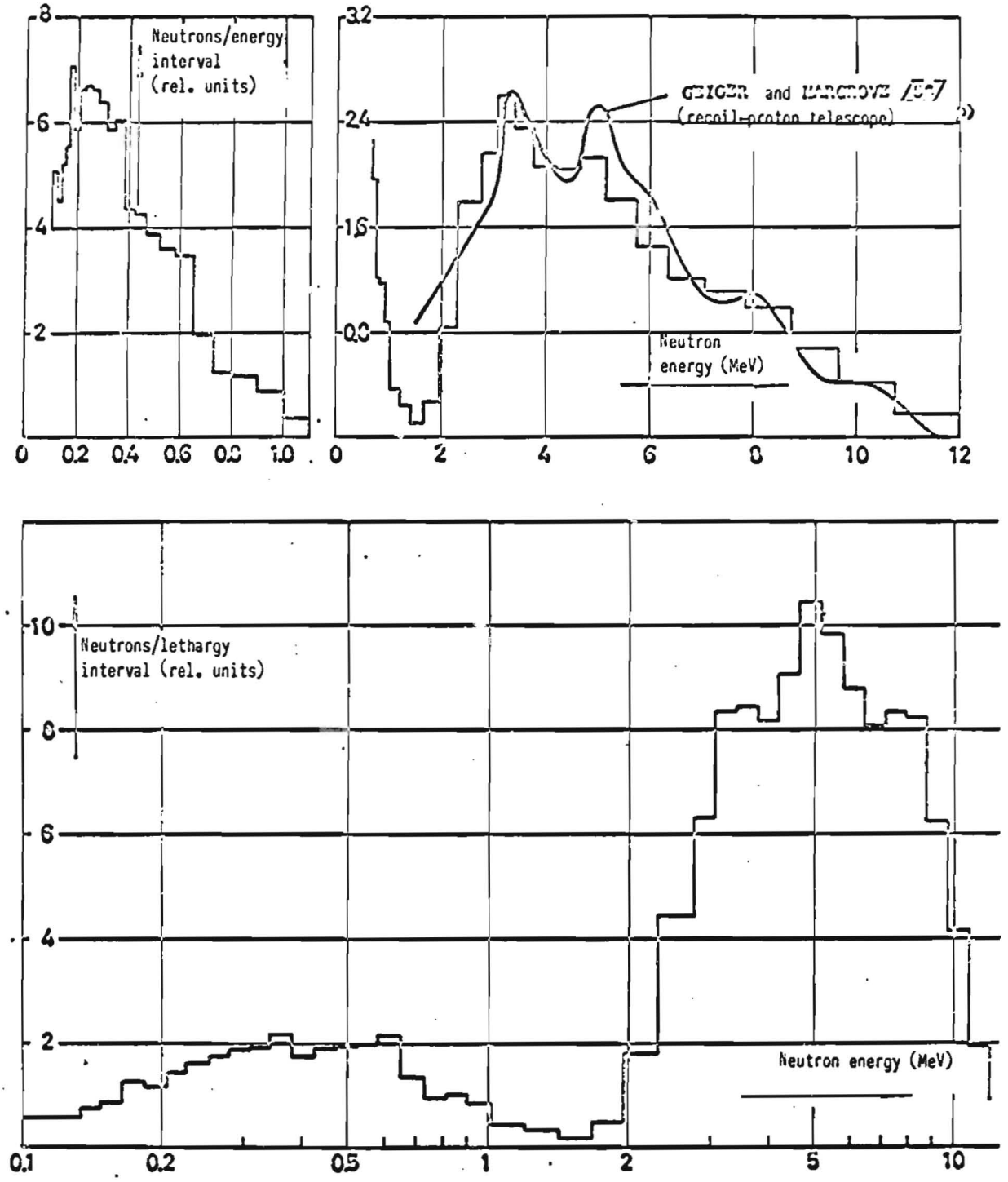

Fig. 51.--Neutron spectrum of the Am-Be (0.4 C)-source.

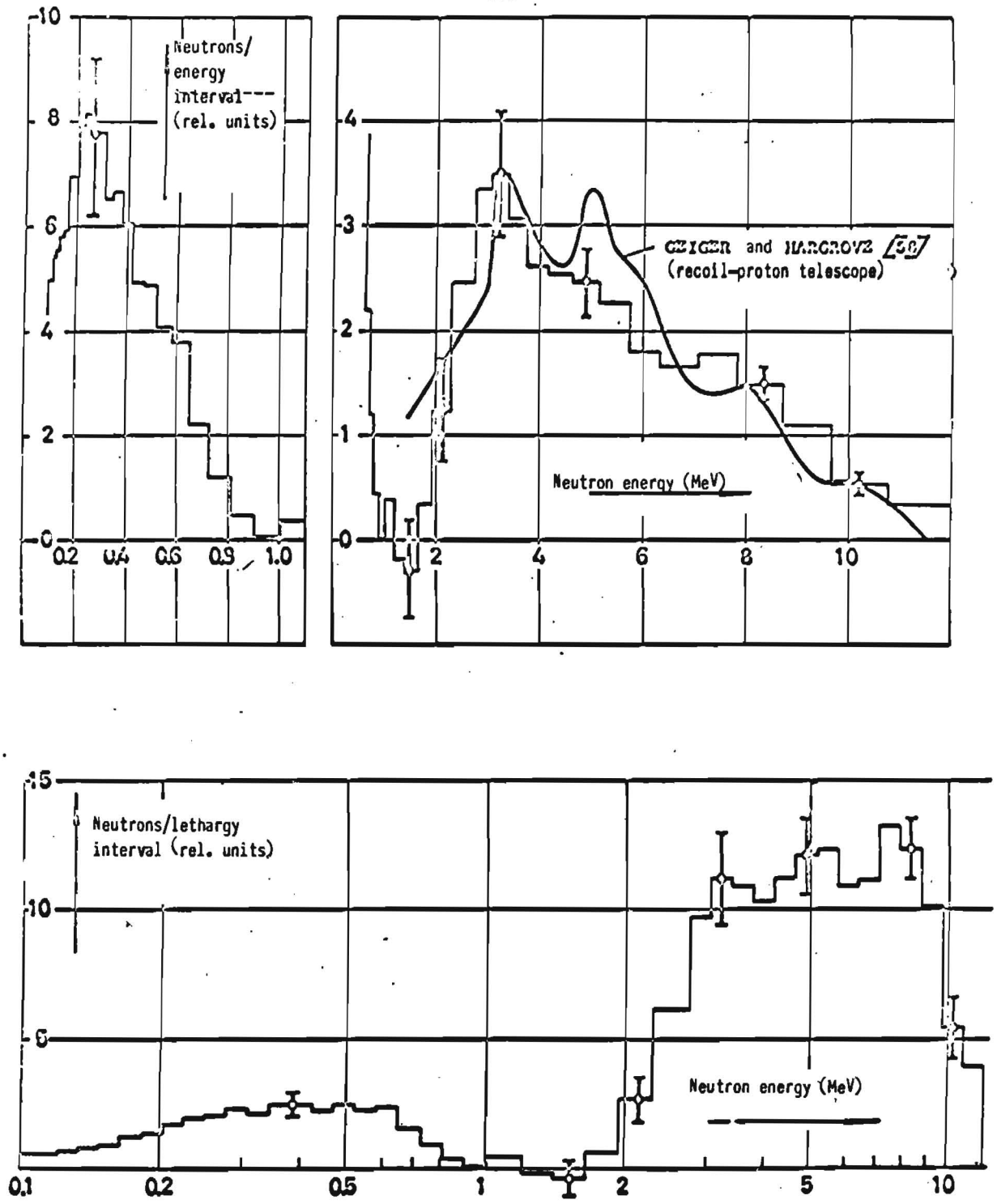

Fig. 52.--Neutron spectrum of the Am-Be (1.5 C)-source.

In their general trend above 2 MeV, the spectra measured here are in agreement with the two comparison spectra but extend to somewhat higher energies and do not have as pronounced a fine structure. The reason for this energy shift presumably resides in inaccuracies of about ±5% in the energy calibration because of the mediocre energy resolution of 20% of the counter used in this region (No. 1, Table 6) and the relatively low energy of the He^3-calibration peak. Although particularly coarse active material was used in the Am-Be (1.5 C)-source and homogeneity was neglected, the fine structure surprisingly is somewhat more defined than in the other two sources. To investigate whether the source spectra already have a weakly defined fine structure or whether the fine structure is lost because of the poor counter resolution, the 3-6 MeV region was measured in addition with counter No. 2 (Table 6) which has an energy resolution of about 5%. The result is shown in Fig. 53. From the clear definition of the minimum between the peaks at 3 and 5 MeV in the spectrum with 5% resolution, we recognize that the fine structure of the source utilized here is comparable to that of other sources and is smeared by the mediocre energy resolution of counter No. 1 (Table 6).

In the various studies on Am-Be-source spectra, the spectrum of only one source was usually measured and the very extensive discrepancies found in some of the spectra measured by different authors were then attributed to differences in the source spectra. For this reason in particular, the spectra of three different sources were determined with the same method here. Fig. 54 shows a comparison of the measured spectra above 3 MeV. The spectra of the Am-Be(5C)- and the Am-Be(0.4 C)-sources are identical within the statistical limits of error of about 5% each. The Am-Be(1.5 C)-source, in contrast, definitely has fewer neutrons between 3 and 5 MeV and more between 7 and 10 MeV than the other two sources. This is to be expected, for the α-particle energy distribution in the source is shifted toward lower energies as a result of the coarse granulometry and transitions to the ground state of the C^{12}-nucleus are consequently favored.

All three spectra show an intense peak at about 400 keV and a pronounced minimum at about 1.5 MeV. The neutron contribution below 1.5 MeV amounts to (22 ± 5) % in the Am-Be(5C)- and the Am-Be(0.4 C)-source and to (18 ± 5) % in the Am-Be(1.5)-source, which is in

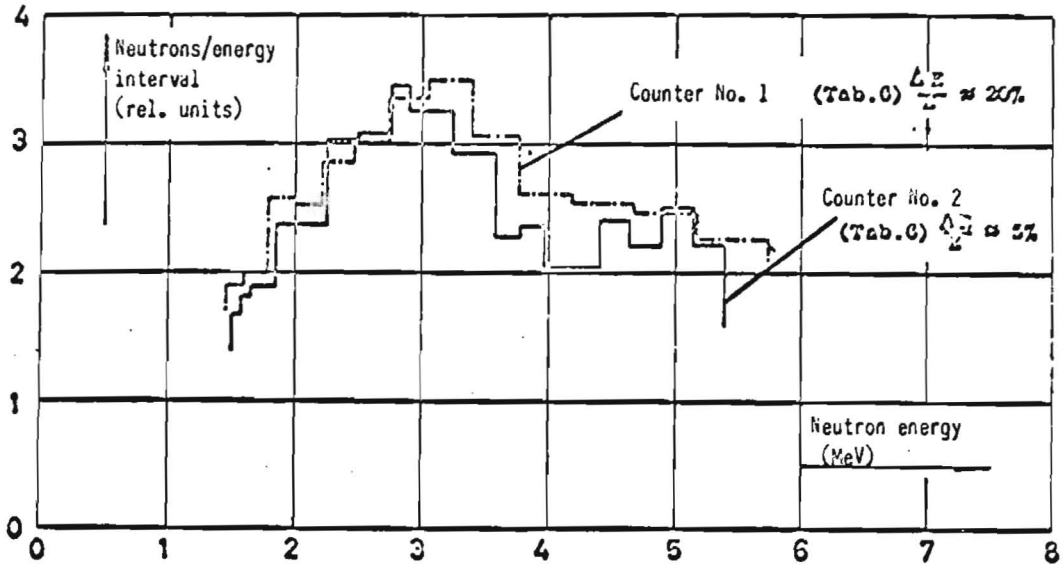

Fig. 53.--Fine structure of the Am-Be sources (Am-Be (1.5 C)).

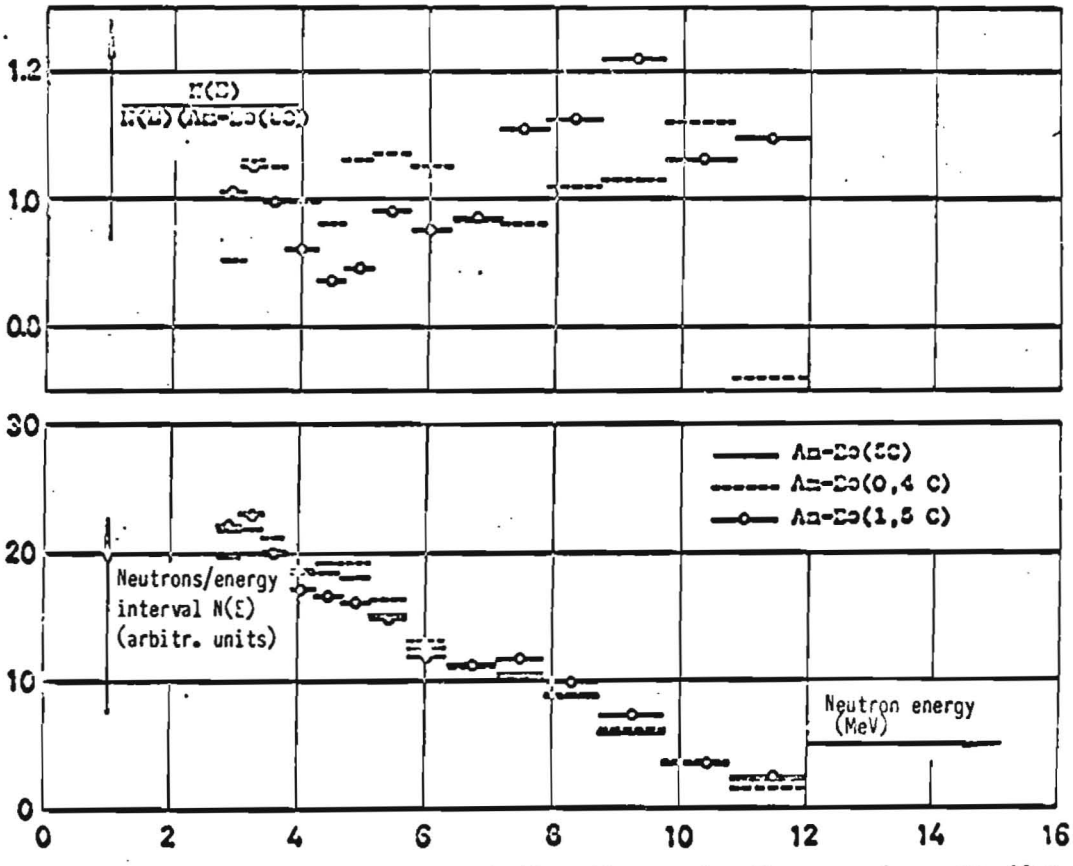

Fig. 54.--Comparison of the three Am-Be-spectra on the range of 3 MeV - 12 MeV.

agreement with the values of other authors within the relatively broad limits of error [56,57]. The Am-Be(1.5 C)-source clearly has fewer low-energy neutrons than the other two sources (this conclusion is possible in spite of the wide limits of error because the systematic errors are identical in the three spectra); this is confirmed by other measurements [58]. The mean energy of the low-energy peak of about 400 keV is in agreement with the value measured by St. Romain et al. [57] and thus supports their interpretation.

4.4.7 Ra-Be-source: The neutrons of Ra-Be-sources are produced by the same reaction (43) as those of Am-Be-sources. The relatively small differences in the spectra of these two sources are primarily the result of the occurrence of several α-groups with energies between 4.8 and 7.7 MeV in the Ra-disintegration scheme.

Spectrum measurements with Re-Be-sources are very difficult, particularly in the lower energy region, because of the high-energy and approximately one thousand times more intense γ-background compared to Am-Be-sources. Some measurements in the energy region above about 2 MeV have been published but they show pronounced discrepancies in some cases [1]. A number of observations indicates the existence of an intense neutron group in the energy region below 1 MeV [4]; a precise determination of the spectrum in this region has not been published to our knowledge.

The source (Buchler and Co., Braunschweig) consisted of a homogeneous mixture of $RaSO_4$ (100 mC) and Be placed into a nickel capsule (29.5 mm height, 18 mm diameter) and had a source strength of $1.2 \cdot 10^6$ n/sec. The measured spectrum is shown in Fig. 55 together with the measurement of Thompson and Taylor [16]. The total measuring time amounted to about 45 h. Measurements were made with counter No. 1 above 3 MeV and with counters No. 3 and 4 (Table 6) below this value.

As indicated in Fig. 55, the intense γ-radiation was somewhat smeared by a small lead cylinder between source and detector. Elastic collisions practically do not change the neutron energy, but about 20% of all neutrons with energies above 3 MeV which fly in the direction of the detector undergo an inelastic collision in the lead cylinder. Monte Carlo calculations show that this notably distorts the source spectrum only below 3 MeV, where the flux (per energy interval) on the average increases by a value corresponding to about 20% of the flux value in the maximum at 4 MeV.

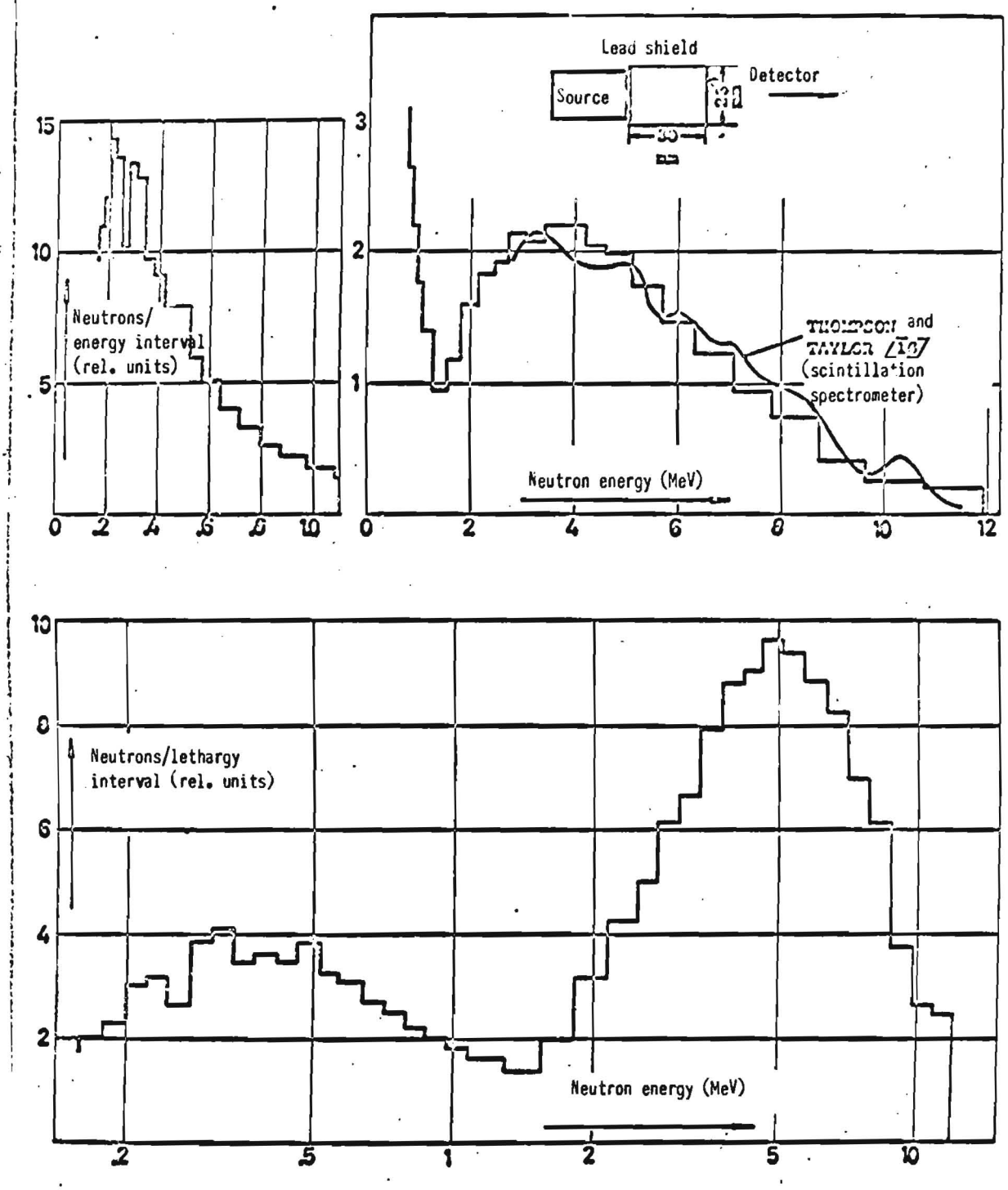

Fig. 55.--Neutron spectrum of the Ra-Be-source.

The measured spectrum is in good agreement with that determined by Thompson and Taylor in the energy region above 3 MeV. As in the Am-Be-sources, a neutron peak is again present in the region below 1 MeV. The mean energy of this peak amounts to about 400 keV as in the Am-Be-sources, indicating the same disintegration process (44) proposed by St. Romain et al. [57]; in this case, however, the intensity of this peak is about twice as high as in the Am-Be sources ([36 ± 8]% of all neutrons are below 1.5 MeV in the measured spectrum). The deformation of the measured spectrum in the low-energy region caused by the lead shield has the result that the minimum at about 1.5 MeV is not as well defined here as in the Am-Be-sources and that the above-indicated intensity value for the low-energy neutron peak must be reduced by about 3% to (33 ± 8) %.

4.5 Source strengths: The source strengths were estimated by integration over the measured spectra by means of the relation obtained from (30):

$$N = 4\pi \cdot d_1 \cdot d_2 \int \varphi^E \, dE \qquad (45)$$

and are compared in Table 9 with manganese bath results [53].

Table 9.--Source strengths (n/sec) of the sources utilized.

	Cf^{252}	Am-Li	Am-7	$Am-B^{10}$	Am-B	Am-Be (0,4 C)	Am-Be (1,5 C)
Manganese bath	$1,03 \cdot 10^6$	$1,09 \cdot 10^5$	$4,53 \cdot 10^5$	$4,33 \cdot 10^5$	$1,21 \cdot 10^6$	$1,10 \cdot 10^6$	$1,32 \cdot 10^6$
From spectrum	$1,7 \cdot 10^6$	$9,3 \cdot 10^4$	$3,7 \cdot 10^5$	$3,5 \cdot 10^5$	$9,3 \cdot 10^5$	$9,7 \cdot 10^5$	$1,27 \cdot 10^6$
Spectrum / Mn bath	1,01	0,85	0,81	0,81	0,77	0,83	0,96

The source strengths determined from the spectrum on the average are about 15% lower than the manganese bath results. An estimate shows that a flux depression of this order of magnitude results from the fact that neutrons are scattered from the counter front face which consists of 3 mm iron. When this is taken into account, the source strengths calculated from the spectra concur with the manganese bath results within the mean systematic error of slightly more than 10%.

5. Summary

This study demonstrated that reliable neutron spectrum measurements are possible with proton recoil counters even below 20 keV and in the region of 1.5-10 MeV, and the spectra of all normally used neutron sources were determined in the entire energy region of interest.

The reliability in the low-energy region was considerably increased by an accurate determination of the relation between proton energy and ionization produced in the counter for protons in hydrogen in the energy region above 1 keV. For the high-energy region too, the relation between proton energy and ionization had to be experimentally verified first for the counter gases utilized. The greatest difficulty in the high-energy region resides in the long range of the protons which increases markedly with energy. By the use of very large counters filled with gas mixtures with a high slowing-down power and under a high pressure, it was possible to create conditions for a sufficiently high probability that the energetic protons would also release their total energy in the counting gas. A specially adapted electronic system had to be used to process the long pulse rise times of such counters. A prerequisite for unfolding of the measured recoil-proton spectra by means of calculated response matrixes was to furnish proof with monoenergetic neutrons that the measured and calculated response functions are in agreement for all counters utilized in the entire energy region. These preliminary measurements were completed by measurements with two SUAK-assemblies. A comparison with the results of time-of-flight- and Li^6-spectrometer measurements showed agreement within the estimated systematic errors.

The differential neutron spectrum of a Sb-Be-source was determined accurately for the first time and the measurements show that with the use of the γ,n-discrimination method, proton-recoil counters furnish good results also in the low-energy region even with an extremely high γ-background. The spectrum measurements of the α,n-sources generally confirm the findings of earlier studies in the energy region above about 2 MeV. All α,n-sources investigated here emit a notable number of neutrons in the energy region below 1-2 MeV for which no differential spectrum measurements have been available thus far with the exception of the Am-Li-source. The low-energy neutron peak which has been postulated to exist on the basis of

theoretical considerations and indirect measurements with Ra-Be- and Am-Be-sources was confirmed and its fine structure was determined. In the Am-B-source, a clearly defined neutron peak is also present in the region below 1 MeV, even though it is less intense compared to Ra-Be- or Am-Be-sources, while the spectrum with the other α,n-sources is relatively continuous in this region. The spectral measurements for three different Am-Be-sources show that the particle size of the radioactive material in particular can notably influence the α,n-source spectra (up to 10%), but generally, these differences are small compared to the discrepancies in the spectra measured by different authors.

At this point, I would like to thank Prof. Dr.-Ing. D. Stegemann for suggesting this study and for his interest in its progress. I am indebted to Prof. Dr. K. Wirtz for permitting its performance at the Institute of Neutron Physics and Reactor Engineering of the Karlsruhe Nuclear Research Center. I am grateful to Dipl.-Phys. G. Fieg for stimulating discussions and suggestions and to Dipl. Phys. E. Korthaus for making the neutron sources available to me.

6. Literature

[1] Hess, W.N.: Neutrons from (α-n) Sources. Ann. Phys. 2, 115 (1959).

[2] Love, T.A. and R.B. Murray: Fast Neutron Spectroscopy. IRE-Trans. NS-8, 91 (1961).

[3] Batchelor, R., R. Aves, and T.H.R. Skyrme: Helium-3 filled proportional counter for neutron spectroscopy. Rev. Sci. Instr. 26, 1037 (1955).

[4] Marion, J.B. and J.L. Fowler (edts).: Fast Neutron Physics, Pt. I (p. 1, 179 and 413), Interscience, New York (1960).

[5] Sayres, A. and M. Coppola: ^{3}He-neutron spectrometer using pulse rise time discrimination. Rev. Sci. Instr. 35, 431 (1964).

[6] Bair, W.A.: An improved helium-3 neutron spectrometer. UCRL-Report No. 16595 (1966).

[7] Pendlebury, E.D.: Neutron cross sections of Li-6 in the energy range 0.001 eV - 15 MeV. AWRE-Report No. 0-60/64 (1964).

[8] Batchelor, R. and H. Parker: Neutron cross sections of He-3 in the energy range 0.001 eV - 14 MeV. 1963 Interum Revision. AWRE-Report. No. 0-78/64 (1964).

[9] Cloth, P and R. Hecker: Determination of the neutron energy distribution of a Am-Be- and a Cf^{252}-source by means of a He^3-semiconductor-sandwich-spectrometer. Nukleonik 12, 163 (1969).

[10] Verdinski, V.V., W.R. Burrus, R.M. Freestone and R.E. Textor: Fast neutron spectrometry with thick organic scintillators in reactor-type measurements. Radn. Meas. in Nucl. Power, paper 3.11 (1966).

[11] Giles, R.: A proportional counter spectrometer for neutrons. Rev. Sci. Instr. 24, 986 (1953).

[12] Perlow, G.J.: Recoil type neutron spectrometer for 0.05 to 1 MeV. Rev. Sci. Instr. 27, 460 (1956).

[13] Bluhm, H. and D. Stegemann: Theoretical and experimental investigations for an improved application of the ^6Li-semiconductor sandwich spectrometer. Nucl. Instr. Math. 70, 141 (1969).

[14] Herold, T.R.: Neutron spectrum of $^{238}Pu\text{-}F_4$. Nucl. Instr. Meth. 71, 40 (1969).

[15] Geiger, K.W. and C.J.D. Jarvis: Neutrons and gamma rays from $Po^{210}\text{-}B^{10}(n,\alpha)$ and $Po^{210}\text{-}B^{11}(n,\alpha)$ sources. Can. J. Phys. 40, 33 (1962).

[16] Thompson, M.N. and J.M. Taylor: Neutron spectra from Am-α-Be and Ra-α-Be sources. Nucl. Instr. Meth. 31, 305 (1965).

[17] Horsley, A.: Neutron cross sections of hydrogen in the energy range 0.0001 eV - 20 MeV. Nucl. Data, Sect. A, 2, 243 (1966).

[18] Beckurts, K.H. and K. Wirtz: Neutron Physics. Springer Verlag, Berlin, 1964.

[19] Benjamin, P.W., C.D. Kemshall and J. Redfearn: The use of gas-filled spherical proportional counter for neutron spectrum measurements in a zero energy fast reactor. AWRE Report No. NR2/64 (1964).

[20] Bennett, E.F.: Fast Neutron Spectroscopy by Proton Recoil Proportional Counting. Nucl. Sci. Eng. 27, 16 (1967).

[21] Rossi, B.B. and H.H. Staub: Ionization chambers and counters. McGraw-Hill Company, London (1949).

[22] Wilkinson, D.H.: Ionization chambers and counters. Cambridge University Press (1950).

[23] Ricker, G.R., Jr.: Pulse risetimes in proportional counters. Rev. Sci. Instr. 40, 227 (1969).

[24] English, W.K. and G.C. Hanna: Grid iron ionization chamber measurements of electron drift velocities in gas mixtures. Can. J. Phys. 31, 768 (1953).

[25] Staub, H.H.: Detection Methods. In: Experimental Nuclear Physics, Vol. I, Ed. E. Sogre, John Wiley, New York (1960).

[26] Gillespie, A.B.: Signal, Noise, and Resolution in Nuclear Counter Amplifiers. Pergamon, London (1953).

[27] Allen, W.D. and A.T.G. Ferguson: The measurements of fast neutron flux over the energy range 0.03 MeV to 3 MeV. Proc. Phys. Soc. London 70A, 639 (1957).

[28] Werle, H., G. Fieg, H. Seufert and D. Stegemann: Investigation of the specific energy loss of protons in hydrogen above 1 keV with regard to neutron spectrometry. Nucl. Instr. Meth. 72, 111 (1969).

[29] Bergman, A.A. et al.: A neutron spectrometer based on measuring the slowing-down-time of neutrons in lead. Proc. Int. Conf. Peaceful Uses Atom. Energy, Geneva (1955), 4 UN, New York, p. 135 (1956).

[30] Strauss, M.G. and R. Brenner: General purpose analog pulse height computer. Rev. Sci. Instr. 36, 1857 (1965).

[31] Fieg, G.: Determination of fast neutron spectra in the 10 keV-1 MeV energy region by means of a spherical hydrogen-filled proton-recoil-proportional counter. Thesis, Karlsruhe Institute of Technology, 1966.

[32] Snidow, N.L.: Wall effect corrections in recoil proton spectrometers-spherical counter. BAW-TM-442, Babcock and Wilcox, 1965.

[33] Brandl, V.: A Monte-Carlo program for proton-recoil counters in cylindrical geometry. KFK 860, EUR 4154.d, 1968.

[34] Benjamin, P.W., C.D. Kemshall and A. Brickstock: The analysis of recoil proton spectra. AWRE Report No. 09/68 (1968).

[35] Küchle, M., F. Mitzel, E. Wattecamps and H. Werle: Measurements of neutron spectra and decay constants with the fast subcritical facility SUAK. Proc. Int. Conf. Fast Critical Exp. and Analysis, ANL-7320, p. 506, 1966.

[36] Bluhm, H., G. Fieg, F. Kappler, M. Küchle, M. Müller, H. Werle, E. Wattecamps: Neutron spectrum measurements in various SUAK assemblies. BNES Int. Conf. Fast Reactors, June 1969.

[37] Coates, M.S., D.B. Gayther, P.D. Goode, and D.J. Tripp: Time-of-flight measurements of the neutron spectrum in a subcritical fast reactor assembly. J. Nucl. Energy 22, 547 (1968).

[38] Hughes, D. and C. Eggler: Cloud chamber energy measurements of photoneutron sources. Phys. Rev. 72, 902 (1947).

[39] Hanson, A.O.: Energies of neutrons from MaTh-D, La-D, γ-Be and Sb-Be Photo-Neutron Sources. Phys. Rev. 75, 1794 (1949).

[40] Möller, U.: Solution of the transport equation by means of the Monte-Carlo method. KFK 297 (1965).

[41] Ryves, T.B. and D.W. Beale: An estimate of the energy of Sb-Be-photoneutrons from a measurement of the Sb^{124}γ-ray energy. Int. J. Appl. Rad. and Isot. 18, 204 (1967).

[42] Mattauch, J.H.E., W. Thiele and A.H. Wapstra: Consistent set of Q-values. Nucl. Phys. 67, 32 (1965).

[43] Schmitt, H.W.: Determination of the energy of antimony-beryllium photo-neutrons. Nucl. Phys. 20, 220 (1960).

[44] Tuttle, J.G.: Measurements of neutron importance in mixed-spectra critical assemblies. AI-Rep. No. 8549, Set. 7 (1963).

[45] Smith, A.B. and P.R. Fields: Spontaneous fission neutron spectrum of Cf 252. Phys. Rev. 108, 411 (1957).

[46] Conde, H. and G. During: Fission Neutron Spectra, Part II, Fission Neutron Spectra of U^{235}, Pu^{239} and Cf^{252}. Ark. Fys. 29, 313 (1965).

[47] Meadows, J.W.: Cf^{252} fission neutron spectrum from 0.003 to 15.0 MeV. Phys. Rev. 157, 157 (1967).

[48] Bonner, T.W.: Measurements of neutron spectra from fission. Nucl. Phys. 23, 116 (1961).

[49] Bowman, H.R., S.G. Thompson, J.C.D. Milton and W.J. Swiatecki: Velocity and angular distributions of prompt neutrons from spontaneous fission of Cf^{252}. Phys. Rev. 126, 2120 (1962).

[50] Bennett, E.F.: The Am-α-Li neutron spectrum. Argonne National Laboratory Report No. ANL-7017, 39 (1965).

[51] Barton, D.M. Measurements of the neutron spectrum from a Po-Li^7 neutron source. Los Alamos Report No. LA-1609 (1953).

[52] Young, D.S.: Paraffin cylinders to measure neutron energies. Los Alamos Report No. LA-1953 (1955).

[53] Szilvasi, A.J.D., K.W. Geiger, and W.R. Dixon: Study of neutrons from a Po-F(α,n)-source. J. Nucl. Energy. Pt. A, 11, 131 (1960).

[54] Lehman, R.L.: Neutron groups in the spectrum of a PuF_4 source. Phys. Rev. 171, 1311 (1968).

[55] Van der Zaam, L.: Calculated neutron spectra from $^9Be(\alpha,n)$ sources. Can. J. Phys. 46, 1527 (1968).

[56] Geiger, K.W. and C.K. Hargrove: Neutron spectrum of an Am^{241}-Be(α,n) source. Nucl. Phys. 53, 204 (1964).

[57] St. Romain, F.A., T.W. Bonner, R.L. Bramblett, and J. Hanna: Low-energy neutrons from the reaction $Be^{9}(\alpha,n)C^{12}$. Phys. Rev. 126, 1794 (1962).

[58] Korthaus, E.: Gesellschaft für Kernforschung mbH. Karlsruhe, personal communication.